EUROPEAN-AMERICAN-JAPANESE
TWO-PHASE FLOW GROUP MEETING

23RD TO 27TH OCT. 2022

EAJTPFGM22
1ST EDITION
CHAMONIX FRANCE
ORGANISATION:
CETHIL

https://eajtpfgm21.sciencesconf.org/

PREFACE

The first edition of the European-American-Japanese Two-Phase Flow Group Meeting will be hosted by Prof. Rémi Revellin (INSA Lyon, France) in Chamonix, France from 23rd oct. to 27th oct. 2022. The idea of the group meeting was first initiated by Prof. Iztok Zun (European Research Community) and Prof. Goichi Matsui (Japanese Society of Multiphase Flow) and led to a series of eight joint European-Japanese meetings. Fruitful and exciting exchange of information occurred during the previous editions (Portoroz - June 1998, Tsukuba - September 2000, Certosa di Pontignano – September 2003, Kyoto - September 2006, Spoleto - September 2009, Kumamoto – September 2012, Zermatt – October 2015 and New-York – April 2018). After the European-Japanese Two-Phase Flow Group Meeting held in New-York in 2018, Prof. John Thome (EPFL, Switzerland) and Prof. Akio Thomiyama (Kobe University, Japan) suggested to begin holding a joint three-way meeting every three years with americas. As a result, the bilateral meeting (European-Japanese) every three years has become a trilateral meeting.

This joint meeting will provide a discussion platform that motivates a fruitful emergence of new ideas that can be immediately put into practice in current research, to set up collaborations with research groups in Europe, Americas and in Japan, and to provide a good insight of the latest research occurring in the most qualified European, American and Japanese laboratories of two-phase flow. The special features of the European – American - Japanese Group meetings are:

- presentations dealing with fresh material (work in progress);
- quality attendance by invitation only (about 60 participants);
- ample time for discussion;
- plenary sessions;
- informal meeting opportunities;

The 2022 Meeting will be held at the **Alpina Electric Hotel****** in Chamonix located in front of the Mont Blanc.

Table of contents

ORGANISERS

Conference Chair

Prof. Rémi Revellin
CETHIL Laboratory UMR 5008
INSA Lyon
Bât Sadi Carnot, 9 Rue de la Physique
69621 Villeurbanne cedex
France
Tel: +33 4 72 43 82 00
remi.revellin@insa-lyon.fr

European Side Conference Co-Chairs

Prof. John R. Thome
Honorary Professor,
École Polytechnique Fédérale de Lausanne (EPFL),
CH-1015 Lausanne. Switzerland
john.thome@jjcooling.com

Prof. Gian Piero Celata
ENEA Casaccia, Institute of Thermal Fluid Dynamics,
Via Anguillarese, 301
Santa Maria di Galeria, Rome. Italy
Tel: + 39 06 3048 3905,
gianpiero.celata@enea.it

Prof. Paolo di Marco
Energy and Systems Engineering (DESE), Università di Pisa,
Largo Lucio Lazzarino, 1
I 56126 Pisa. Italy
Tel: + 39 050 2217107,
p.dimarco@ing.unipi.it

Japanese Side Conference Co-Chairs

Prof. Akio Tomiyama
Graduate School of Engineering, Department of Mechanical Engineering, Faculty of Engineering,
Kobe University
1-1 Rokkodaicho, Nada Ward, Kobe
Hyogo Prefecture 657-0013, Japan
Tel: +81 78 881 1212
tomiyama@mech.kobe-u.ac.jp

American Side Conference Co-Chairs

Gretar Tryggvason
Charles A. Miller Jr. Distinguished Professor and Department Head
Department of Mechanical Engineering
223 Latrobe Hall, 3400 N. Charles Street
Johns Hopkins University
Baltimore, MD, 21218-2681
Phone: 410-516-5970
gtryggv1@jhu.edu

VENUE

The European American Japanese Two-Phase Flow Group Meeting will take place at the **Alpina Eclectic Hôtel****** in the centre of Chamonix. The hotel is easily accessible from the major French and European cities! An ideal location in the world's mountaineering capital. Back from a day of presentations or simply because you feel like it, treat yourself to a relaxing moment at the foot of Mont Blanc in the spa and wellness center of the hotel.

Alpina Eclectic Hôtel
79 av. du Mont Blanc
74400 Chamonix-Mont-Blanc

https://www.alpinachamonix.com/en/

To reach the destination
By plane
Geneva International Airport and Shuttle link to Chamonix (88 km). Shuttle online reservation https://www.mountaindropoffs.com/ or https://alpybus.com/chamonix or https://www.chamexpress.com/Chamonix.html
Bus shuttle (cheapest one): https://www.checkmybus.com/

By Train
- Chamonix train station (SNCF)
- TGV train line: Saint-Gervais-les-Bains-le-Fayet SNCF train station (20 km)
- TER train line: Saint-Gervais-les-Bains-le-Fayet SNCF train station (20 km)

By car
- From France: Highway "Autoroute Blanche" (A40)
- From Switzerland: Highway to Martigny, then Col de la Forclaz and finally Col des Montets
- From Italia: by the Mont-Blanc tunnel located at 15km from the hotel

INFORMATION

Power and Electrical Plugs

Power plugs in France have the particularity of being male and female at the same time. In most countries, plugs only have prongs, and sockets are only receptacles for those prongs. However, electric plugs have 2 prongs and a receptacle in France. Electrical outlets in France usually deliver power at 220-240 volts, 50 Hz.

Currency

The euro (€) has been France's currency since January 1, 2002. The euro is used in 19 of the 27 countries that make up the European Union.

The French currency, the euro, is made up of bills in the following denominations — 5, 10, 20, 50, 100, 200 and 500 — and coins are 1 euro, 2 euros, and 1, 2, 5, 10, 20, and 50-centime pieces. Some shops do not accept bills of 100, 200 and 500 €.

Time Zone and Date

The time zone of Chamonix is GMT+2.

General information

- France country code: +33, for example +33 4 50 53 47 77 (Hotel Alpina Chamonix)
- To call inside France, use 0 as prefix to area code; for example 04 50 53 47 77 (Hotel Alpina Chamonix)
- To call foreign countries 00 + country code + area code + number; for example 00 41 27 966 68 68 (example for Switzerland).

Emergency phone numbers (land line phones)
- Medical Emergencies: 15
- International Emergencies: 112
- Police: 17
- Fire: 18

Weather and Clothing

Chamonix is situated at 1'035 m, and thus subject to fast changing weather conditions. In October, the average temperature in Chamonix is about 10°C (max 13°C, min 8°C).

For our excursion on a Montenvers train on Tuesday to the « Mer de Glace » for lunch you should plan to have a winter coat for the temperature and wind up there.

Smoking

In France smoking is not permitted in indoor public spaces.

KEYNOTE SPEAKERS

Prof. (Emeritus) John R. Thome
JJ Cooling Innovation Sàrl
Lausanne
Switzerland
Industrialization of Micro-Two-Phase Flow and Heat Transfer Research: Where Are We?

John R. Thome is Technical Director of JJ Cooling Innovation Sàrl in Lausanne, Switzerland, which develops new micro-two-phase cooling technologies for: power electronics, automotive, datacenters, edge computing, aerospace, 5G, batteries, food and beverage industries. These comprise Passive cooling (gravity/thermosyphons and self-excited/PHPs) and Active cooling (pumped and compressor driven systems), see (https://www.jjcooling.com). He is Professor Emeritus of Heat Transfer at the EPFL in Lausanne (1998-2018) where he directed the LTCM lab (https://archiveweb.epfl.ch/ltcm.epfl.ch). He is the author of five books and editor-in-chief of the *Encyclopedia of Two-Phase Heat Transfer and Flow* (16 volumes). He chairs the Virtual International Research Institute of Two-Phase Flow and Heat Transfer (http://2phaseflow.org) that has some 30 participating members. He has written over 250 journal papers with 30'000+ citations. He received the 2017 Nusselt-Reynolds Prize, the 2019 IEEE ITHERM Award, the 2019 ASME InterPack Medal and the 2010 ASME Heat Transfer Memorial Award, among others.

Prof. Asano Hitoshi
Department of Mechanical Engineering
Kobe University
Japan
Effect of Boiling Bubbles on Gas-Liquid Interfacial Structure
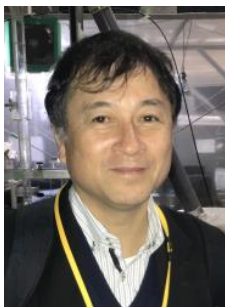
Hitoshi Asano is a professor of Department Mechanical Engineering of Kobe University, Japan. He graduated from Kobe University in 1990. He started research on two-phase flow dynamics in Kobe University after 3.5 years working in Daikin Industries. He obtained degree of Dr. Eng. from Kobe University in 2000, and was promoted to associate professor in 2001. From 2001 to 2002 he visited

Stuttgart University as a research fellow of the Alexander von Humboldt foundation. His interest is focused on thermo-fluid dynamics with evaporation and condensation in compact heat exchangers for HVAC systems and in two-phase flow cooling systems for space structures. He is Fellow of the Japan Society of Mechanical Engineers, and a member of Scientific Council of International Center for Heat and Mass Transfer.

Prof. Joseph Katz
Department of Mechanical Engineering
Johns Hopkins Whiting School of Engineering
USA

Multiphase Flow Phenomena Associated with the Breakup, emulsification, and Transport of Crude Oil by Surface Waves and Subsurface Plumes
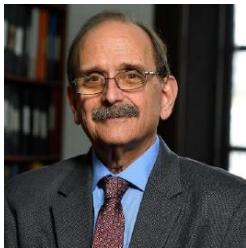
Joseph Katz received his B.S. degree from Tel Aviv University, and his M.S. and Ph.D. from California Institute of Technology, all in mechanical engineering. He is the William F. Ward Sr. Distinguished Professor of Engineering, and the director and co-founder of the Center for Environmental and Applied Fluid Mechanics at Johns Hopkins University. He is a Member of the National Academy of Engineering, as well as a Fellow of the American Physical Society, American Society of Mechanical Engineers (ASME), and American Society of Thermal and Fluids Engineering. He has served as the Editor of the Journal of Fluids Engineering, and as the Chair of the board of journal Editors of ASME. His research extends over a wide range of fields, with a common theme involving experimental fluid mechanics, and development of optical and ultrasonic diagnostics techniques for laboratory and field applications. His group has studied laboratory and oceanic boundary layers, flows in turbomachines, flow-structure interactions, biomedical flows, swimming behavior of marine plankton in the laboratory and in the ocean, as well as cavitation, bubble, and droplet dynamics, the latter focusing on interfacial phenomena associated with oil spills.

PROGRAM

Sunday 23rd Oct.

14:30	16:30	Lobby	Registration	
16:00	16:30	Main room, 1st floor	Welcome coffee	
16:30	16:45	Main room, 1st floor	Opening	Rémi Revellin - John Thome - Akio Tomiyama - Gretar Tryggvason
16:45	**17:45**	**Main room, 1st floor**	**Keynote lecture**	**Chairman: John Thome**
16:45	*17:45*		*Multiphase Flow Phenomena Associated with the Breakup, emulsification, and Transport of Crude Oil by Surface Waves and Subsurface Plumes*	Joseph Katz, Johns Hopkins University, USA
19:00	21:00	Restaurant "Le Vista", 7th floor of the hotel	Cocktail - dinner	

Monday 24th Oct.

09:00	**10:00**	**Main room, 1st floor**	**Keynote lecture**	**Chairman: Rémi Revellin**
09:00	10:00		*Industrialization of Micro-Two-Phase Flow and Heat Transfer Research: Where Are We?*	John Thome, JJ Cooling Innovation Sàrl, Switzerland
10:00	10:20	Main room, 1st floor	Coffee break	
10:20	**12:00**	**Main room, 1st floor**	**Experimental**	**Chairman: Paolo Di Marco**
10:20	10:40		*Heat Transfer of Flow Boiling Carbon Dioxide in Vertical Upward Direction*	Rémi Revellin, INSA Lyon, France
10:40	11:00		*Bubbly flows in a column with submerged hollow fiber membranes*	Ryo Kurimoto, Kobe University, Japan
11:00	11:20		*Liquid Velocity and Turbulence Measurements in Air-water Bubbly Flows using PIV-PLIF*	Xiaodong Sun, University of Michigan
11:20	11:40		*Low to Moderate Frequency AC Electric Field Effects on Convective Boiling in the Bubbly Flow Regime*	Anthony Robinson, Trinity College Dublin, Ireland
11:40	12:00		*Multiscale deformation and breakup in turbulence*	Rui Ni, Johns Hopkins University, USA
12:30	14:00	Restaurant "Le Vista", 7th floor of the hotel	Lunch	
14:00	**16:00**	**Main room, 1st floor**	**Numerical**	**Chairman: Gretar Tryggvason**
14:00	14:20		*Bubble Cloud Formation by the Backscattering of High Intensity Focused Ultra Sound from a Bubble Interface*	Hiroyuki Takahira, Osaka Metropolitan University, Japan
14:20	14:40		*Hybrid quadrature moment methods for polydisperse cavitating flows.*	Tim Colonius, California Institute of Technology, USA
14:40	15:00		*Interface-resolved Boiling Simulation in Complex Geometries for Machine-Learning Model Development*	Igor Bolotnov, North Carolina State University, USA
15:00	15:20		*Numerical simulation of conjugate heat transfer effects on flow boiling in a multi-microchannel evaporator*	Mirco Magnini, University of Nottingham, UK
15:20	15:40		*Stability of two-phase stratified flows in circular pipes*	Ilya Barmak, Tel Aviv University, Israel
15:40	16:00		*Study on High-Precision Simulation Method of Condensation*	Kei Ito, Kyoto University, Japan
16:00	16:20	Main room, 1st floor	Coffee break	
16:20	**17:40**	**Main room, 1st floor**	**Modeling**	**Chairman: Mirco Magnini**
16:20	16:40		*Effect of Inclination Angle on Evaporating Flow in Parallel Pipes*	Yehuda taitel, Tel Aviv University, Israel
16:40	17:00		*MIT-Boil experience and future challenges: update after 10 years of collaborative research*	Emilio Baglietto, MIT, USA
17:00	17:20		*Selected Aspects of Flow Boiling of R1233zd(E) at Medium and High Reduced Pressures*	Dariusz Mikielewicz, Gdansk University, Poland
17:20	17:40		*Two-phase frictional pressure gradient: to what extent are the ANN-based methods able to replace the deterministic models?*	Luca Viscito, University of Naples Federico II, Italy
19:00	21:00	Restaurant "Le Vista", 7th floor of the hotel	Dinner "Buffet montagnard"	

Tuesday 25th Oct.

09:00	10:00	Main room, 1st floor	Experimental	Chairman: Emilio Baglietto
09:00	09:20		Experiment on boiling entrainment from a falling liquid film	Tomio Okawa, The University of Electro-Communications, Japan
09:20	09:40		Heat transfer and pressure drop characteristics of single and two-phase flows in a finned rectangular channel	Yasushi Saito, Kyoto University, Japan
09:40	10:00		Simultaneous measurement of liquid film thickness and heat transfer during downflow condensation of R134a and R245fa inside a vertical minichannel	Stefano Bortolin, University of Padova, Italy
10:00	10:20	Main room, 1st floor	Coffee break	
10:40	15:00	Refuge du Montenvers	Excursion by train with lunch at the top	
15:00	16:00	Main room, 1st floor	Experimental	Chairman: Xiaodong Sun
15:00	15:20		Development and application of ultrasound techniques to multiphase flows	Fria Hossein, University College London, UK
15:20	15:40		Generation of Microbubble Encapsulated Vesicles and the Manipulations using Ultrasound Field	Shu Takagi, University of Tokyo, Japan
15:40	16:00		Behaviour of bubble chain in gallium eutectic alloy under influence of transverse magnetic field	Hideki Murakawa, Kobe University, Japan
16:00	17:00	Main room, 1st floor	Keynote lecture	Chairman: Akio Tomiyama
16:00	17:00		Effect of Boiling Bubbles on Gas-Liquid Interfacial Structure	Hitoshi Asano, Kobe University, Japan

Wednesday 26th Oct.

09:00	**10:00**	**Main room, 1st floor**	**Numerical**	**Chairman: Tim Colonius**
09:00	*09:20*		*ACoolTPS ? A Framework for Simulating Two-Phase Flows*	Gustavo Anjos, Federal University of Rio de Janeiro, Brazil
09:20	*09:40*		*Drag reduction of a spherical bubble with oscillation in shear-thinning power-law fluid*	Kazuyasu Sugiyama, Osaka University, Japan
09:40	*10:00*		*Influence of density and viscosity on deformation, breakage, and coalescence of bubbles in turbulence*	Alessio Roccon, TU-Wien, Austria
10:00	10:20	Main room, 1st floor	Coffee break	
10:20	**12:20**	**Main room, 1st floor**	**Experimental**	**Chairman: Hitoshi Asano**
10:20	*10:40*		*Active and Passive techniques for enhancing pool boling in normal and reduced gravity*	Paolo Di Marco, University of Pisa, Italy
10:40	*11:00*		*Pool Boiling: Aspects of Heat transfer Enhancement*	Tassos Karayiannis, Brunel University London, UK
11:00	*11:20*		*Spherical Re-entrant Cavities for Pool Boiling Enhancement*	Roger Kempers, York University, Canada
11:20	*11:40*		*The percolation law of the boiling crisis*	Matteo Bucci, MIT, USA
11:40	*12:00*		*Effect of Bilayer Porous Metal body on Critical Heat Flux Enhancement in a Saturated Pool Boiling*	Shoji Mori, Kyushu University, Japan
12:00	*12:20*		*Cavitation Inception, Development, and Noise Emissions Due to the Interaction of a Pair of Line Vortices*	Steven Ceccio, University of Michigan, USA
12:30	14:00	Restaurant "Le Vista", 7th floor of the hotel	Lunch	
14:00	**16:00**	**Main room, 1st floor**	**Experimental**	**Chairman: Tassos Karayiannis**
14:00	*14:20*		*Capturing Two-phase Flow beyond Steady States Using Periodic Oscillations Induced by Flow Instability*	Caleb Brooks, University of Illinois, USA
14:20	*14:40*		*Fragmentation of Liquid Drop Falling through Miscible Liquid due to Rayleigh-Taylor Instability*	Kosuke Hayashi, Kobe University, Japan
14:40	*15:00*		*Gas Removal from Closed-End Small Holes using Pressure Fluctuation*	Toshiyuki Sanada, Shizuoka University, Japan
15:00	*15:20*		*Gas-liquid flow hydrodynamics in jumpers of subsea gas production systems*	Alexander Yurishchev, Tel Aviv University, Israel
15:20	*15:40*		*String Cavitation Flow in Multi-Hole Fuel Injector and Spray*	Akira Sou, Kobe University, Japan
15:40	*16:00*		*Study of Plateau-Rayleigh instability in stratified liquid-liquid pipe flow: PIV/PLIF experiments and numerical solution*	Oscar Rodriguez, University of São Paulo, Brazil
16:00	16:20	Main room, 1st floor	Coffee break	
16:20	**17:20**	**Main room, 1st floor**	**Numerical**	**Chairman: Gustavo Anjos**
16:20	*16:40*		*Direct Numerical Simulation of Atomization of Vaporizing Liquids*	Yue Ling, Baylor University, USA
16:40	*17:00*		*High-Fidelity Multi-Scale Modeling Framework for Predicting Turbulent Spray Atomization*	Olivier Desjardins, Cornell University, USA
17:00	*17:20*		*Direct numerical simulation of freezing droplets*	Dominique Legendre, IMFT, France
19:00	21:00	Restaurant "Le Vista", 7th floor of the hotel	Gala Dinner	

Thursday 27th Oct.

08:40	10:00	Main room, 1st floor	Modeling	Chairman: Dariusz Mikielewicz
08:40	09:00		*A Dual-Scale LES Model for Sub-Filter Dynamics of Phase Interfaces During Atomization*	Marcus Herrmann, Arizona State University, USA
09:00	09:20		*Dispersion of a passive scalar around a Taylor bubble*	Davide Picchi, University of Brescia, Italy
09:20	09:40		*Interface Retaining Coarsening of Multiphase Flows*	Gretar Tryggvason, Johns Hopkins University, USA
09:40	10:00		*Subgrid-scale models for turbulent particle-laden flows from dilute to dense regimes*	Jesse Capecelatro, University of Michigan, USA
10:00	10:20	Main room, 1st floor	Coffee break	
10:20	11:40	Main room, 1st floor	Experimental	Chairman: Anthony Robinson
10:20	10:40		*Role of solid and soft particles in tuning microfluidic dripping to jetting transitions*	Loïc Chagot, University College London, UK
10:40	11:00		*Experimental analysis of the flow-induced noise, structure acceleration and two-phase flow jet velocity at the outlet of a thermal expansion valve*	Gherhardt Ribatski, University of São Paulo, Brazil
11:00	11:20		*Experimental Observation and Temperature Measurement of Lateral Hydrate Growth on a Sessile Droplet*	Christos Markides, Imperial College London, UK
11:20	11:40		*Influence of Air Entrainment on Quenching of a Solid Sphere*	Shigeo Hosokawa, Kansai University, Japan
11:40	11:45	Main room, 1st floor	Closure	Rémi Revellin

ACoolTPS – A Framework for Simulating Two-Phase Flows

G. R. Anjos[1] and P. Valluri[2]

[1]COPPE/Department of Mechanical Engineering, Federal University of Rio de Janeiro – Rio de Janeiro, Brazil,

[2] IMT/ Chemical Eng, School of Engineering, University of Edinburgh – Edinburgh, United-Kingdom

Contact E-mail : gustavo.rabello@coppe.ufrj.br

The present work aims at developing a new flexible computational framework based on modern programming language to simulate macro and microscale two-phase flows with dynamic boundaries in complex geometries. Such a technique is extremely useful for periodic and very large domains which requires exhaustive computational resources, consequently, reducing the required numerical domain. In this presentation the one-fluid interface tracking Finite Element (FE) method is used to solve the equations governing the motion of two immiscible incompressible fluids in the Arbitrary Lagrangian-Eulerian framework (ALE). The equations are written in axisymmetric coordinates; however, the proposed moving boundary technique can be extended to 3-dimensional flows and any other methods using the ALE framework such as the finite volume method. The two-phase interface mesh separating fluids is a segregated mesh, therefore a layer of defined thickness is set to assure smooth transition of properties among phases and no exhaustive remeshing is required at the fluid regions. Validations and results will be presented.

Figure 1 shows five different snapshots of the current numerical simulation highlighting 1) the unstructured quadrilateral mesh and the interface region in time $t = 2.2$, 2) the smoothed Heaviside function defining the inner and outer regions occupied by the two immiscible fluids in time $t = 5.08$, 3) the vertical velocity in time $t = 8.8$, 4) the horizontal velocity in time $t = 12.92$ and 5) the pressure field in time $t = 17.56$.
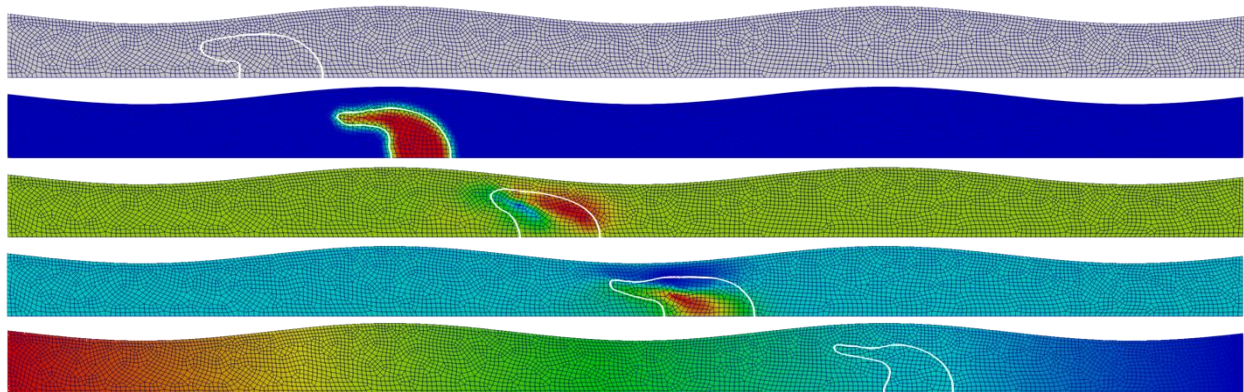

Figure 1. Snapshots of the current numerical simulation of two-phase flows using unstructured quadrilateral mesh showing 1) the fluid mesh in time $t = 2.2$, 2) the smoothed Heaviside function in time $t = 5.08$, 3) the vertical velocity in time $t = 8.8$, 4) the horizontal velocity in time $t = 12.92$ and 5) the pressure field in time $t = 17.56$.

Effect of Boiling Bubbles on Gas-Liquid Interfacial Structure

H. Asano[1], T. Ubara[1], K. Sawatari[1], K. Sugimoto[1] and H. Murakawa[1]

[1]Department of Mechanical Engineering, Kobe University
Contact E-mail : asano@mech.kobe-u.ac.jp

In the development of compact heat exchangers for refrigeration and air-conditioning systems, we are facing to several requirements. Those are further improvement in overall heat transfer coefficient, reduction in heat resistance, adaptation to new refrigerants with low GWP (global warming potential), and reduction in usage of refrigerant. A simple way to satisfy the requirements is to apply a mini-channel heat exchanger with multiport tubes with the hydraulic diameter of submillimeter. The other way to reduce the usage of refrigerant, especially for a large capacity chiller, is to substitute a flooded evaporator to a falling film evaporator. In each case of evaporating flow in minichannel and falling film evaporation, liquid film evaporation is dominant in the refrigerant heat transfer. It is well known that the heat transfer coefficient becomes higher for thinner liquid film. In other words, thicker liquid film leads to lower heat transfer coefficient and larger wall superheat. Nucleate boiling in liquid film is expected to enhance the heat transfer. While vapor bubble formation enhance the heat transfer in liquid film, breakup of bubbles often causes local dry patch formation. Therefore, it is important to clarify the effect of boiling bubbles on liquid film structure. Here, experimental results on falling film evaporation with nucleate boiling on a horizontal cylinder are shown.

Figure 1 shows a schematic diagram of experimental apparatus. Hydro-fluoro-olefin 1233zd(E) whose GWP is 1 was used as the refrigerant. The refrigerant was supplied to the test cylinder from three needle nozzles via dummy tube with machined cavities (GEWA-B5L by Wieland) to spread the liquid film uniformly. The detail of the test section is shown in Fig. 2. The test tube was heated by a cartridge heater with the same heating length as the test section. Wall temperature was measured by 7 T-type thermocouples soldered at the bottom of the test section to avoid disturbances to the liquid film. To avoid wettability change due to oxidation, an oxide layer was formed by heating at 300 ℃ in the preliminary preparation. The saturation temperature was maintained at 5, 20, 35 ℃. Subcooling degree of the supplied liquid was maintained within 0.5 K. The detail of the measurement accuracy was reported by Ubara et al. [1].

The measured heat transfer coefficient plotted against heat flux is shown in Fig. 3. The closed and open symbols show the results measured in the heat flux increasing and decreasing processes, respectively. The solid lines show the correlation of pool boiling heat transfer suggested by Jung et al.[2]. The film flow rate per unit length was enough to cover the heat transfer surface under the adiabatic condition. Figure 4 shows covering ratio of the heat transfer

surface by liquid film measured from observed images (Fig. 5) in the heat flux increasing process. It can be seen in Fig. 3 that heat transfer was dominated by nucleate boiling in liquid film under the moderate heat flux condition. Under the high heat flux condition, deterioration in the heat transfer coefficient was observed. It was shown in Fig. 4 that the deterioration was mainly caused by the decrease in the covering ratio. Focusing on the effect of saturation temperature, covering ratio became higher with the higher saturation temperature. It was observed that while breakup of larger vapor bubbles caused dry patch formation, smaller vapor bubbles from larger number of nucleation sites had positive effect for spreading the liquid film.
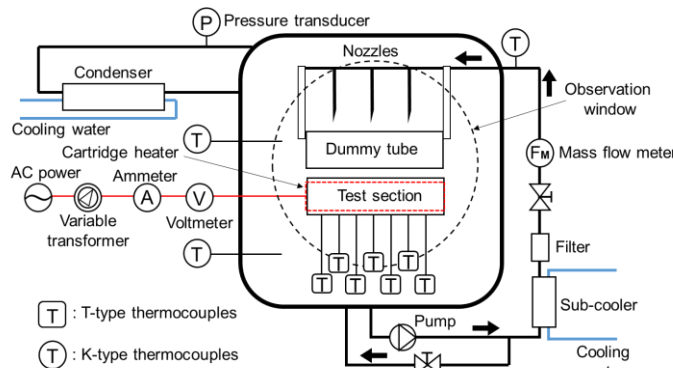
Figure 1. Schematic diagram of experimental apparatus.
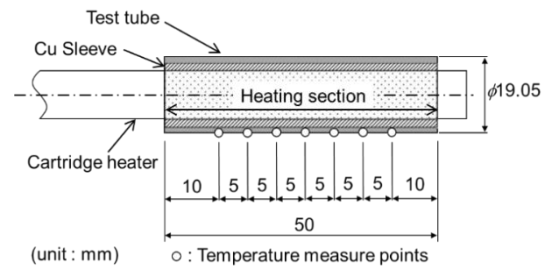
Figure 2. Test section configuration.
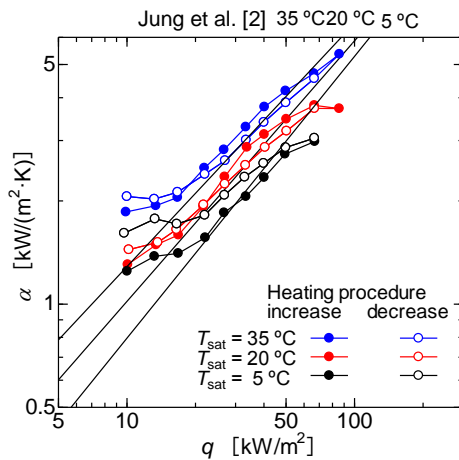
Figure 3. Heat transfer coefficient against heat flux ($\Gamma = 0.0334$ kg·m^{-1}·s^{-1}).
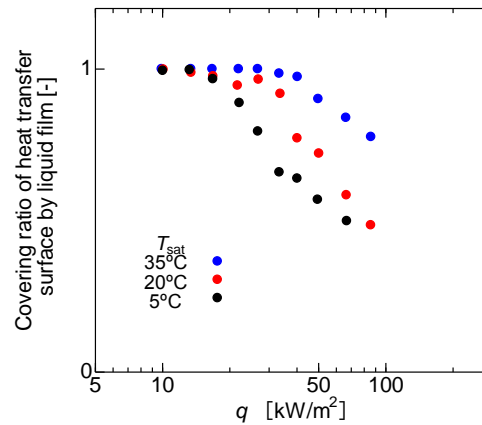
Figure 4. Covering ratio in heat flux increasing process against heat flux ($\Gamma = 0.0334$ kg·m^{-1}·s^{-1}).
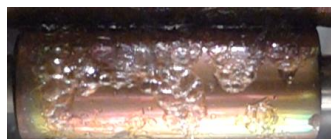
(a) $T_{sat} = 5℃$ (b) $T_{sat} = 20℃$ (c) $T_{sat} = 35℃$
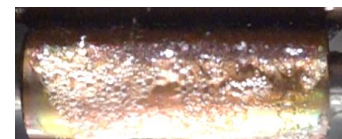
Figure 5. Falling film evaporation behavior at $\Gamma = 0.0334$ kg·m^{-1}·s^{-1} and $q = 66.9$ kW·m^{-2}.

References
[1] T. Ubara et al., *Applied Thermal Engineering*, 196 (2021), 117329.
[2] D. Jung et al., *Int. J. of Refrigeration*, 26 (2003), pp. 240–248.

MIT-Boil experience and future challenges: update after 10 years of collaborative research

E. Baglietto, M. Bucci

Department of Nuclear Science and Engineering
Massachusetts Institute of Technology, USA
emiliob@mit.edu

Benefitting from a strong international collaboration, the group at MIT has devoted considerable effort on advancing the ability to model multiphase flow and boiling in an industrially applicable Multiphase CFD framework (M-CFD). Following originally in the footsteps of Lahey and Drew [1], we have attempted to move from the classic multifield approach (CMFD), and extend the applicability of the methods through local representation of the fundamental meso-scale interfacial and wall phenomena. The effort has consistently leveraged the growing availability of both experimental and numerical databases, in combination with the advancements in data analysis techniques and computational resources, to advance the understanding and propose modeling formulations with increasing applicability. Some examples of the most refractory challenges have been wall lubrication, lateral forces and interaction of turbulence with liquid/gas structures [2][3]. A valuable review of the evolution of the approach has been recently published by Lahey [4].

Among the many objectives, the central effort has been devoted to advancing the ability to generally predicting boiling heat transfer, potentially up to its critical limit [5], across varying flow conditions, heater materials and coolant characteristics, where existing models and correlations only provide very limited applicability. Gilman and Baglietto [6] proposed an initial representation of boiling heat transfer mechanisms starting from the experimental measurements of Philips [7], indicating a dominant contribution of single-phase heat transfer mechanisms (forced agitation driven by bubble ebullition cycles and movement). Most importantly the work of Gilman indicated that the heat flux partitioning cannot be characterized by an a priori representation but must be dynamically determined by the complex interaction of the various micro-hydrodynamic mechanisms.

Figure 1: Experimental and MIT-Boil predictions for varying surface characteristics

The tight integration of the modeling work with the experimental effort has allowed expanding the reach of high-resolution measurements to quantify the contribution of the individual heat transfer components [8], confirming the initial postulations of Gilman and providing greater confidence in the potential of the approach. However, assembling a new modeling framework represented a massive undertaking, which necessarily relied on a tightly integrated experimental and modeling effort, to develop closure models that addressed the complete bubble life-cycle. In particular new models have been developed for: (1) the size and dynamics of the bubbles on the surface; (2) the amount of the liquid microlayer and dry area under each bubble; (3) the amount
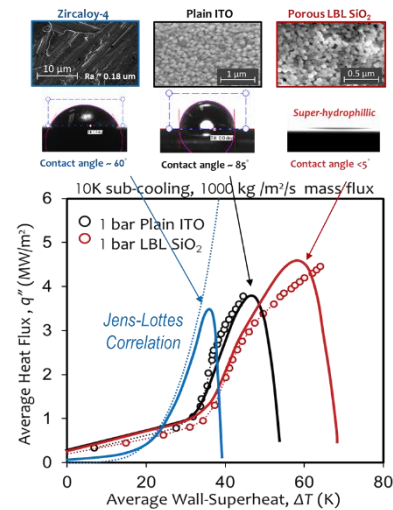
of surface area influenced by sliding bubbles; (4) the quenching of the boiling surface following bubble departure, and; (5) statistical bubble interactions on the surface. The resultant new mechanistic boiling heat transfer model is referred to as the MIT Boiling model. Kommajosyula [9] has consistently assessed the MIT boiling approach across the available Kennel, Jens & Lottes and Thom databases, demonstrating increased applicability across a broad range of conditions, and outperforming all correlations even on their own databases.

Most recently, the MIT-Boil model has been leveraged to re-evaluate the flow boiling experiments of R12 refrigerant DEBORA, demonstrating the greatly increased maturity of the M-CFD approach, while also identifying and ranking areas for future improvements. In parallel the models are currently being extended and evaluated for applicability to boiling simulations at high void fractions, up to critical heat flux, in support of CANDU reactor fuel analysis.

The generality of the MIT-Boil framework has recently supported launching an exciting new challenge, to support design and development of future in-space cryogenic storage and transfer systems, which are critical to the future NASA human missions beyond low earth orbit. While the MIT-Boil incorporates a fairly general framework for the meso-scale mechanistic models of boiling, its robust extension requires novel high-resolution information for cryogenic coolants across varying gravity conditions. To this end we have recently developed high-resolution, non-intrusive optical techniques and applied them in a special cryogenic facility both at earth and micro-gravity conditions, studying pool and flow boiling of LN2 (as a simulant for cryogenic fuels) at operating pressure (80 psi) and across different flow rates (including stagnant flow) in a parabolic flight campaign.

REFERENCES

1. Lahey Jr., R.T., Drew, D.A., 1992. On the development of multidimensional two-fluid models for vapor/liquid two-phase flows. Chem. Eng. Commun. 118 (1), 125–139.

2. E. Baglietto, E. Demarly, R. Kommajosyula, N. Lubchenko, B. Magolan and R. Sugrue, 2019 - A Second Generation Multiphase-CFD Framework Toward Predictive Modeling of DNB, Nuclear Technology, 205 (1-2), 1-22.

3. B. Magolan, E. Baglietto, 2019 - Assembling a bubble-induced turbulence model incorporating physical understanding from DNS, International Journal of Multiphase Flow, Volume 116, 185-202.

4. R. T Lahey Jr, E. Baglietto, I. A Bolotnov, 2021. Progress in multiphase computational fluid dynamics, Nuclear Engineering and Design 374, 111018.

5. E. Baglietto, E. Demarly, R. Kommajosyula, 2019 - Boiling Crisis as the Stability Limit to Wall Heat Partitioning, Applied Physics Letters, 114.

6. Gilman, L., Baglietto, E., 2017. A self-consistent, physics-based boiling heat transfer modeling framework for use in computational fluid dynamics. Int. J. Multiphase Flow 95, 35–53.

7. Phillips, B.A., 2014. Experimental Investigation of Subcooled Flow Boiling Using Synchronized High-Speed Video, Infrared Thermography, and Particle Image Velocimetry, PhD Thesis, Massachusetts Institute of Technology.

8. Richenderfer, A., Kossolapov, A., Seong, J.H., Saccone, G., Demarly, E., Kommajosyula, R., Baglietto, E., Buongiorno, J., Bucci, M., 2018. Investigation of subcooled flow boiling and CHF using high-resolution diagnostics. Exp. Thermal Fluid Sci. 99, 35–58.

9. Kommajosyula, R., 2020. "Development and assessment of a physics-based model for subcooled flow boiling with application to CFD", PhD Thesis, Massachusetts Institute of Technology.

Data-Driven Multiphase Flow Insight with Deep Learning

S. Balachandar

Department of Mechanical & Aerospace Engineering, University of Florida

Contact E-mail : bala1s@ufl.edu

Euler-Lagrange (EL) and Euler-Euler (EE) techniques have been widely employed for solving particle, droplet, and bubble-laden flows. Since flow around the individual particles is not resolved, the accuracy of the technique depends on the fidelity of the point-particle force laws used. The main focus of this talk is the use of emerging machine learning techniques along with physical insight into the averaging processes involved in the EL and EE techniques can yield closures that recover fully-resolved-like accuracy at orders of magnitude lower cost.

The standard EL approach has been limited to (i) particles of size much smaller than the grid-scale and (ii) dilute flows where inter-particle interaction is weak. We will discuss recent developments that begin to ease these limitations. As the grid size approaches the particle size, we face the unpleasant prospect of force law becoming less accurate due to the self-induced flow generated, which corrupts the estimation of undisturbed flow velocity. We will discuss theoretical approaches to properly correcting for the self-induced flow. We will also present the data-driven hierarchical interaction model which rigorously extends the point-particle technique to higher volume fractions. This model systematically accounts for the precise location of all the neighboring particles.

In this talk we will discuss the deep-learning framework pursued by our group as well as relevant research by other groups for the development of accurate multiphase closure models, with a summary on what seems possible in the future, and how the community can benefit from the data revolution.

Stability of two-phase stratified flows in circular pipes

I. Barmak[1], A. Gelfgat[1] and N. Brauner[1]

[1] School of Mechanical Engineering, Tel Aviv University, Tel Aviv 6997801, Israel
Contact E-mail: brauner@tauex.tau.ac.il

In this work, we investigate the linear stability of two-phase stratified flow in a circular pipe. For this purpose, we formulate the linearized 3D governing equations in each phase, coupled by the linearized boundary conditions at the pipe walls and the fluid-fluid interface. The problem is solved numerically in bipolar coordinates, in which the pipe walls and a fluid-fluid interface of constant curvature coincide with the coordinate lines. Previous studies on linear stability of two-phase stratified flow were formulated either in the framework of the simplified mechanistic Two-Fluid models or in the simpler two-plate geometry. However, due to those simplifications, the implications of circular pipe geometry on stability characteristics are still unknown.

In the stability analysis, the base flow, assumed laminar, steady, and fully developed, and the unperturbed fluid-fluid interface, assumed plane, are subject to three-dimensional perturbations of all wavenumbers propagating in the axial direction. The stability characteristics are validated by comparison with those we obtain independently using the well-established Immersed Boundary Method in Cartesian coordinates.
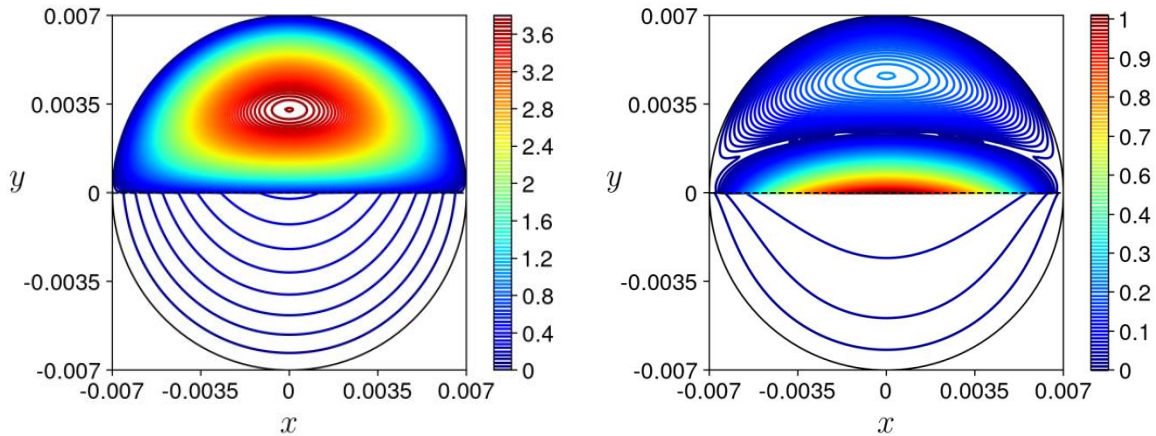
Figure 1. Air-water stratified flow in a horizontal pipe (of diameter 0.014m) for critically stable operational conditions (water/air flow rate and viscosity ratios are 0.07 and 55, respectively): (a) base flow velocity; (b) axial velocity of the critical perturbation.

The resulting stability boundaries, the critical perturbations that trigger flow instability and their patterns (e.g., Fig. 1) will be reported for gas-liquid and liquid-liquid stratified pipe flows of particular practical importance.

Interface-resolved Boiling Simulation in Complex Geometries for Machine-Learning Model Development

I.A. Bolotnov, A. Iskhakova and N.T. Dinh

North Carolina State University, USA
Contact E-mail: igor_bolotnov@ncsu.edu

Boiling phenomenon is one of the most challenging physics to simulate numerically at any resolution scale. Over the past decade there has been a significant effort at NC State to implement and validate the boiling simulation capabilities using interface capturing approach within highly scalable finite-element based flow solver, PHASTA. While the validated simulations at these resolutions are valuable addition to study complex two-phase flow phenomena, coarser modeling scales are more suitable for engineering applications. However, the coarse-grid simulation capabilities rely on sub-grid models which often have quite high uncertainties for many flow conditions. The objective of this work is to formulate and demonstrate a machine learning-based framework which will eventually lead to robust and fast physics-based capabilities to simulate two-phase boiling flows in complex geometries.

Level-set method is used in the PHASTA code for interface capturing simulations [1]. Evaporation/condensation algorithm has been implemented to couple the energy equation with mass/momentum conservation [2]. Using Bubble Tracking algorithm [3], average temperature gradient is collected for each bubble. With this, local heat flux across the interface is found as

$$q'' = -\left(\frac{R_0}{R_1}\right)^2 \cdot k_l \frac{\partial T}{\partial r},$$

where R_0 is the bubble radius, R_1 is the radius of temperature gradient collection shell [4], k_l is the liquid phase thermal conductivity. The performance of this algorithm has been verified against analytical bubble growth model [5] and validated against experimental data [6].

Recently, the predictive capabilities of Evaporation and condensation algorithm have been expanded to flow boiling [7]. As shown in Figure 1, multiple bubble nucleation is present in the vertical channel with fins. The code also showed a good performance with higher wall superheat values.

Figure 1. Example of flow boiling simulation in PHASTA [7]
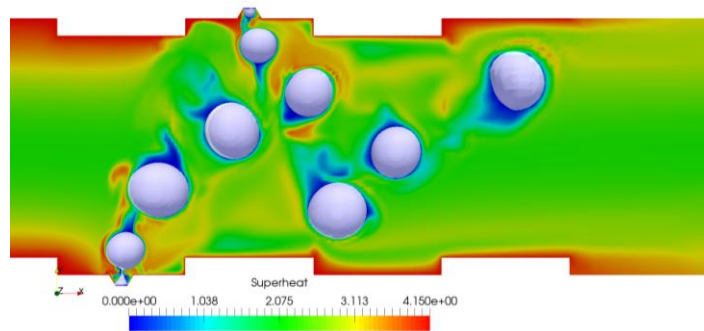
Full resolution simulation of nucleate boiling phenomenon is quite computationally expensive. Therefore, it is limited to smaller domain applications and relatively short time scales (e.g., tens of nucleation events per nucleation site). Those limitations can be relaxed if much coarser computational meshes can be used while maintaining the physical representation of the

phenomenon. Traditionally, these capabilities require sub-grid models to inform the unresolved physics in the solution process. In the presented framework, we demonstrate basic approach to utilize the machine-learning based models which are training on high-resolution simulations to provide appropriate closures for the coarse-grid simulation.

As an example, a coarse-grid solution can be informed by high-resolution data through machine-learning based training and validation process. The schematic of the proposed workflow is shown in Figure 2. For simplicity, a bubble rising in a stagnant fluid is considered. Local information on velocity and mesh size is set as inputs, whereas the difference (correction) between the high-fidelity data and inputs is defined as the output value. Once a reliable model performance is achieved, this correction term could be used on the fly in the coarse-grid solution.
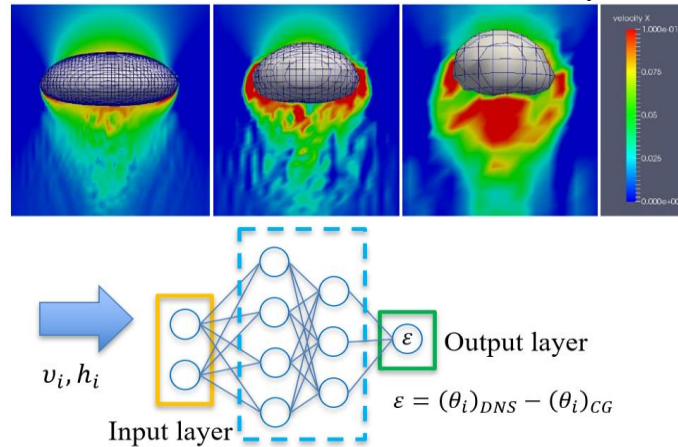
Figure 2. A workflow example of using high-res simulations for error correction of low-resolution simulations.

References

[1] M. Sussman, A. Almgren, J. Bell, P. Colella, L. Howell and M. Welcome, "An adaptive level set approach for incompressible two-phase flows," *Journal of Computational Physics,* pp. 81-124, 1999.

[2] M. Li and I. Bolotnov, "The evaporation and condensation model with interface tracking," *International Journal of Heat and Mass Transfer,* vol. 150, p. 119256, 2020.

[3] J. Fang and I. Bolotnov, "Bubble tracking analysis of PWR two-phase flow simulations based on the level set method," *Nuclear Engineering and Design,* vol. 323, pp. 68-77, 2017.

[4] M. Li and I. Bolotnov, "Interface Tracking Simulation of Phase-Change Phenomena: Boiling and Condensation Verification," in *ASME 2016 conference proceedings*, Washington, DC, July 10-14, 2016.

[5] L. Scriven, "On the Dynamics of Phase Growth," *Chem. Eng. Sci.,* vol. 10, no. 1-2, pp. 1-13, 1959.

[6] M. Li, "High Resolution Boiling Simulation Using Interafce Tracking Method," 2019.

[7] A. Iskhakova, Y. Kondo, K. Tanimoto, N. Dinh and I. Bolotnov, "High-Fidelity Flow Boiling Simulations in a Minichannel with Offset Strip Fins," in *Advances in Thermal Hydraulics*, Anaheim, CA, USA, 2022.

EAJTPFGM22
CHAMONIX
— FRANCE —

Simultaneous measurement of liquid film thickness and heat transfer during downflow condensation of R134a and R245fa inside a vertical minichannel

**S. Bortolin[1], A. Berto[1], P. Lavieille[2], M. Azzolin[1]
M. Miscevic[2] and D. Del Col[1]**

[1]University of Padova, Department of Industrial Engineering
Via Venezia 1, 35131 Padova, Italy
[2]Université Paul Sabatier, Laboratoire Plasma et Conversion d'Energie
118 Route de Narbonne, Bat3R1, 31062 Toulouse, France
Contact E-mail: stefano.bortolin@unipd.it

Simultaneous determination of heat transfer coefficient and liquid film thickness during annular flow condensation in small diameter channels is complex and very rare in the literature, although the availability of such experimental data is fundamental for better understanding the occurring physical mechanisms and for the design of compact heat exchangers. In the present work, heat transfer coefficient and liquid film thickness have been simultaneously measured during vertical downflow condensation inside a 3.38 mm diameter channel. Condensation tests have been run at mass flux between 30 kg m^{-2} s^{-1} and 150 kg m^{-2} s^{-1} with refrigerants R134a [1] and R245fa [2], respectively at 30 °C saturation temperature and 40 °C saturation temperature. These two fluids have been selected as they exhibit different values of vapor density (and thus of vapor velocity) at the considered test conditions.

The test section is composed of two heat transfer sectors connected with a glass tube. The glass tube has been realized with a special external shape that produces a magnification of the observed liquid film thickness and allows the use of a chromatic confocal sensor. The instantaneous liquid film thickness and interfacial waves are detected by combining two complementary optical methods: shadowgraph technique (applied to a sequence of flow pattern images recorded by a high speed camera, Figure 1) and chromatic confocal imaging (Figure 2).

The heat transfer coefficient of the tested fluids is found to increase with vapor quality and mass velocity, although the effect of the mass velocity becomes negligible for $G \leq 75$ kg m^{-2} s^{-1} in the case of R134a and for $G \leq 50$ kg m^{-2} s^{-1} in the case of R245fa. Flow pattern visualizations for both R134a and R245fa show that the flow is always annular with waves. Depending on the operating conditions, the vapor-liquid interface is characterized by the presence of high amplitude disturbance waves carrying a significant portion of the condensate and smaller wave structures rippling the liquid substrate. It is found that the appearance of high-amplitude waves and the resulting thinning of the liquid film between two consecutive disturbance waves enhance the heat transfer at $G = 90\text{-}100$ kg m^{-2} s^{-1} for R134a and at $G = 50\text{-}$

75 kg m^{-2} s^{-1} for R245fa. The inception of these waves can be predicted by the turbulent-wavy transition criterion developed by Azzolin et al. [3].

The experimental liquid film thickness data of the two tested fluids have been analysed in terms of mean and base thickness, waves frequency and waves velocity. In the case of R134a, the mean velocity of the disturbance waves, determined by cross correlation, is almost halved compared to R245fa. The film thickness values of R245fa are smaller compared to R134a due to the lower density of the vapor phase, which promotes the thinning of the film and the earlier formation of high amplitude waves. The mean and the base liquid film thickness is found to decrease with increasing mass velocity under the effect of vapor shear stress for $G \geq 75$ kg m^{-2} s^{-1} in the case of R134a and for $G \geq 50$ kg m^{-2} s^{-1} in the case of R245fa. Instead, an increase of the liquid film thickness has been observed when increasing the mass velocity from 30 kg m^{-2} s^{-1} to 50 kg m^{-2} s^{-1}: this trend is opposite to the one found at high mass velocity and it is due to the transition from shear stress-driven to gravity-driven downward flow condensation.

The accuracy of several well-known models for the prediction of heat transfer coefficient, film thickness and void fraction has been assessed with comparison to the experimental data of both R134a and R245fa.
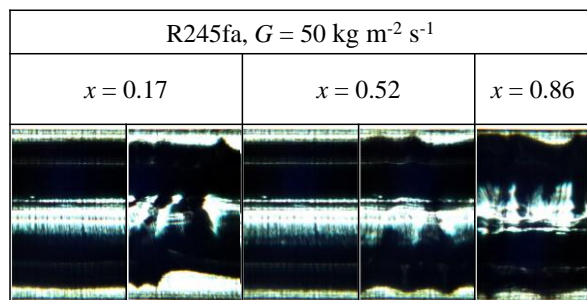
Figure 1. Flow visualizations of R245fa at mass velocity G equal to 50 kg m^{-2} s^{-1} and different vapor qualities x during condensation in vertical downflow inside a 3.38 mm diameter channel.
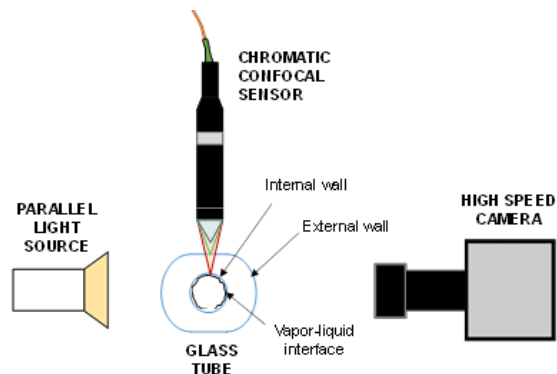
Figure 2. Sketch of the optical system for the measurement of the liquid film thickness consisting of a glass tube, a LED light source, a high-speed camera and a chromatic confocal sensor.

References

[1] Berto A., Lavieille P., Azzolin M., Bortolin S., Miscevic M., Del Col D. Film thickness, interfacial waviness and heat transfer during downflow condensation of R134a, Appl. Therm. Eng. 214 (2022), 118808, https://doi.org/10.1016/j.applthermaleng.2022.118808

[2] Berto A., Lavieille P., Azzolin M., Bortolin S., Miscevic M., Del Col D. Liquid film thickness and heat transfer measurements during downflow condensation inside a small diameter tube, Int. J. Multiph. Flow, 140 (2021), 103649, https://doi.org/10.1016/j.ijmultiphaseflow.2021.103649

[3] M. Azzolin, S. Bortolin, D. Del Col, Convective condensation at low mass flux: Effect of turbulence and tube orientation on the heat transfer, Int. J. Heat Mass Transf. 144 (2019), 118646, https://doi.org/10.1016/j.ijheatmasstransfer.2019.118646

Capturing Two-phase Flow beyond Steady States Using Periodic Oscillations Induced by Flow Instability

C.S. Brooks and T. Zhang

Department of Nuclear, Plasma, and Radiological Engineering,
University of Illinois at Urbana-Champaign,
104 South Wright Street, Urbana, IL 61801, USA
Contact E-mail: csbrooks@illinois.edu; taiyang2@illinois.edu

Measurement of transient two-phase flow can face challenges in collecting sufficient samples to extract macroscopic mean behaviors. Theoretically, those means are treated as continuous and differentiable functions of space and time, which are defined with a strong requirement of proper averaging operations smoothing microscopic fluctuations from inherent randomness and discontinuities across interfaces. In reality, limitations can however occur during a single realization of a fast transient where convergence criteria for specific instruments, such as a threshold of bubble counts for a conductivity probe, might only be met with a running-average window larger than the target time scale. Ensemble-averaging over many repetitions, which is often avoided and replaced by the long-term time-averaging during steady states treated as stationary ergodic processes, is still the legitimate approach to compensate this sampling insufficiency but at the potential cost of extra difficulty in reproducing transients.
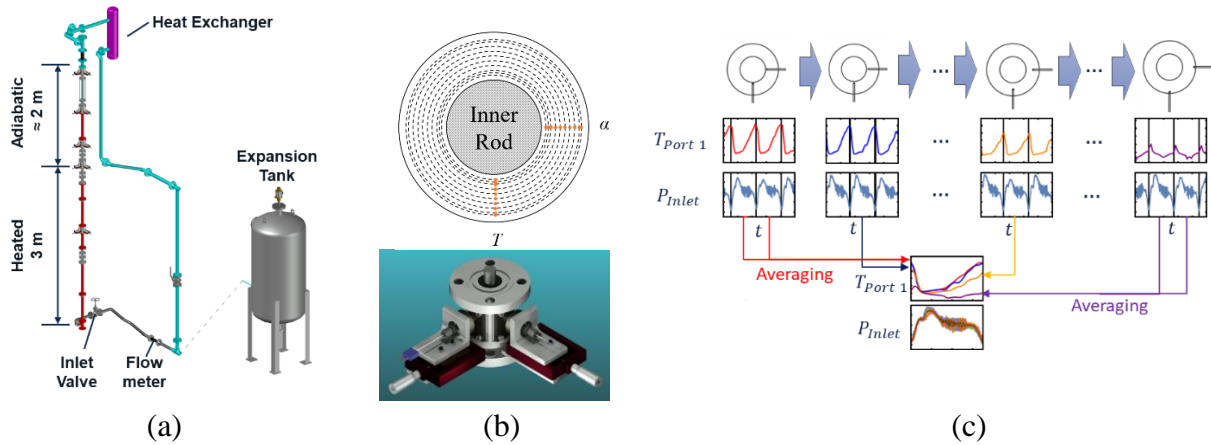
Figure 1. (a) Facility, (b) instrumentation port with probe traversing mechanisms, (c) measurement procedure and post-processing concepts for reconstructing a mean cycle by ensemble averaging.

The current work presents a practice and its methodology in capturing periodic two-phase flow naturally induced by flashing instability in low-pressure natural circulation. These conditions are encountered low-frequency limit cycle oscillations during stability tests of a 5-meter-tall single-channel loop, Fig.1(a). Five customized traversing mechanisms on its annular hot-leg allow scanning measurement points of thermocouples and four-sensor conductivity probes across the flow area, Fig.1(b). The empirical periodicity justifies the description of mean

flow using one representative cycle as the ensemble average over multiple cycles captured during a single test. Dedicated yet generalizable measurement procedures and post-processing concepts are correspondingly developed, Fig.1(c). One parameter with a clean waveform, such as the volumetric flow rate or pressure at the single-phase inlet, is continuously recorded as an "oscillation-phase indicator" based on whose signals the mean period is obtained and time stamps are extracted separating oscillation cycles. Based on these time stamps, other signals from different cycles, locations, and instruments are then aligned onto one representative cycle on which the ensemble averages are obtained.

Utilizing the periodicity, two-phase flows beyond steady states are captured with ensemble averages over many periods and with same spatial resolutions achievable under steady states (Fig, 2). For a typical conditions with a period around O(10s), over 100 cycles can be covered without significantly increasing experimental time cost. The steady-state local measurement strategy of traversing point-measurement instruments is still applicable, maintaining the 10-point radial resolution. Conductivity probes with a running-sampling-window around only 1s can register sufficient bubbles to calculate local mean void fraction with clean waveforms by accumulating signals over more than 10 realizations. The stability tests therefore produce a comprehensive dataset covering more than 150 conditions including stable steady states, stability boundaries, and periodic mean two-phase flow with rich transient phenomena induced by the flashing instability.

This practice contributes experience in practically collecting two-phase flow dataset beyond steady states, generates a benchmark for simulation codes with naturally induced transient phase-change phenomena, and provides valuable materials for further investigation on the performance and requirements of conductivity probes for transient measurements.
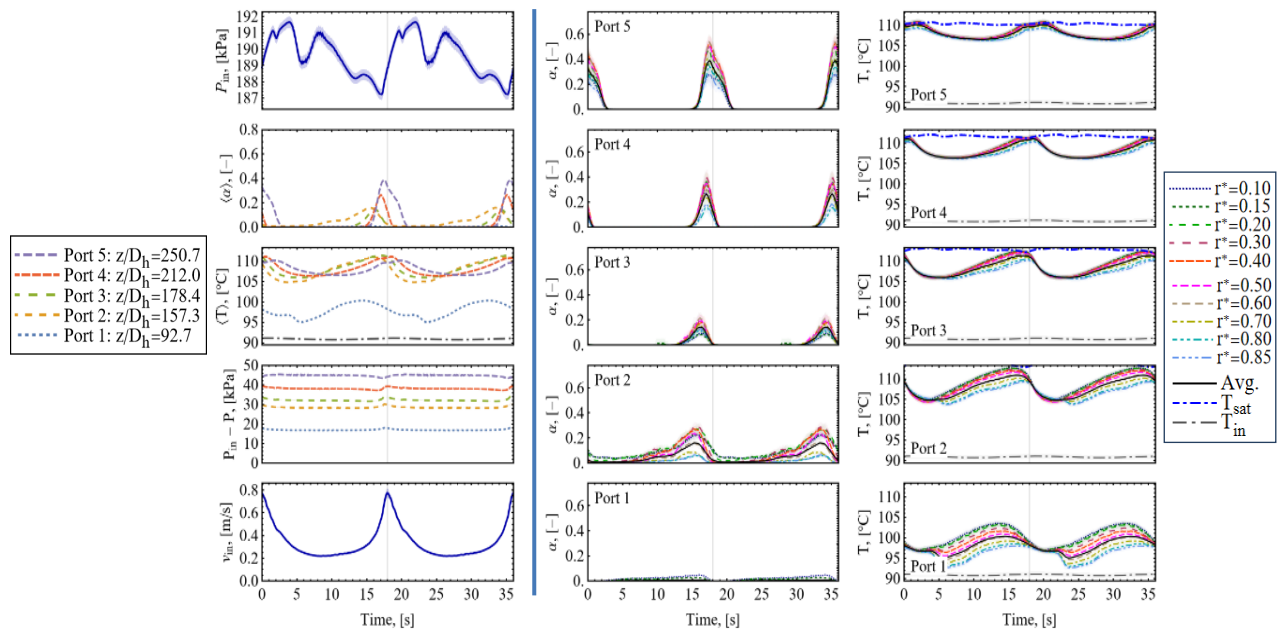

Figure 2. An example of captured mean behaviors of periodic two-phase flow.
Colors represent measurements at different axial or radial locations and the shades represent uncertainty. Left: area-averaged quantities. Right: local void fraction and temperature.

Subgrid-scale models for turbulent particle-laden flows from dilute to dense regimes

J. Capecelatro[1], M. Herzog[1], A. Lattanzi[2], and S. Subramaniam[3]

[1]University of Michigan, [2]Berkeley Lab, [3]Iowa State University
Contact E-mail : jcaps@umich.edu

Particle dynamics in turbulent flows are complex and involve significant interaction between scales. In the dilute limit, particles may respond to length and time scales present within an intrinsically turbulent flow. At higher concentrations, particles may respond to wakes generated by neighboring particles (see Fig. 1). The velocity fluctuations inherent to the former characterizes turbulent kinetic energy (TKE), while the latter gives rise to so-called pseudo-turbulent kinetic energy (PTKE). In the context of large-eddy simulation (LES) and Reynolds-averaged Navier–Stokes (RANS), models are needed to account for subgrid-scale (SGS) fluid velocity fluctuations (TKE or PTKE) on particle dispersion.

Stochastic models are commonly employed for dilute particle-laden flows but are far less established for dense suspensions that exhibit PTKE. Despite their pervasive application, existing stochastic models are incapable of capturing the correct instantaneous spatial distribution of particles (e.g., preferential concentration). So-called structural SGS models aim to capture two-point particle statistics through reconstruction of the fluid velocity field. Such examples include approximate deconvolution, fractal and spectrally optimized interpolation, and stochastic vortex structure models. However, such approaches are limited in their ability to accurately reconstruct SGS motion and remain relatively unexplored [1]. Marchioli (2017) [1] notes that an ideal SGS model would combine the strengths of structural and stochastic models, allowing for accurate predicting of one-point and two-point statistical moments and geometric particle dispersion. Here, we propose a stochastic model for PTKE and present a spatially correlated stochastic model capable of predicting one-point and two-point statistics.

We first introduce a system of Langevin equations that form a hierarchy in terms of the physics they can resolve [2]. Two canonical flow configurations are then considered: (i) flow through dense homogeneous suspensions of particles (PTKE-driven homogeneous heating/cooling) and (ii) the classical situation of a dilute concentration of inertial particles in homogeneous isotropic turbulence (TKE). In the former case, we employ a force Langevin model to describe neighbor-induced hydrodynamic interactions, as shown in Fig. 1. The inclusion of a fluctuating drag force, modeled as an Ornstein-Uhlenbeck (OU) process, allows for accurate predictions of granular temperature evolution.
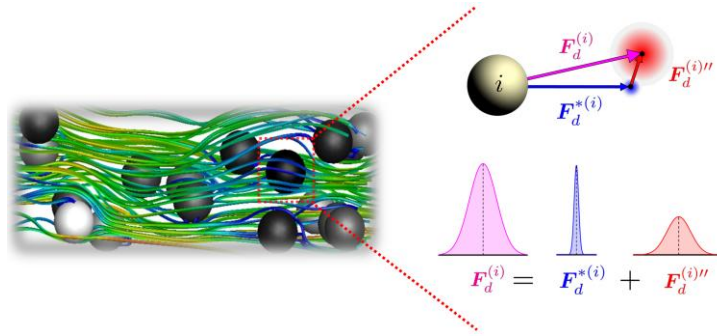
Figure 1. Neighboring particles disturb the local flow field within a particle-laden suspension, leading to variation in drag. A statistical description is adopted for the drag on an individual particle that allows specification of higher-order statistics.

In the latter case, particles spontaneously cluster due to non-linear interactions with carrier-phase turbulence. We present a new framework that embeds two-point statistics into the stochastic increment of the fluid velocity "seen" by a particle. A covariance matrix is assembled using particle-pair information that is readily available in LES and RANS. Decomposition of this covariance matrix allows for it to be applied in the OU process, transforming the independent random increments into spatially correlated random increments. The construction and decomposition of the covariance matrix presents several challenges, as its size scales with the number of particles. Because the two-point statistics decay rapidly with particle pair separation, the covariance matrix is sparse. We explore methods for exploiting the sparsity to allow for an efficient implementation in LES and RANS.

References

[1] Marchioli, C., Large-eddy simulation of turbulent dispersed flows: A review of modelling approaches, *Acta Mech*anica **228** (3), pp. 741-771, 2017.
[2] Lattanzi, A. M., Tavanashad, V., Subramaniam, S., & Capecelatro, J., Stochastic models for capturing dispersion in particle-laden flows. *Journal of Fluid Mechanics* **903**.

Cavitation Inception, Development, and Noise Emissions Due to the Interaction of a Pair of Line Vortices

D. Knister, H. Ganesh, S. L. Ceccio

University of Michigan

Contact E-mail : ceccio@umich.edu

Hydrodynamic cavitation commonly occurs on objects of naval interest. In many cases, the flows around lifting surfaces on a ship are most prone to cavitation. The flow over and in the wake of lifting surfaces typically contain a range of concentrated vortical structures with varying size, strength, and orientation. The cores of single liquid vortices can develop reduced pressures (and even liquid tensions) that can lead to the formation of cavitation bubbles. The interaction of multiple vortices can also lead to cavitation inception, and it is often the case that the strongest vortices (*e.g.* the vortices with the highest circulation) do not cavitate first. Rather, the interaction between multiple vortices can lead to instabilities and vortex stretching, where the weaker vortices are stretched by stronger vortices and develop significant transient pressure reductions, leading to inception in these weaker vortices.

To understand this phenomenon, a canonical flow of two counter rotating vortices undergoing a Crow instability is examined experimentally. Volumetric velocimetry measurements are obtained *via* Shake-the-Box Particle Tracking Velocimetry. After demonstrating Reynolds number independence over a range of conditions, these measurements are then used for estimation of core pressures in the vortices as well as quantification of stretching in the vortical cores. The measurements demonstrate that, at least for the flows considered, the steady low pressure due to the presence of a vortex is important, but the unsteady pressure drop associated with stretching in the vortex is critical for the weaker vortex to see pressures low enough to lead to inception.

The velocimetry measurements allow us to determine the distribution of transient minimum pressures achieved within the vortex cores in relationship to the kinematics of the flow field. The freestream cavitation nuclei distribution is independently measured with a Cavitation Susceptibility Meter. These data, combined with the distribution of known pressure transients, are used to predict the rate of discrete cavitation events and compared to the observed rates of bubble creation.

The acoustic emission of the incipient cavitation bubbles is also measured, and we show how the characteristic noise pulses created by cavitation events are related to both the underlaying vortex dynamics coupled with the critical pressure of the incepting nuclei and the bubble/vortex interactions.
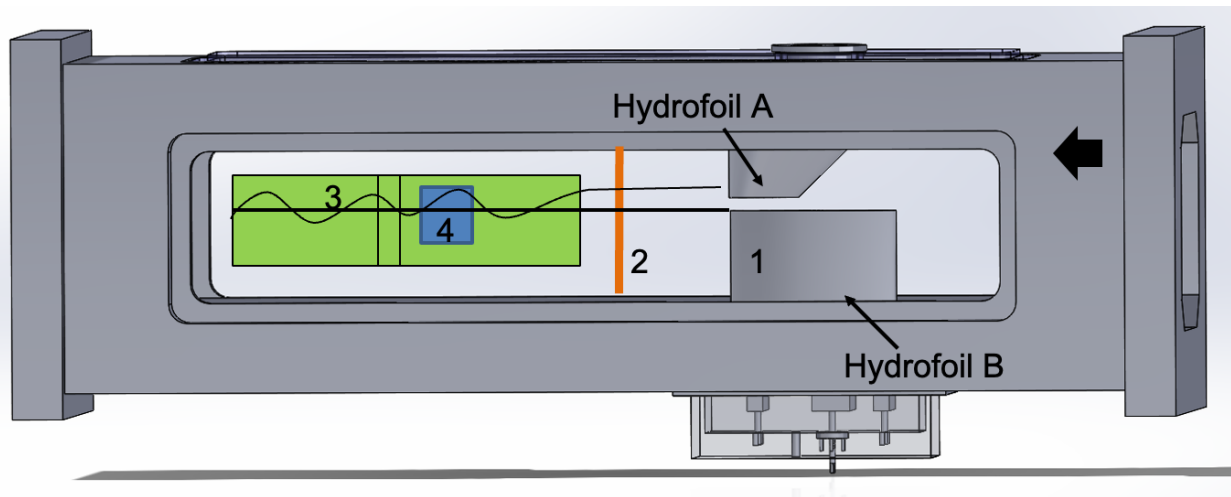

Figure 1. Experimental setup to generate pairs of stretched vortices; (1) pair of vortices generated by hydrofoils; (2) stereo PIV taken in transverse plane; (3) high speed videos; (4) Volumetric PIV interrogation volume
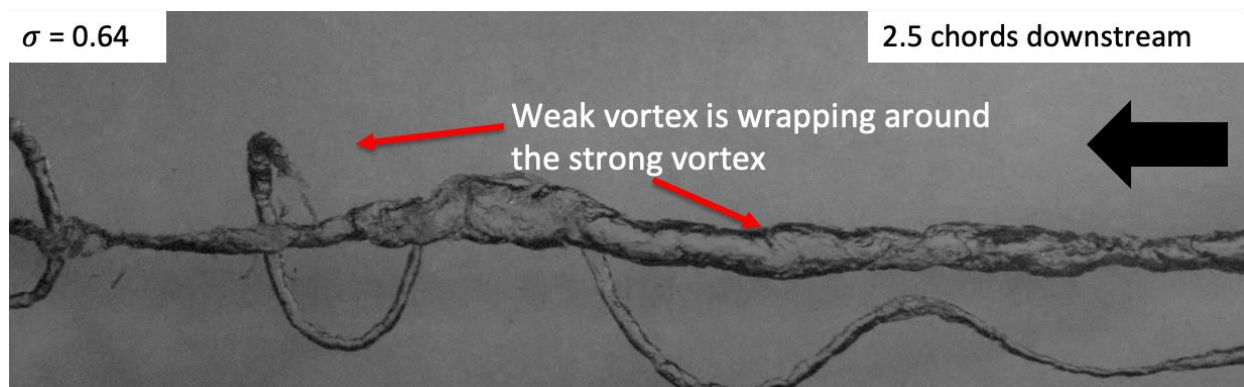

Figure 2. Example image of developed cavitation in the counter-rotating vortex pair.

Role of solid and soft particles in tuning microfluidic dripping to jetting transitions

L. Chagot, S. Migliozzi and P. Angeli

ThAMeS: The Advanced Multiphase Systems, UCL

Chemical Engineering Department, UCL, London, WC1E 7JE, UK

Contact E-mail : l.chagot@ucl.ac.uk

Colloids are rapidly emerging as alternatives to surfactants to stabilize droplets (Deshmukh et al. (2015), Ridel et al. (2016)) and control the transition regimes.

For classic surface-active agents as SDS, CTAB or TX100, recent studies (Roumpea et al. (2018), Kalli and Angeli (2022)), show that the transition to different microfluidic regimes for droplet generation is modified by the surfactant concentration due to the development of an uneven Marangoni stress along the droplet neck during the formation process (Kalli and Angeli (2022), Antonopoulos et al. (2021)).

Although many studies focused on the role of colloid concentrations and attributes on the final properties of stabilized emulsions (i.e. Pickering/mickering emulsions) (Chevalier and Bolzinger (2013), Fernandez-Rodriguez et al. (2021)), most of them ignore the microfabrication aspect, and nothing is known on the effect of solid or soft particles in altering the regime transitions in microfluidic droplet formation.

In this study, the transition between the dripping and the jetting regime (Fig. 1), in absence of Marangoni stresses, is investigated for microdroplets generated in a microchannel. This work is part of the EPSRC Programme Grant PREMIERE, and aims to improve the droplet control in both lab and industrial processes.
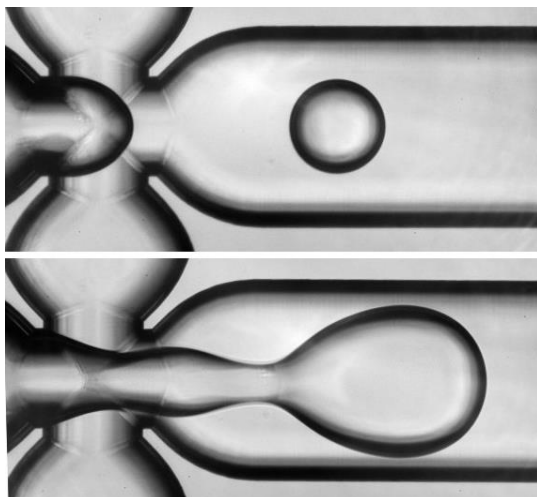

Figure 1 Example of dripping regime (top) and jetting regime (bottom) for pure water droplets generated in dodecane.
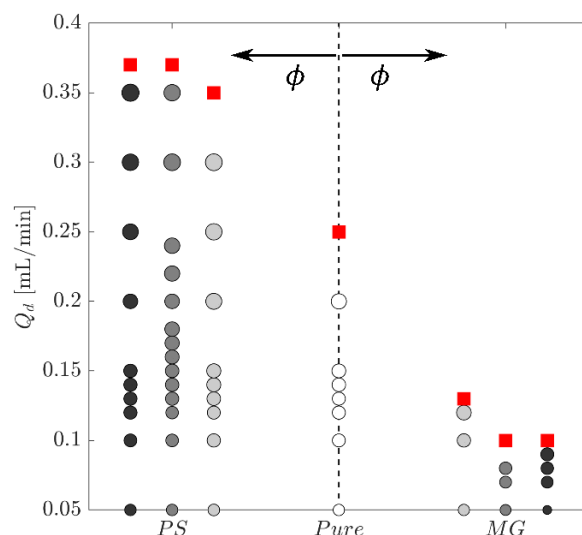

Figure 2 Evolution of the droplet size and the transition between dripping/jetting (red squares) for different particles (PS) and microgels (MG) concentrations at Q_c=0.6mL/min. The size of the circles are directly correlated to the size of the droplets.

Experimental investigations were conducted by using as droplet phase pure water containing solid polystyrene particles (380nm) or soft Poly(N-isopropylacrylamide)(PNIPAM) microgels (330nm) and dodecane as outer phase. Droplets were generated in a flow-focusing glass microchannel at different colloid concentrations ϕ. For different concentrations, the transition regime between dripping and jetting was studied and compared to the pure case ($\phi = 0$). Droplets were illuminated via a LED light and the ultra-fast process of droplet formation was tracked in space and time through a 12 bit high-speed camera (1280×800 pixels), equipped with a 20× microscope lens.

Results show while a high concentration of microgels triggers the transition to the jetting regime at lower flow rates, a high concentration of solid particles shifts the transition to higher flow rates compared to the particle-free case (Fig. 2). Therefore, both solid and soft particles can be used to control the transitions between drop formation regimes in microchannels.

References:

Antonopoulou, E., Harlen, O. G., Rump, M., Segers, T., & Walkley, M. A. (2021). Effect of surfactants on jet break-up in drop-on-demand inkjet printing. *Physics of fluids*, *33*(7), 072112.

Chevalier, Y., & Bolzinger, M. A. (2013). Emulsions stabilized with solid nanoparticles: Pickering emulsions. *Colloids and Surfaces A: Physicochemical and Engineering Aspects*, *439*, 23-34.

Deshmukh, O. S., van den Ende, D., Stuart, M. C., Mugele, F., & Duits, M. H. (2015). Hard and soft colloids at fluid interfaces: Adsorption, interactions, assembly & rheology. *Advances in colloid and interface science*, *222*, 215-227.

Fernandez-Rodriguez, M. A., Martín-Molina, A., & Maldonado-Valderrama, J. (2021). Microgels at interfaces, from mickering emulsions to flat interfaces and back. *Advances in colloid and interface science*, *288*, 102350.

Kalli, M., Chagot, L., & Angeli, P. (2022). Comparison of surfactant mass transfer with drop formation times from dynamic interfacial tension measurements in microchannels. *Journal of Colloid and Interface Science*, *605*, 204-213.

Kalli, M., & Angeli, P. (2022). Effect of surfactants on drop formation flow patterns in a flow-focusing microchannel. *Chemical Engineering Science*, *253*, 117517.

Ridel, L., Bolzinger, M. A., Gilon-Delepine, N., Dugas, P. Y., & Chevalier, Y. (2016). Pickering emulsions stabilized by charged nanoparticles. *Soft Matter*, *12*(36), 7564-7576.

Roumpea, E., Kovalchuk, N. M., Chinaud, M., Nowak, E., Simmons, M. J., & Angeli, P. (2019). Experimental studies on droplet formation in a flow-focusing microchannel in the presence of surfactants. *Chemical Engineering Science*, *195*, 507-518.

Hybrid quadrature moment methods for polydisperse cavitating flows.

T. Colonius[1] and S. Bryngelson[2]

[1]California Institute of Technology, [2]Georgia Institute of Technology
Contact E-mail : colonius@caltech.edu

Traditional engineering approaches to cavitating flows include, most prominently, homogeneous models that represent a mixture of liquid and vapor with a volume fraction and need to be supplemented with *ad hoc* source terms representing phase change. Rigorous, interface-resolving approaches, have, on the other hand, seen rapid progress in the past decades, but resolution requirements preclude their use for many applications. Bubbly flow models are an attractive alternative when cavitation forms numerous well-separated and primarily spherical bubbles. Both Lagrangian [1] (volume-averaged) and Eulerian [2] (ensemble phase-averaged) approaches have been proposed, and these require meso-scale closures for the dynamics of individual bubbles. The Lagrangian approach is deterministic in nature, in the sense that bubbles are sampled from a distribution for each simulation. As bubble nucleation is generally thought of as a stochastic process, this means that an ensemble of these simulations is required to fully characterize the flow. The Eulerian approaches are stochastic in nature and can be directly solved for the statistics of the flow, but, most generally, they require the evolution of a high-dimensional population balance equation (PBE) whose independent variables include all bubble-dynamic variables required for the mesoscale closure.

To reduce the computational burden, Eulerian modes up to now have been restricted to assuming that the only the bubble equilibrium radius (nuclei size) is a random variable. In this presentation, our recent development of a more general approach where the PBE is solved efficiently using quadrature method of moments (QMOM). The bubble radius, and bubble radial velocity are treated as random variables, in addition to the equilibrium radius. Figure 1 shows how the model works. The PBE is discretized via quadrature, and a set of moments is evolved with the flow. The abscissae (nodes) and weights are adaptive and efficiently obtained by inverting the moments. The quadrature is then able to estimate additional moments (beyond those carried by the PBE) that are required for closure of the flow equations. In particular, we use conditional, hyperbolicity preserving (CHyQMOM) approach [3], which is computational favorable when there are multiple independent variables.

We show [4] that with just two quadrature points for the bubble radius and radial velocity, this method can track the evolving statistics of modestly nonlinear bubble dynamics with reasonable accuracy at long times and at low cost. For highly nonlinear bubble dynamics, more quadrature points are needed, but, as is common in QMOM models, numerical instabilities can occur when increasing the set of carried moments. To address this problem, we hybridizing the QBMM with recurrent neural networks and realizability constraints [5]. Specifically, long short-term memory recurrent neural networks (LSTM RNNs) are trained on Monte Carlo truth data. They correct the baseline placement of quadrature points in the bubble dynamic phase space and introduce additional quadrature points where appropriate to decrease model-form errors in significantly non-Gaussian regimes. This approach decreased the relative moment errors by at least a factor

of ten. Finally, we will discuss generalizations of this model needed to address generic, polydisperse cavitating flows.
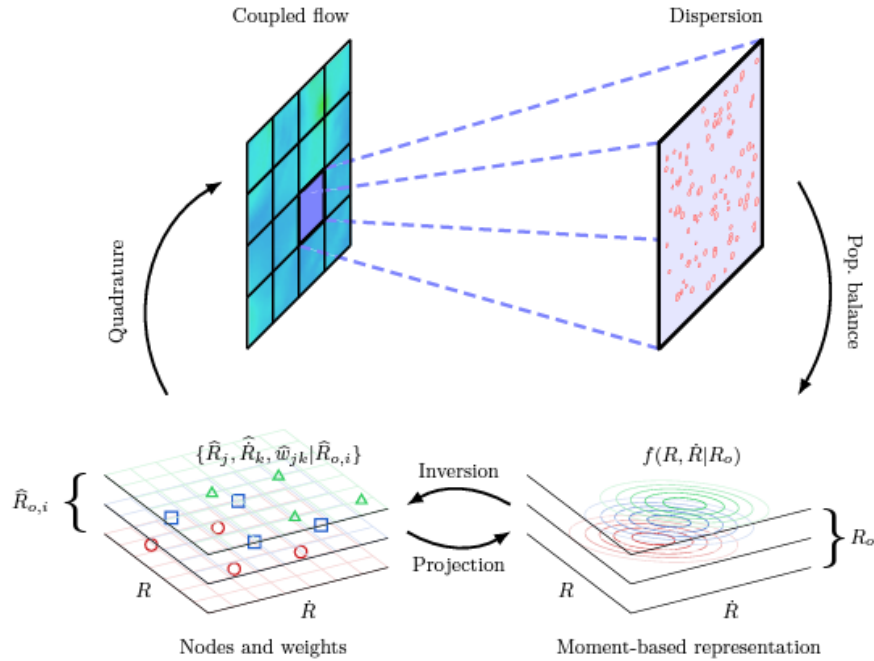

Figure 1. Illustration of the quadrature-based moment method for a fully coupled bubbly flow.

References

1. van Wijngaarden, L. (1968) On the equations of motion for mixtures of liquid and gas bubbles, *J. Fluid Mech.* 33, 465–474.
2. Zhang, D. Z., & Prosperetti, A. (1994) Ensemble phase- averaged equations for bubbly flows. *Physics of Fluids*, *6*(9), 2956-2970.
3. Patel, R. G., Desjardins, O., & Fox, R. O. (2019) Three-dimensional conditional hyperbolic quadrature method of moments. *Journal of Computational Physics: X*, *1*, 100006.
4. Bryngelson, S. H., Fox, R. O., & Colonius, T. (2021) Conditional moment methods for polydisperse cavitating flows. arXiv: 2112.14172.
5. Bryngelson, S. H., Charalampopoulos, A., Sapsis, T. P., & Colonius, T. (2020) A Gaussian moment method and its augmentation via LSTM recurrent neural networks for the statistics of cavitating bubble populations. *International Journal of Multiphase Flow*, *127*, 103262.

High-Fidelity Multi-Scale Modeling Framework for Predicting Turbulent Spray Atomization

A. Han, L. Vu, and O. Desjardins

Sibley School of Mechanical and Aerospace Engineering, Cornell University
Contact E-mail : olivier.desjardins@cornell.edu

The high-fidelity computational prediction of turbulent liquid atomization presents enormous challenges, in part because of the wide range of length and time scales involved in the spray break-up process. While direct numerical simulation (DNS) approaches have been increasingly applied to the study of liquid-gas flows in recent years, their computational cost is typically too large to enable the prediction of spray properties such as drop size distribution, especially under flow conditions relevant to most engineering applications. Of course, large-eddy simulation (LES) approaches, even with high resolution, have the potential to be much cheaper than DNS, yet their application to liquid atomization has remained difficult due to the lack of model closures.

Whether considering DNS or high-resolution LES of liquid atomization, a key difficulty consists in ensuring that the outcome of break-up events is mesh-independent, since the shrinking length scales that emerge during break-up cannot be formally resolved on a fixed grid. In this work, we propose to tackle this challenge with a novel multi-scale modeling framework wherein topology change events are explicitly modeled. To that end, we first recognize that if the simulation resolves scales below the Kolmogorov–Hinze scale – where turbulent inertia and surface tension are in balance – it can be expected that only surface tension-dominated interfacial structures will subsist at the sub-grid scale: these consist of metastable interface topologies such as sheets, ligaments, and droplets, as illustrated in Fig. 1. Consequently, we augment an unsplit geometric volume-of-fluid (VOF) scheme with R2P, a two-plane interface reconstruction method that outperforms the classical PLIC method by allowing for conservative sub-grid scale tracking of simple topologies like sheets and ligaments. A connected component labeling algorithm analyses the Eulerian field on the fly and identifies sheets and ligaments as Lagrangian objects, which can then be fed as input to various physics-informed break-up models. Several options for such break-up model are discussed.

Even setting aside the multi-scale challenge of break-up itself, the atomizing flow spans a wide range of length and time scales. In this work, multiple computational domains are interfaced, with each domain tackling a different length scale of the spray atomization problem. Upstream, we simulate the internal gas flow of the nozzle using a single-phase LES. This

generates the gas inflow conditions for a VOF LES of the spray formation region, where our sub-grid scale break-up model generates Lagrangian droplets which are then evolved in an Euler-Lagrange LES performed on a much larger domain, wherein turbulent spray dispersion is simulated. As illustrated in Fig. 2, we demonstrate the effectiveness of the methodology by comparing a simulation of turbulent airblast atomization to experimental data such as effective liquid path length, liquid core length, flapping frequency, but also droplet size distribution, showing favorable agreement for all metrics.
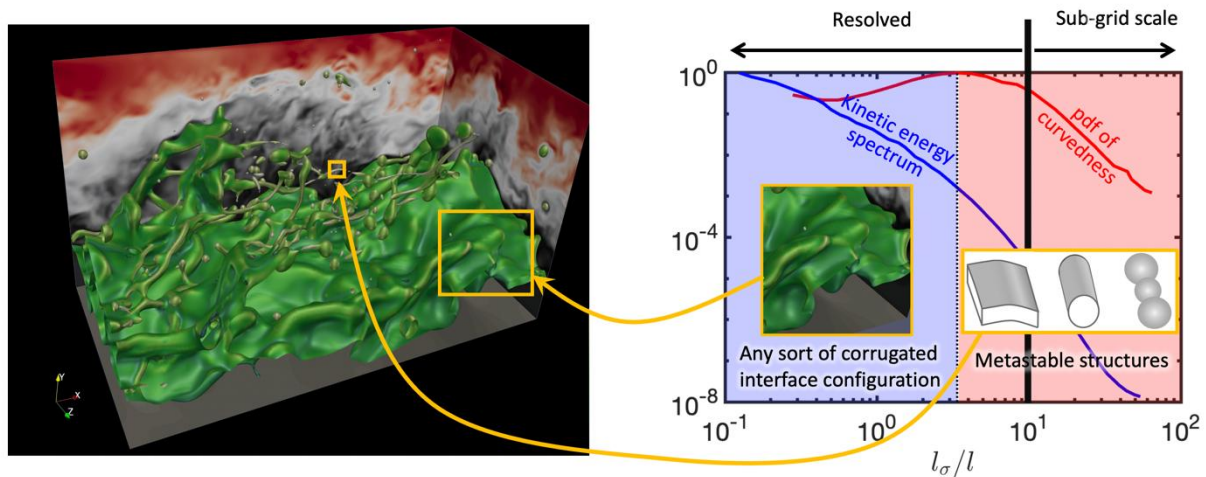

Figure 1. Sample turbulent atomizing liquid-gas flow on the left, and illustration of the dependence of interfacial topology on length scale on the right. Interfacial scales larger than the Kolmogorov–Hinze scale l_σ exhibit complex corrugations due to turbulence. Below l_σ, surface tension dominates leading to flat surfaces, sheets, ligaments, and spheroids.
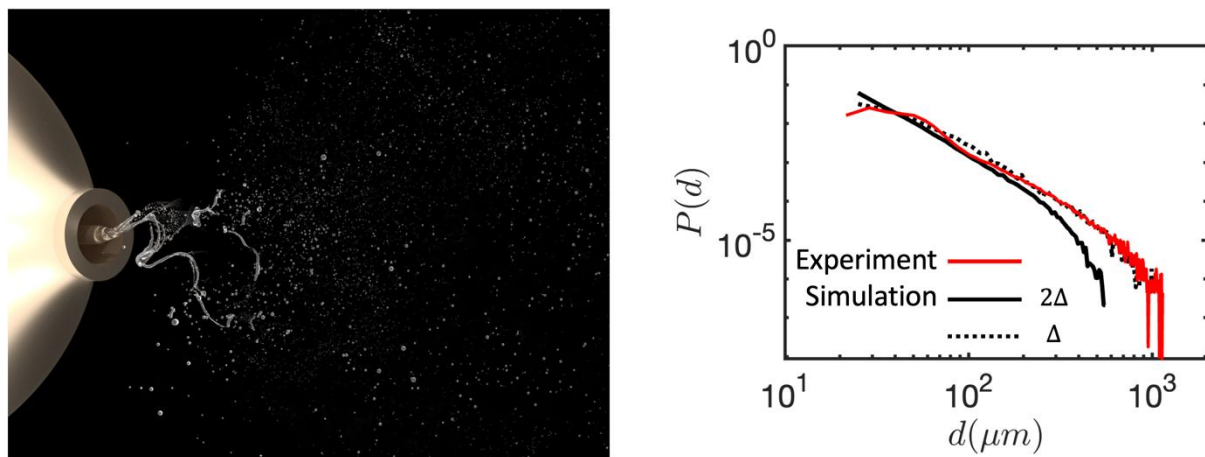

Figure 2. Snapshot of multi-scale LES of turbulent airblast atomization on the left. Validation of droplet size distribution predictions against experiments by A. Aliseda and N. Macchicoane at University of Washington are shown on the right.

Active and Passive techniques for enhancing pool boling in normal and reduced gravity

Paolo Di Marco, Alekos I. Garivalis

[1]DESTEC, University of Pisa, Largo L. Lazzarino 1, 56122 Pisa, Italy
Contact E-mail : p.dimarco@ing.unipi.it

Introduction

Pool boiling heat transfer is one of the most effective ways to remove heat available nowadays – excluding forced convection. Buoyancy force, driven by gravity, is recognized as one of the external actions that contribute most to the bubble detachment and vapor removal from the wall region. Thus, in microgravity conditions, the boiling process changes. As described by Straub, primary mechanisms of boiling occur at the microscale level close to the heated surface and are weakly dependent on gravity, while secondary, far-heater, mechanisms include the bubble removal and are mainly driven by gravity. Recently, efforts were done with engineered surfaces, and the use of micropillars showed enhancement in heat transfer coefficients and Critical Heat Flux. Even if the role of the engineered surfaces on the enhancement is still debated, it is expected to be independent on gravity, as relies on capillary forces. One aim of this study is to verify this experimentally; the second aim is to use an electric field to introduce an external action capable to remove vapor from the boiling region, in behalf of gravity force. The experiments conducted during parabolic flights will clarify the role of the structures and electric field in boiling enhancement with potential applications for space devices.
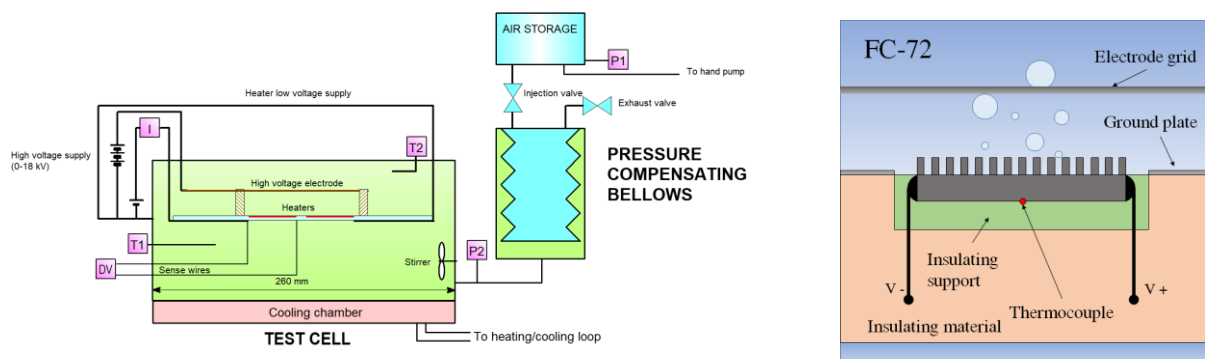

Figure 1. Experimental apparatus and test section (PF 73 and 78)

Experimental apparatus

The experimental apparatus (see Fig. 1) allows to perform pool boiling experiments during parabolic flights. It consists of a test cell with a volume of 2.3 litres, filled with FC-72 (saturation temperature at 1 bar is 56.6 °C). The pressure and temperature of the liquid can be adjusted by means of dedicated subsystems. The test section consists of a 10 mm x 10 mm, electrically-heated, silicon chip, and the boiling process occurs on its top (see Figure 1). Microstructures of different sizes are etched on the surface exposed to the fluid. The heat provided by the DC power supply (ELC ALR3206D) through the two copper wires soldered at

the chip sides is transferred almost entirely to the liquid: heat losses less than 5% have been estimated. The heat flux is calculated by measuring the voltage and current through the heater and dividing by its surface; a temperature sensor (thermocouple or PT-100) is placed below the heater in the middle and provides the temperature of the surface - as the Biot number is small, a small difference of temperature occurs in the silicon. To generate the electric field in the boiling region, a stainless steel grid is placed at 6 mm from the surface; a steel plate covers the surface to ensure grounding. A DC voltage of 15 kV was applied between the grid and the ground. Results were collected during three ESA parabolic flight campaigns (PF71, PF78 and PF78) with microstructures of different size and different subcooling degrees.

Results and discussion

Due to the limited space, only CHF enhancement results are summarized herein in Figure 2.

It can be noted that the overall CHF enhancement is always superior in microgravity conditions, but the effect of microstructures alone is reduced in microgravity. In fact, by breaking the large bubble hovering over the heated surface, the electric field transforms the bubble dynamics, restoring the one observed on Earth. This allows the microstructures to work more efficiently, i.e., there is a synergistic effect. This is confirmed by visualizations of boiling patterns, and suggests that substantial increase of boiling performance in microgravity conditions relies on improvement of far-heater boiling patterns.

It is worth noting that the enhancement encountered in PF73 and 78 is less than the surface increase due to the microstructures, while in PF71 it was greater. This leaves room to optimization of the micropillar structure and size, to be performed in the future.
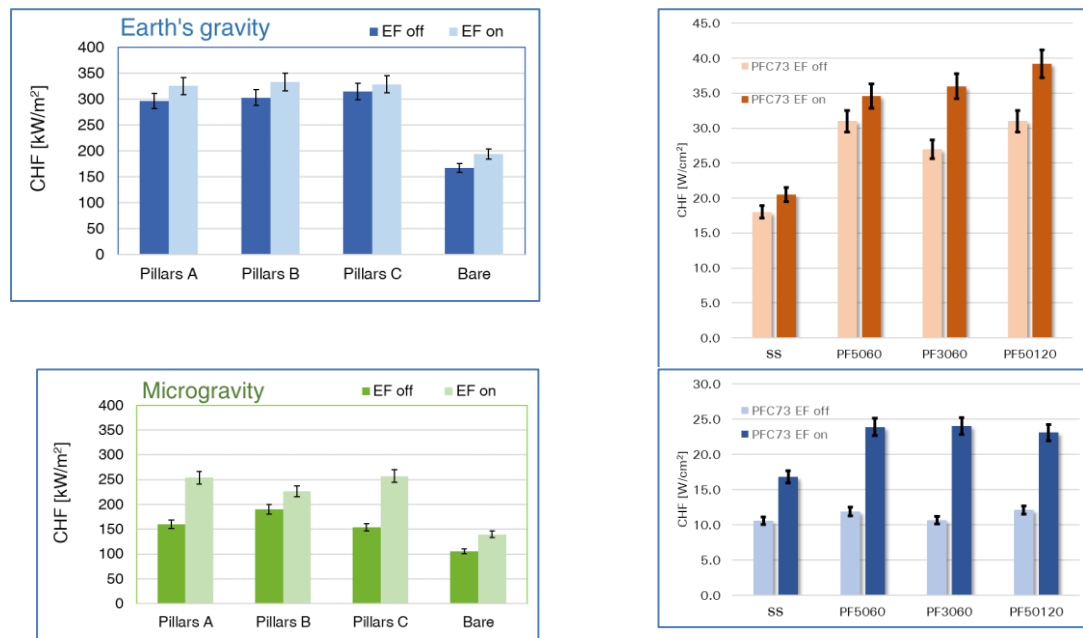

Figure 2. CHF values, PF71 (left) and PF 73 (right);
upper row: Earth results; bottom row, microgravity results.

Spherical Re-entrant Cavities for Pool Boiling Enhancement

A. Elkholy, J. McArdle, R. Kempers

Department of Mechanical Engineering, York University, Toronto, Canada
Contact E-mail : kempers@yorku.ca

Many studies have used re-entrant features to enhance the boiling heat transfer coefficient (HTC) due to its ability to provide stable bubble nucleation sites, even at low heat fluxes. However, the re-entrant features implemented in previous studies consisted of 2D-shaped channels or grooves, not cavities. In the current work, laser powder bed fusion (L-PBF) was employed to additively manufacture 3D spherical re-entrant cavities from AlSi10Mg which could not be produced via conventional machining methods.

The boiling surfaces are shown in Fig. 1 and consists of a uniform pattern of spherical re-entrant cavities with pore diameters ranging from 0.4 to 0.8 mm, cavity diameters from 1.5 to 2.5 mm, and spacings between 2.4 to 3.25 mm. All the experiments were performed with ethanol and Novec 7100 at saturated conditions.
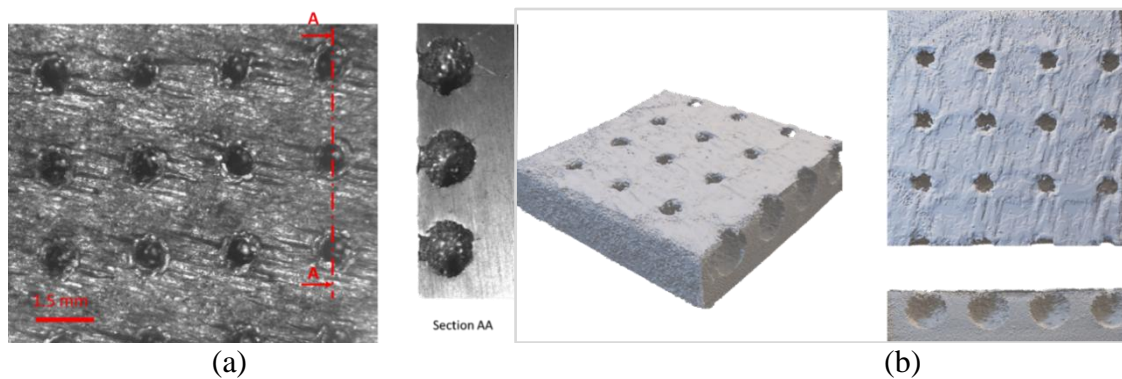
Figure 1: a) Microscopic photos for the boiling sample with re-entrant cavities., b) 3D reconstructed geometry the re-entrant cavities using µCT imaging

A high-accuracy pool boiling facility recently constructed at York University (Fig. 2) was used to characterize the boiling performance of these surfaces. This apparatus is unique in that it was designed to support the characterization of relatively large boiling surfaces (30 x 30 mm) to allow for the investigation larger scale arrays of features.

Figure 2 (a) Cross-sectional view of the boiling vessel, b) top-side accessories, c) heating system

High-speed imaging was used to characterized bubble grown and departure. Compared to a solid bare surface, the re-entrant cavities yielded more nucleation sites which were organized and yielded roughly equal sized bubbles as shown in Fig. 3.
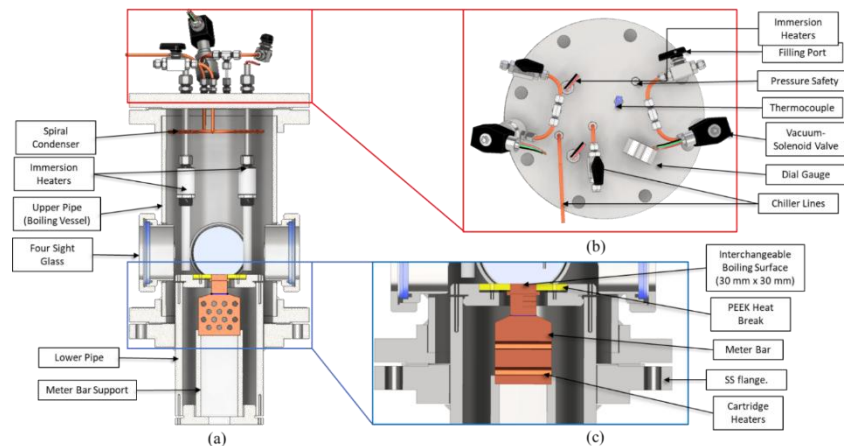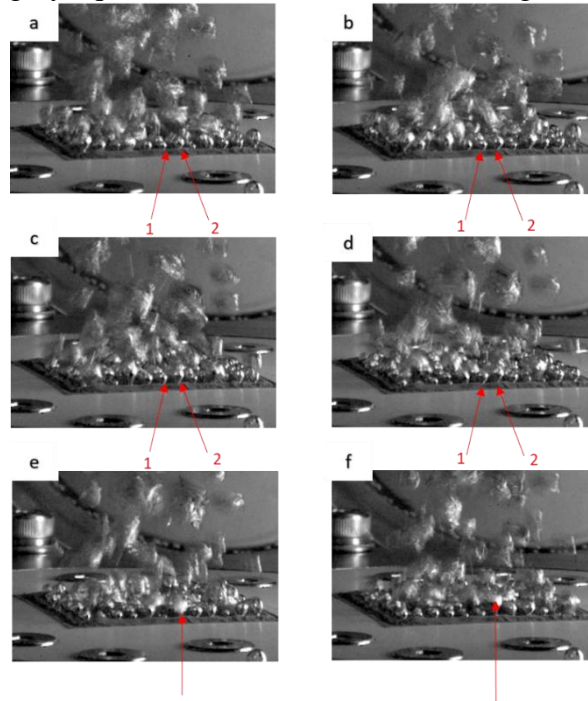

Figure 3: Successive bubble growth for the surface with re-entrant cavities at a heat flux q" of 3.45 W/cm2 at a) 0 ms,(b) 20 ms, c) 30 ms, d) 40 ms, e) 50 ms, f) 60 ms

The experimental results demonstrated that the surface with re-entrant cavities had a significant effect on the HTC, which reached up to 285% of improvement at low heat fluxes compared to the bare surface (Fig. 4). This is referred to the re-entrant cavities' capability to promote an organized coalescence mechanism, which increased the bubbles' departure frequency. Higher frequency and nucleation site density yielded a notable enhancement of the HTC compared to the bare surface.

Figure 4: Comparison between the 3D printed bare surface and the re-entrant cavities for a) the pool boiling curve and, b) boiling HTC

Effect of Inclination Angle on Evaporating Flow in Parallel Pipes

Ron Rene Hayat[2], Dvora Barnea[1] and Yehuda Taitel[1]

[1]School of Mechanical Engineering, Tel Aviv University, Tel-Aviv 69978, Israel
[2]Soreq NRC, Yavne 8180000, Israel
Contact E-mail : taitel@eng.tau.ac.il
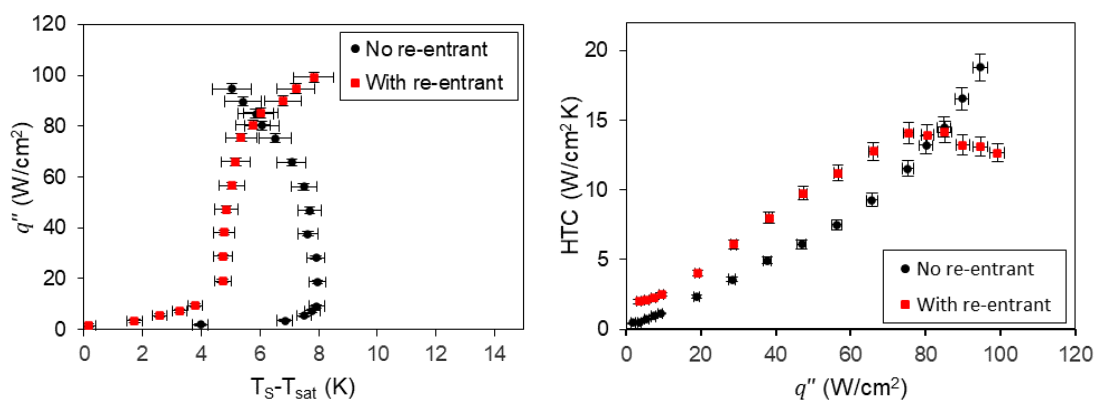
The effect of inclination angle on evaporating flow in a single and two identical parallel pipes is presented. Three types of flow behaviour occur in a single pipe. (1) The dependence of pressure difference on the flow rate is a monatomic increasing function. (2) The pressure difference vs. flow rate has a range of decreasing pressure vs. flow rate (negative slop region). (3) Negative pressure difference takes place in a certain range of flow rates. For the case of two parallel pipes we may identify equal flow distribution, uneven flow distribution (maldistribution) and maldistribution with oscillations.

Fig. 1 is a schematic presentation of the system that is analysed.
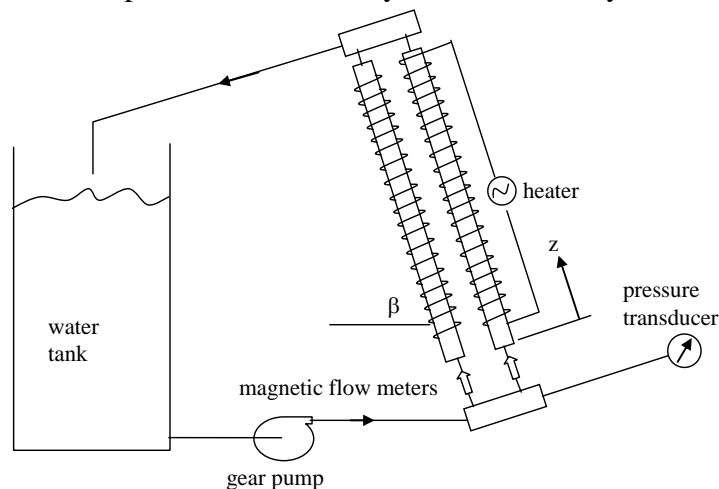
Figure. 1. Schematic layout of parallel pipes system with evaporation

Fig 2 shows the pressure difference vs. flow rate for a single pipe at inclination angles ranging from vertical up to vertical down. One can observe 3 regions. For high upward inclination angles (above the upper horizontal red line) ΔP is a monotonic function of the flow rate. At upward slightly inclined and horizontal flow we get the typical N shape pressure vs. flow rate curve (between the 2 red lines). The third region, where the flow moves downwards, is characterised by a zone of negative pressure drop (due to gravity).
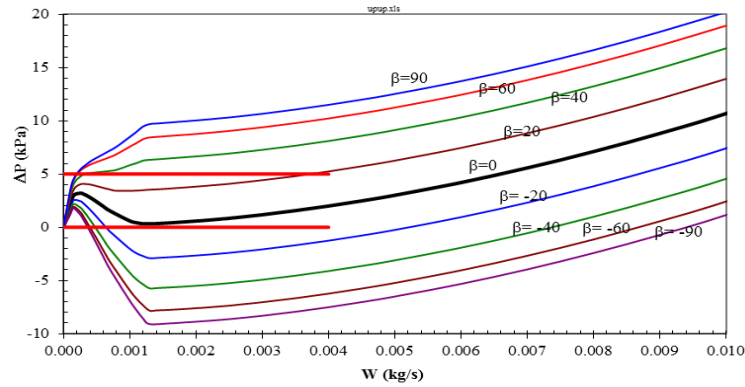
Figure 2. Pressure difference vs. flow rate and inclination angle,
Q_{in} =600 W/m, P_{out}=1 bar, L=1 m, D=3 mm.

Fig 3 presents the steady state flow rate ratio for downward flow in two parallel pipes, β=0, -40, -90 deg. The blue curves are stable steady state solutions, the red are unstable solutions. The dashed lines represent the range where downward flow takes place in one pipe while upward flow is observed in the second pipe. In this range oscillations in the pressure and flow rates occur. Fig. 4 presents the pressure difference for the same conditions as in fig. 3.
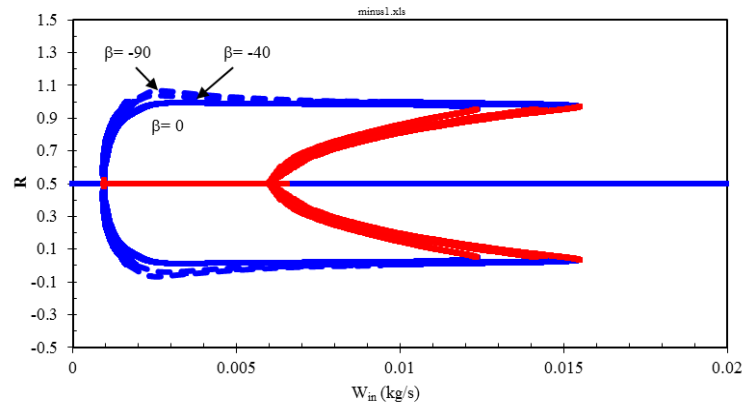
Figure. 3. Pressure difference vs. total inlet mass flow rate for two parallel heated pipes.
Q_{in} = 1200W/m, D=3mm, L=1m, P_{out}=1bar, β=0^0 , -40^0 and -90^0.
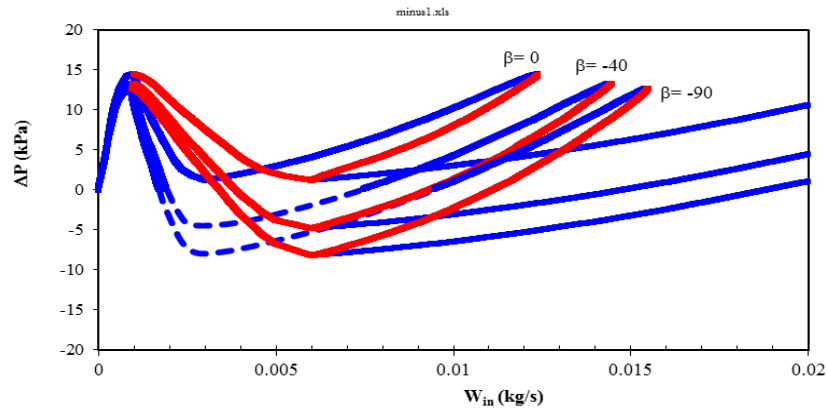
Figure. 4. Pressure difference vs. total inlet mass flow rate for two parallel heated pipes.
Q_{in} = 1200W/m, D=3mm, L=1m, P_{out}=1bar, β=0^0 , -40^0 and -90^0.

Influence of Air Entrainment on Quenching of a Solid Sphere

S. Hosokawa[1] and R. Dohtsu[1]

[1]Kansai University
Contact E-mail : hosokawa@kansai-u.ac.jp

Quenching of high-temperature solid can be seen in various situations such as the hardening process of metal parts and cooling of the molten core of a nuclear reactor. In many cases, quenching occurs in the atmospheric condition and the depth of the coolant is not so deep compared with the size of the cooled body. Hence, air will be entrained near the solid body falling into a coolant. Although many studies have been carried out on the quenching of high-temperature solid, the effects of the entrained air on the quenching process of a high-temperature solid sphere have been rarely investigated. The present study aims to investigate the effect of entrained air on the quenching process of a solid sphere. We carried out quenching experiments of a solid sphere at various falling speeds and depths of the sphere since the amount of entrained air surrounding the sphere depends on the speed and depth.

Figure 1 shows the schematic of the experimental apparatus. The experimental apparatus consists of the solid sphere with the thermocouple, the linear actuator, the electric furnace, the data logger and the cooling water tank filled with tap water. The material of the solid sphere is Inconel 600, and the diameter is 30 mm. The thermocouple is inserted into the sphere and the tip is located at the center of the sphere. The tank is made of transparent polycarbonate resin to observe the cooling process. The cooling water temperature was adjusted to 60 °C using a heater, and the sphere was heated to 900 °C at the center of the electric furnace. The sphere was moved vertically at a constant speed by the linear actuator and stopped at a certain depth in the water tank. The temperature at the center of the sphere was recorded with the data logger and the boiling flow pattern around the sphere was recorded by using the high-speed video camera (Photron, FASTCAM mini WX100). The falling speed V_0 of the sphere was changed from 0.30 m/s to 0.96 m/s. The depth h of cooling position, which is the distance from the water surface to the center of the final sphere position, ranged from 0.1 and 0.2 m.

Figure 2 shows the time change of the temperature at the center of the sphere. The temperature drops almost linearly just after the start of cooling, and then it drops sharply around 800 - 550 °C depending on the
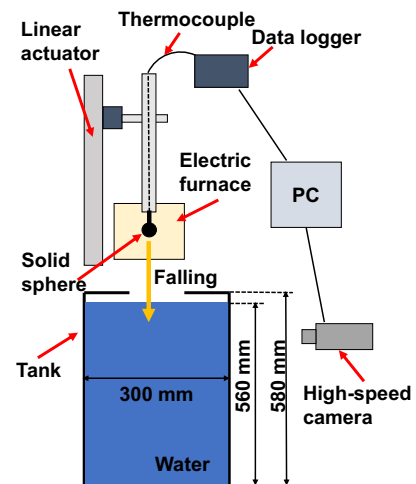

Figure 1. Experimental apparatus

experimental condition. The former region corresponds to the film boiling, and the latter corresponds to the nucleate boiling. The time duration of the film boiling clearly depends on V_0, and increases with V_0. Since the air entrainment around the sphere is enhanced by increasing V_0, this implies that the entrained air around the sphere contributes to inhibit the transition from the film boiling to the nucleate boiling. This is because the non-condensable gas molecules of the entrained air remain in the vapor film during the film boiling and the film thickness becomes thicker than that without non-condensable gas molecules. The time duration of the film boiling also depends on h, and increases as h decreases. As h increases, the amount of the entrained air released from the neighborhood of the sphere to the atmosphere may increase due to the longer passage in the water. Hence, this indicates that the increase in h decreases the remaining amount of the entrained air around the sphere and the stability of the vapor film also decreases due to the lack of non-condensable gas molecules in the film. These results implies that the non-condensable gas in the vapor film inhibit the transition from the film boiling to the nucleate boiling, that is, the duration of the film boiling becomes longer by the presence of the non-condensable gas in the film.

To confirm this inference, an experiment was carried out in the low dissolved oxygen concentration (DO) condition, in which oxygen, i.e. one of the main components of the entrained air, dissolved into the water, and therefore, the non-condensable gas concentration in the film decreases due to the dissolution. The DO was decreased by adding sodium sulfite into the water and the measured DO was 0.0 mg/l. The result is shown in Figure 3 together with the result without sodium sulfite (DO = 4.7 mg/l) at the same V_0 and h. As DO decreases, the temperature at which the transition from the film boiling to the nucleate boiling occurs increases and the duration of the film boiling decreases. In other words, it is confirmed that the stability of the vapor film is enhanced by the presence of the dissolved oxygen in the water. This indicates that the stability of the vapor film is enhanced by the presence of the non-condensable gas molecules in the film and therefore the transition from the film boiling to the nucleate boiling occurs at lower temperature in the case of the presence of the non-condensable gas molecules in the film due to air entrainment.
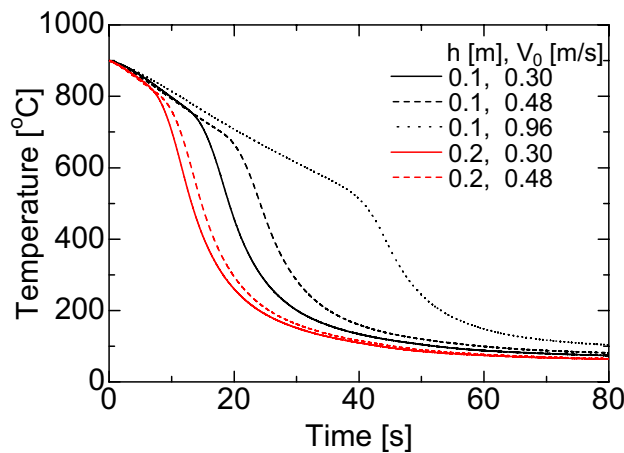

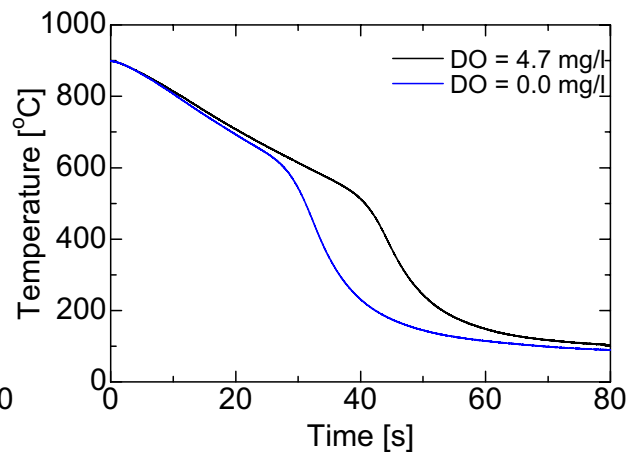Figure 2. Influence of falling speed and depth

Figure 3. Influence of DO
(h = 0.1 m, V_0 = 0.96 m/s)

Development and application of ultrasound techniques to multiphase flows

F. Hossein., M. Matterazzi., M. Errigo., P. Bormann., P. Lettieri., P. Angeli.,

Department of Chemical Engineering, University College London, London, WC1E 7JE, United Kingdom
Contact E-mail : *f.hossein@ucl.ac.uk

Multiphase flows underpin many and diverse areas of engineering, manufacturing, and energy, including pharmaceuticals, spent nuclear fuel reprocessing, and food production. It is paramount importance to predict the behaviour of these complex systems. Despite extensive research in this area, the available experimental techniques are limited to optically transparent geometries, refractive index matching (e.g., PIV, LDA), or expensive with strict safety requirements instrumentation (e.g., X—Ray, MRI). Ultrasound techniques are relatively cheap, easy to setup and can provide complementary information while they can be applied to non-transparent systems. In this work we have developed ultrasound techniques and applied to solid-liquid flows in fluidized beds and liquid-liquid flows in stirred vessel, to measure different parameters, such as, particle or droplet size distribution, velocity profiles, and volume fraction. The experimental measurement techniques applied are ultrasound attenuation spectroscopy, ultrasound Doppler velocity profiling, and ultrasound wave propagation speed. The experimental setups, signal post processing including inversion algorithms are also investigated for the characterization of dispersed phases in stirred vessel and fluidized beds. For the solid-liquid system, the experiments were performed in a vertical fluidized bed with an inner diameter of 5 cm, and height of 70 cm, made of borosilicate glass, which contains glass beads (particle density = 2500kg/m^3), and for the two liquid system, the application and validation of the ultrasound techniques were performed in dispersed liquid-liquid [silicone oil dispersed in water/glycerol] flows in stirred vessel. For a straight validation both ultrasound and planar laser-induced fluorescence PLIF were used to capture the dynamic of oil drops in an aqueous continuous phase in liquid-liquid flows. For the measurement of volume fractions the ultrasound wave propagation speed through solid-liquid and liquid-liquid were used. Ultrasound propagation speed was found for silicone oil dispersion in water/glycerol to be between 1601 m/s and 1662 m/s for droplet volume fractions spanning from 0.53% to 4.2%, and it was found to be between 1504 m/s to 1565 m/s for glass particle in solid-liquid flows with volume fractions spanning from 27% to 70%. Combining the ultrasonic attenuation measurements and the *Optimum Regularisation Technique (ORT)* inversion algorithm, the size distributions of silicone oil droplets ranging from 0.25 mm to 2 mm in two liquid flows and particles in solid-liquid flows ranging from 0.5 mm to 1.25mm, were measured. The Doppler shift effect was used for the measurement of particle velocity profiles in solid-liquid systems. The experimental results show that ultrasound techniques are a powerful tool for the study of concentrated solid-liquid and liquid-liquid systems, and the techniques can offer unprecedented capabilities for the study multiphase systems in fluidization, pipe flows and stirred vessels.
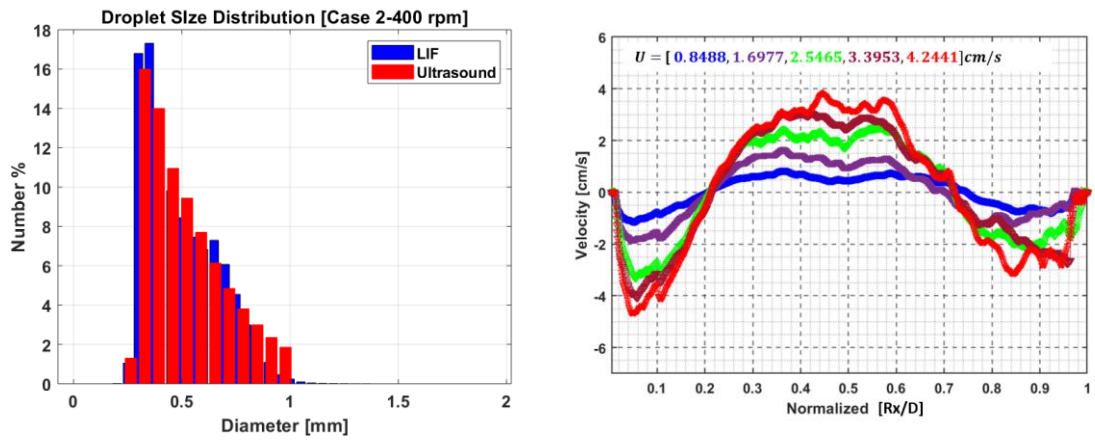
Figure 1. **Left,** oil drop size distribution measured in stirred vessel by PLIF and Ultrasound technique, **Right,** Particle velocity profile measured by ultrasound technique in solid-liquid fluidized bed.

Study on High-Precision Simulation Method of Condensation

K. Ito[1], N. Odaira[1], D. Ito[1], Y. Saito[1] and S. Miwa[2]

[1]Kyoto University, [2]The University of Tokyo
Contact E-mail : ito.kei.3n@kyoto-u.ac.jp

Boiling and condensation phenomena have been a hot issue in the field of gas-liquid two-phase flow reseaches. For example, in the study on nuclear reactors, the boling phenomena is crucially important to predict the critical heat flux in a BWR core. The evaluation of condensation phenomena is also important for the design of some devices, e.g. a steram injector (SI). The SI is expected to work as a passive pump which supplys water into the core without any external power supply, and therefore the SI has been studied and developed to mitigate the influence of a severe accident. In the SI, steam flows along water jet and the direct contact condensation (DCC) occurs at the steam-water interface. The thermal energy of steam is converted to the kinetic energy by the DCC, which makes the discharge pressure higher than the steam inlet (suction) pressure. However, the DCC in the SI is highly complicated phenomena which has not been clarified perfectly by past experimental, numerical and theoretical researches in several decades. The most significant issue is that the SI can fall into an inoperative condition when the discharged pressure reaches its maximum value. Though such an inoperative condition is considered to be caused by the instability at the steam-water DCC interface and/or the condensation shock generated by the DCC, the onset mechanism of inoperative condition has not been clarified yet. Therefore, to reveal the appropriate operating condition of the SI, it is important to study the detailed process of the DCC. In fact, several measurements and simulaitons have been conducted to investigate the DCC in detail. However, the measurements of physical quantities at steam-water DCC interface is highly difficult and also the numerical simulation methods have significant issues on the simulation stability to accurately reproduce the DCC behaviors.

In this study, the authors develop a high-precision simulaiton method of condensation, in which the simulaiton accuracy and stability are enhanced by taking into account the precise physical mechanism of condensation process at stearm-water interface. First, the authors employ the high-precision volume-of-fluid method, one of major interface-tracking methods, as the basic simulation method due to its superior reproducibility of a gas-liquid interface dynamics compared with other methods, e.g. the two-fluid method. Then, the calculation method of interface advection by condensation is examined and an appropriate calculation method is developed and proposed. In addition, the calculation method of temperature gradient, which determines the calculation of condensation quantity, is also examined to enhance the simulation accuracy of condensation quanitity. Finally, as the verification of modified simulation methods, well-known Stefan problem is solved and the simulation resutls are compared with the theoretical solution.

In most conventional simulaiton method of condensation, the phase-change, i.e. the change in volume fraction (f) in the volume-of-fluid method, is calculated in each computational cell. Therefore, the limit of condensation quantity, i.e. the production of condesed liquid, during

one timestep is resticted by the volume of steam in a cell. Namely, the timestep size must be very small in such a simulation to reduce the simulation error. In our new simulaiton procedure, the interface is advected through the cell boundaries and the condensation quantity can be calculated accurately even with relatively large timestep. Figure 1 shows the concept of modified calculation method of interface advection. As shown in left figure, the interface advection velocity (v_c), normal to the interface, is calculated based on the temparature gradient at the interface before the condensation. Then, the interface is advected through the cell boundaries, i.e. beyond the cell where the interface originally exists, and the condensation region is determined as the area between the initial and advected interface as shown in dotted zone in right figure. To achieve this modified calculation method, partial volume calculation algorithm for three-dimensional arbitrary shape cell is developed.
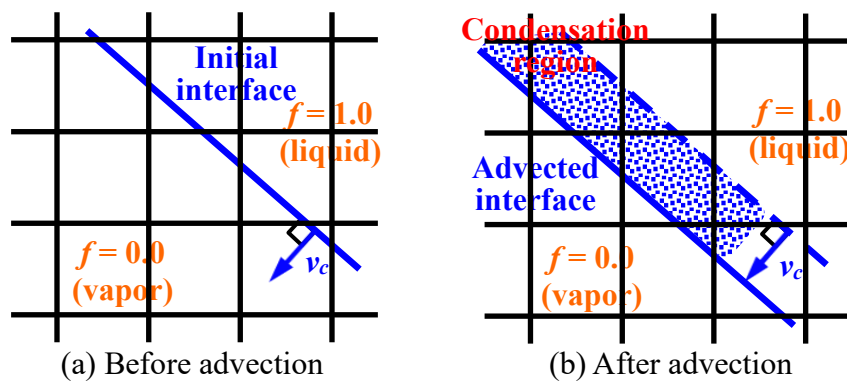
(a) Before advection　　　　　　(b) After advection
Figure 1. Concept of interface advection

Figure 2 shows the calculation result of quasi-one-dimensional Stefan problem on an unstructured triangular mesh. The comparison of the modified method (Fig. 2(a)) and the conventional method (Fig. 2(b)) clearly shows that the interface movement is calculated accurately only by the modified method, that is, the physically-appropriate condensation simulation is achieved by the modified method. The superior simulation accuracy of the modified method is also shown in the comparison with the theoretical solution of interfacial position as shown in Fig. 2(c).

(a) Modified method　　　　(b) Conventional method　　　(c) Comparison with theory
Figure 2. Simulation result of Stefan problem

Experimental Observation and Temperature Measurement of Lateral Hydrate Growth on a Sessile Droplet

Muhammad A. Kamel[1], Aleksei S. Lobasov[1,2], Surya N. L. Narayan[1], Konstantin S. Pervunin[1] and Christos N. Markides[1,2]

[1] Clean Energy Processes (CEP) Laboratory, Department of Chemical Engineering, Imperial College London, SW7 2AZ London, United Kingdom
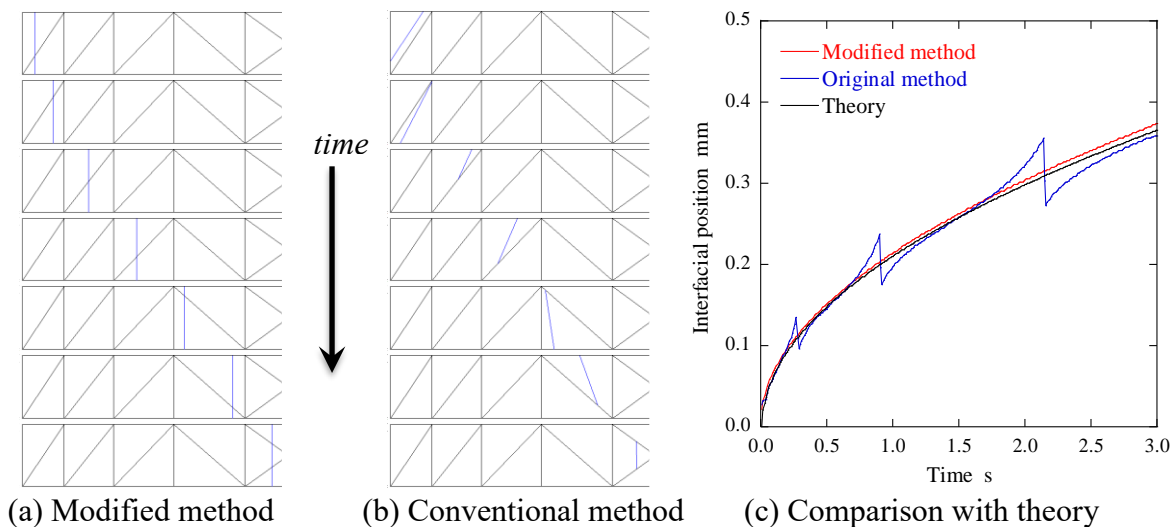[2] Kutateladze Institute of Thermophysics, Siberian Branch of the Russian Academy of Sciences (IT SB RAS), 630090 Novosibirsk, Russia
Contact E-mail: c.markides@imperial.ac.uk

Multiphase flows are commonly encountered in engineering applications, particularly in the oil and gas industry where challenges are arising from operation in deeper and colder waters. Here, accumulation of solid deposits in pipelines, for example, hydrates, waxes, scales, corrosion and asphaltenes, is the main cause of plugs or blockages, thus placing greater emphasis on flow assurance. In mature fields, an increase in the water to gas (or oil) ratio impacts the flow and spatial distribution of the two phases, which creates a favourable condition for hydrate formation at a certain temperature and pressure. Hydrates are inclusion compounds that form initially as thin solid films at the interface between two immiscible liquids, one of which is water. The phase change process is accompanied by heat release due to the exothermic nature of hydrate formation. Hence, the mechanism of film growth can be controlled by either influencing the flow of one of the liquids towards the film front or by managing the heat from the newly created solid phase or both. The aim of this study is to capture the dynamics of interfacial heat transfer during nucleation and growth of hydrates.

Experiments on hydrate formation were performed in a dedicated cell equipped with visualisation windows to allow optical access to a water drop placed at the centre of the cell. In each test run, a single drop of deionised water was injected at room temperature into liquid cyclopentane. Cooling of the drop occurred by natural convection and was achieved by circulating a mixture of ethylene glycol and water in a 1:1 volume ratio through the outer section of the hydrate cell. The circuit was connected to a recirculating cooler for final heat removal. When the temperature of the drop fell below the hydrate equilibrium temperature, a driving force was established for the crystallisation process, leading to the formation of a hydrate layer (film) at the interface upon hydrate nucleation. The dynamics of the phase-change process were captured by one-colour planar laser-induced fluorescence (1c PLIF) in both the drop and surrounding phase to provide spatiotemporally information on the lateral growth of the hydrate layer along the interface and of the temperature field inside and around the drop during the process.

The temperature measurement was performed by utilising Sulforhodamine B (dissolved in water) and Nile Red (dissolved in cyclopentane). Both dyes are temperature sensitive with sensitivity coefficients of 1.5 and 1.8%/°C, respectively. Thin laser light sheets were generated using two Litron

Nd:YAG lasers (532 nm, 50 mJ@100 Hz and 200 mJ@15 Hz) equipped with LaVision and Dantec Dynamics sheet optics, with a time delay between consecutive pulses of the two lasers set to 55.31 μs. The sessile water drop was illuminated from the bottom of the cell, while the surrounding cyclopentane phase was illuminated from the top, as shown in Fig. 1a. LIF signals from the different phases were captured, from a viewing angle perpendicular to the laser sheet, using a double-frame LaVision Imager MX 2M-160 (12 bit, 1936×1216 pixels, 100 Hz) CMOS camera equipped with a Sigma 105 mm f/2.8 EX DG macro lens and a 550-nm long-pass filter at a frequency of 2 fps.
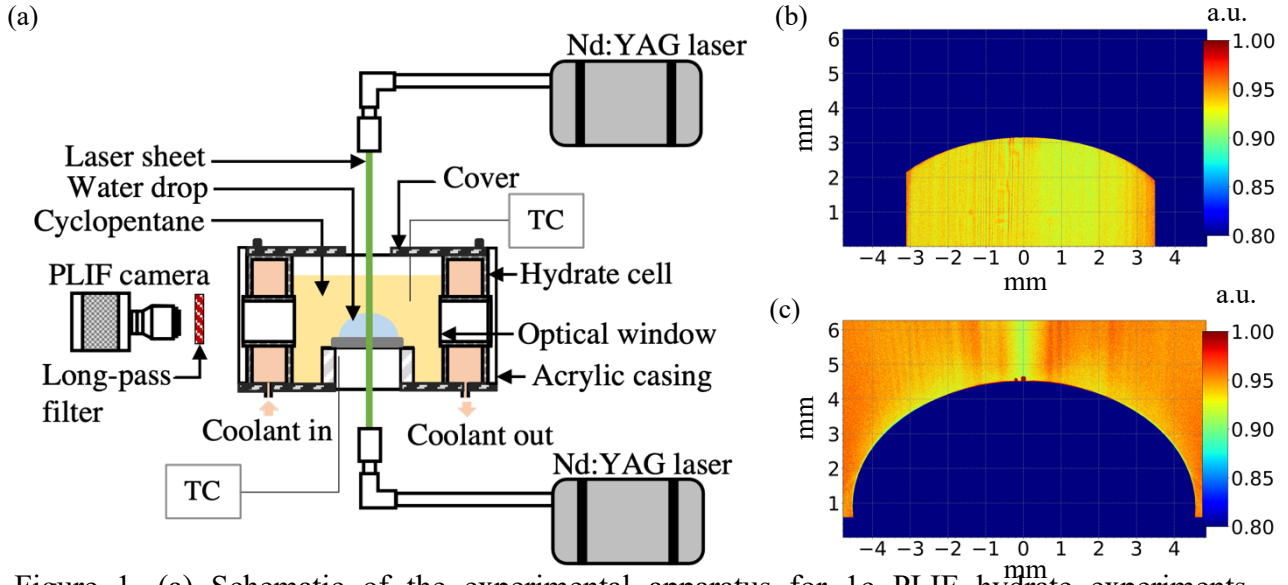

Figure 1. (a) Schematic of the experimental apparatus for 1c PLIF hydrate experiments. (b) Fluorescence intensity inside the drop. (c) Fluorescence intensity in the surrounding phase.

The measurement of temperature fields with PLIF provides insights into the heat transfer process as the hydrate film propagates along the drop interface. Heat release during the formation of a hydrate crystal is diffused into the surrounding phase, the drop phase and the hydrate film. As the thermal conductivity of a solid hydrate is lower than the liquid cyclopentane, the heat transfer to the hydrate film is assumed negligible. The hydrate film was also observed to grow into the cyclopentane phase, thus suggesting that the front, where heat exchange occurs, is in the cyclopentane phase.

Figs. 1b and 1c show examples of fluorescence intensity fields inside the drop and in the surrounding phase, respectively, which are inversely related to appropriate temperature fields. The heat balance at the propagating hydrate front can, therefore, be expressed as:

$$\rho_h \Delta h_f v_f = \alpha_c (T_{c,i} - T_{c,\infty})$$

where ρ_h is the density of hydrate, Δh_f is the latent heat of the hydrate formation, v_f is the velocity of the hydrate front, α_c is the heat transfer coefficient in the cyclopentane phase, $T_{c,i}$ is the hydrate-cyclopentane interfacial temperature and $T_{c,\infty}$ is the bulk temperature in the cyclopentane phase. The heat transfer coefficients are compared for different bulk temperatures ranging from -7 °C to 1 °C to reveal the significance of heat transfer in the mechanism of hydrate lateral growth.

Pool Boiling: Aspects of Heat Transfer Enhancement

Tassos G. Karayiannis[1] and Mohamed M. Mahmoud[2]

[1]Brunel University London, Department of Mechanical and Aerospace Engineering
Uxbridge, UB8 3PH, UK
tassos.karayiannis@brunel.ac.uk

[2]Zagazig University, Faculty of Engineering
Zagazig 44519, Egypt
mbasuny@zu.edu.eg

The pool boiling is one of the most effective heat transfer modes used in systems where large amount of heat need to be transfer with preferably small temperature differences between the surface and the fluid. It is also the starting point, i.e. the background knowledge required, in the design of systems where flow boiling is employed. This applies to both large heat exchanger systems used in the power, chemical and refrigeration industries or the more recent designs of small to micro scale heat exchangers to cool high heat flux electronic devices. Therefore, pool boiling received significant attention by the research community over the past years. A lot of effort has also been applied in further enhancing the pool boiling heat transfer rates and extending the upper possible operational limit, the Critical Heat Flux.

Heat transfer enhancement techniques are classified as active and passive. Active techniques require the use of an external force and include surface or fluid vibration, surface rotation or the application of high intensity electric fields. Passive techniques include rough, treated surfaces or coated surfaces, all aimed at increasing the number of nucleation sites.

The presentation includes reference to past work on the use of electric fields – a technique term Electrohydrodynamic Enhancement (EHD) of boiling with a brief mention of the technique applied to condensation for completeness. It will then focus, for its larger part, on the most commonly passive enhancement technique, which is surface modification by creating micro and/or nanostructures and coatings on the surface to be cooled. The current challenges in benchmarking and evaluating the performance of smooth and enhanced surfaces will first be discussed. The work presented will include reasons for discrepancies among researchers on the performance of enhanced surfaces even for the same fluid and surface preparation technique. The performance of smooth and surfaces roughened by standard techniques is discussed in this context and the effect of fluid explained.

The various passive heat transfer enhancement techniques adopted by researchers will then be presented and critically assessed. In this study we digitised and compared pool boiling data for two fluids, namely water (high surface tension, low wettability) and FC-72 (low surface tension and latent heat, high wettability, representing refrigerants) on two enhanced substrate materials, i.e. copper to represent metallic surfaces and silicon, which is used in small scale applications, in order to elucidate the reasons for the reported past discrepancies and present recommendations for heat transfer enhancement. Finally, recent comparative results with Novec 649 boiling on copper substrates coated with nickel-copper of different porosity will be discussed.

The presentation contributes to the debate and the understanding of the effect of fluid-surface combinations and provides general guidelines for researchers and industrialist when evaluating the performance of enhanced surfaces. We expect this to help in concluding on the best surface structure and manufacturing technique, matching fluids of interest with particular applications.

Multiphase Flow Phenomena Associated with the Breakup, emulsification, and Transport of Crude Oil by Surface Waves and Subsurface Plumes

J. Katz[1]

[1]Department of Mechanical Engineering, Johns Hopkins University, Baltimore, MD, USA
Contact E-mail : katz@jhu.edu

This presentation summaries a series of laboratory studies aimed at characterizing a series of interfacial phenomena affecting the breakup and weathering of surface slicks and subsurface plumes of crude oil after an oceanic spill. Experiments performed in a wave tank examine the time evolution of size and spatial distribution of subsurface droplets generated as single plunging waves of varying heights impinge on fresh oil slicks of varying properties (density, viscosity, and interfacial tension). Test have also been performed after premixing the oil with dispersant (Corexit 9500) at varying concentrations, which drastically reduce the oil-water interfacial tension. The time evolution of turbulence in the tank is also measured. Without dispersant, the initial droplet size distributions are consistent with predictions of classical turbulence-based Weber number scaling. Their subsequent temporal evolution can be modeled by combining effects of turbulent diffusion and buoyant rise of the droplets. Premixing the crude oil with dispersant causes tip streaming that decreases the droplet sizes to the micron range, two orders of magnitude below the Kolmogorov scales. Hence, their size distribution is no longer consistent with turbulence-based scaling.

Aerosolization of oil is caused by the initial splash and by subsequent bubble bursting. Premixing with dispersant increases the concentration of airborne oil-containing nano-droplets by one to two orders of magnitude. In contrast, the dispersant causes a reduction in concentration of volatile organic compounds. Subsequent experiments focusing on aerosolization of oil-dispersant mixtures by bursting of bubbles have shown that the nano-aerosols appear only when the bursting bubbles are large enough to generate film droplets, and the interfacial tension is low enough to increase the thermal length scale to a few nanometers. Tests involving a series of crude oils with very different properties have shown that all of them generate nano-aerosols. The concentration of nanodroplets decreases with increasing Capillary number based on the rise velocity of the bubbles and the oil viscosity and interfacial tension. Subsequent observations have shown that the nano-droplets are generated below the surface prior to bubble injection owing to thermal capillary instability. The bubble plume transport these droplets to the surface, and they become airborne once the bubbles burst.

Extended mixing of crude oil with seawater generates poly-dispersed water-in-oil emulsions that have one to three orders-of-magnitude higher viscosity. Mixing of the emulsions based on light oils with dispersant partially separates the water from the emulsion. In contrast, dispersant has little effect on emulsified heavy crude oils. Micro emulsions also form as oil droplets rises and cross an oil-water interface. These droplets do not mix with the bulk oil since

they remain coated by submicron water films that persist long after crossing. These films eventually break up owing to droplet deformation induced by electrostatic forces.

Another series of studies has focused on the structure of subsurface oil jets and plumes. The fragmentation of a vertical buoyant oil jet is elucidated by refractive index matching using silicon oil and sugar water. Visualizations of the mid plane demonstrate that compound oil droplets containing water droplets, some with smaller oil droplets, form regularly. Their fraction increases with droplet diameter, reaching 78% for 2mm droplets. The process leading to the formation of compound droplets from interfacial ligaments has been visualized (Figure 1). While the exterior surfaces of the oil droplets are deformed by the high shear field, the interior interfaces remain spherical, indicating quiescent domains.

Detailed 2D PIV and planar laser induced fluorescence measurements performed in the near field of the oil jet provide the ensemble-averaged phase and velocity distributions, as well as the Reynolds stresses for each phase and combined. The data elucidate processes affecting the mixing and momentum exchange between phases. Spreading rate of the oil volume fraction and the decrease in its centerline concentration are lower than those of the axial momentum and centerline velocity. Universal profiles of phase distribution and axial momentum scaled with the half widths and centerline values develop after six diameters. The mean velocity in the oil is higher than that in the water, and once the profiles become universal, the difference between them is consistent with the buoyant rise velocity of the oil droplets. The spatial distributions and trends of the Reynolds stresses in the two phases are different initially but diminish with axial distance. Reason for discrepancies and evolution trends can be explained by examining the corresponding production rates. Finally, in the presence of cross flow, entrainment of small droplets into the core of the counter-rotating vortex pair defines the lower boundary of the plume while large droplets escape and define the upper boundary. Hence, reduction of droplet sizes by dispersant increases the fraction of oil entrained into the vortex pair and lowers the upper boundary of the plume.
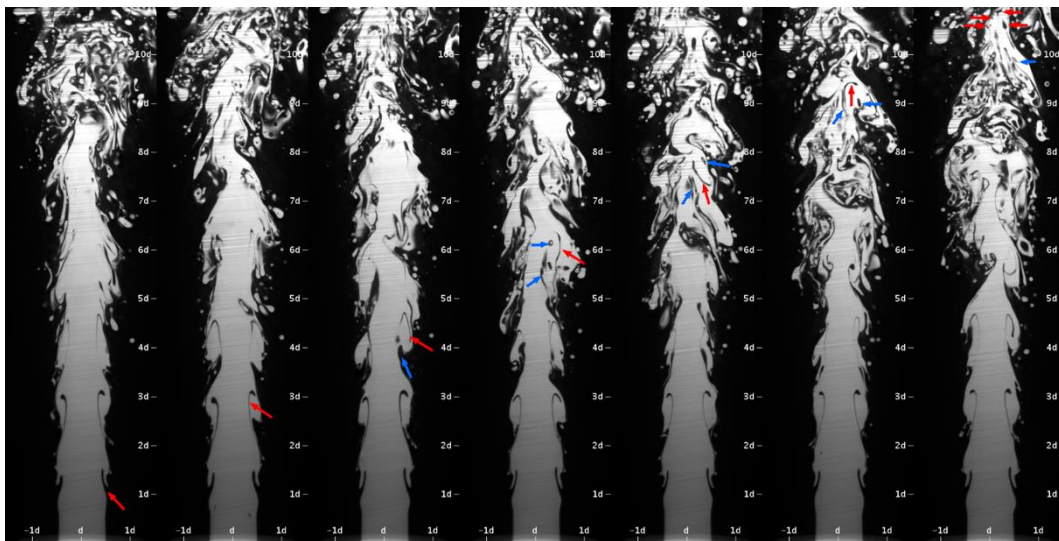

Figure 1: Time evolution of a vertical oil jet in water, showing the entrainment of water leading to the formation of compound droplets; Re=1358, delay between exposures is 300 μs.

A Dual-Scale LES Model for Sub-Filter Dynamics of Phase Interfaces During Atomization

D. Kedelty, A. Goodrich, and M. Herrmann

School for Engineering of Matter, Transport and Energy
Arizona State University
Contact E-mail : marcus.herrmann@asu.edu

While significant progress has been made in the past decade to predict atomization using detailed numerical simulations, these come at significant computational cost since the range of scales that must be resolved exceeds those of a single phase turbulent flow significantly. A switch to a Large Eddy Simulation (LES) approach would be desirable, however, the underlying assumption of LES methods that the dynamics of the unresolved sub-filter scale can be inferred from the resolved scales is questionable when atomization occurs.

Similar to viscosity in single-phase flows, surface tension scales with the inverse of a length-scale, but unlike viscosity, it can act to either dissipate surface corrugations preventing breakup, giving rise to the Kolmogorov-Hinze scale, or enhance surface corrugations due to the Rayleigh-Plateau instability, resulting in breakup. Which process is dominant on the sub-filter scale seems to depend entirely on the sub-filter interfacial geometry, i.e., if the phase interface is in the shape of ligaments, surface tension promotes breakup, whereas in other geometries, surface-tension can inhibit breakup. Unfortunately, the sub-filter geometry cannot always be inferred from the filtered interfacial geometry alone. LES approaches going beyond the traditional modeling approach of inferring sub-filter dynamics from the resolved scales may thus be required for two-phase flows with atomization.
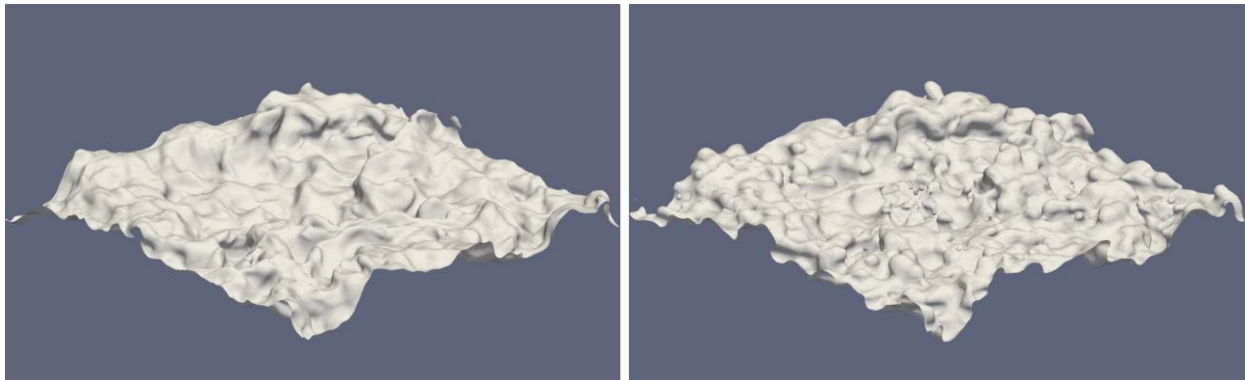

Figure 1: DNS (left) and Dual Scale LES (right) realization of an initially planar interface in decaying homogeneous isotropic turbulence at $t/t_\lambda = 0.1$ with $Re_\lambda = 156$ and $We_\lambda = 1.1$.

In this presentation, a dual scale LES modeling approach will be discussed that can handle the dual nature of surface tension on the sub-filter scale. The model maintains a fully resolved

realization of the phase interface on a dual scale, shifting the modeling task to reconstructing the fully resolved interfacial advection velocity from the filter-scale velocity. The unclosed terms related to the phase interface appearing in the filtered Navier-Stokes equations on the LES scale can then be evaluated directly by explicitly filtering the dual scale resolved realization of the phase interface.

To reconstruct the resolved dual scale interface velocity, effects of sub-filter surface tension, turbulent eddies, shear, acceleration, and phase transition are taken into account. Special care must be taken that the reconstructed dual scale velocities remain consistent with the filter scale velocities and that they satisfy the continuity equation. Results showing the viability of the dual-scale LES approach in canonical test cases including initially planar surfaces and sheets in turbulent flow fields, see for example Fig. 1, will be discussed.

Bubbly flows in a column with submerged hollow fiber membranes

## R. Kurimoto[1], S. Takaya[1], K. Hayashi[1] and A. Tomiyama[1]

[1]Graduate School of Engineering, Kobe University
Contact E-mail : kurimoto@mech.kobe-u.ac.jp

Experiments on bubbly flows in a square column with submerged hollow fiber membranes were carried out to understand characteristics of bubbly flows about packed hollow fiber membranes. The width and height of the bubble column were 100 and 1150 mm. 39 hollow fiber membranes made of PVDF with 2 mm diameter were submerged in the column. Relaxation rates of the membranes were 0.0 and 5.0 x 10^{-3}. The range of the gas volumetric flux was 7.7 x 10^{-3}-2.8 x 10^{-2} m/s. Water and xanthan gum-water solution of 0.9 g/L were used as the liquid phase.

Figures 1 and 2 show flow images at the bottom and middle regions of the column in water and xanthan gum-water solution, respectively. Many small bubbles rise in water since bubbles released from the diffuser break up at the tie plate for the membranes. In contrast, large bubbles rise in xanthan gum-water solution without breakup at the tie plate. We measured removal rates of sludge attached to the membranes to understand effects of the difference in the flow characteristics due to the liquid phases on membrane fouling. The total and local void fractions and bubble diameters at the diffuser and the lower tie plate were also measured.
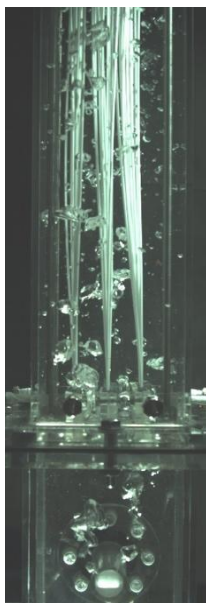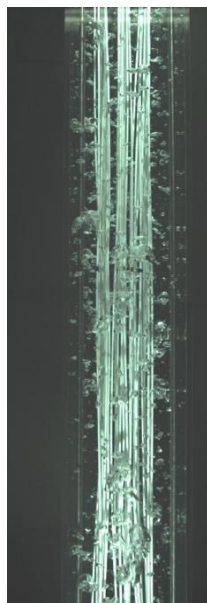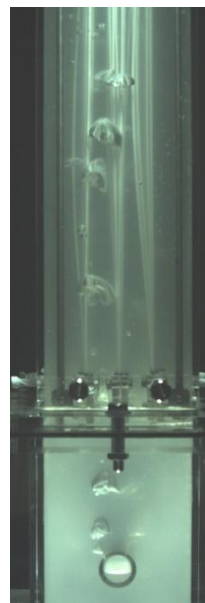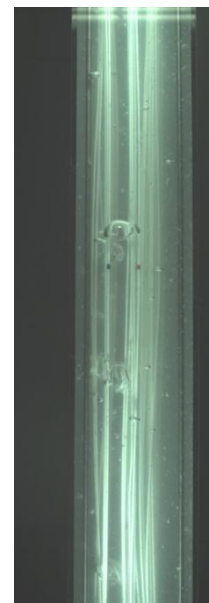

| Bottom region | Middle region | Bottom region | Middle region |
| Fig. 1 Bubbly flow in water | | Fig. 2 Bubbly flow in xanthan gum-water solution | |

Direct numerical simulation of freezing droplets

D. Legendre[1] and S. Lyu[2] and C. Sun[2]

[1]Institut de Mécanique des Fluides de Toulouse (IMFT), Université de Toulouse, CNRS-Toulouse, France
[2]Dep. Energy and Power Engineering, Tsinghua University, 100084 Beijing, China,
Contact E-mail : legendre@imft.fr

This work is devoted to the development of a new hybrid VOF-IBM method for the simulation of freezing liquid films and freezing drops [1]. The VOF and IBM methods of the JADIM IMFT inhouse code [2, 3] are coupled with the temperature equation to be able to solve the icing front propagation in a liquid located on a cold surface, with considering the dilatation induced by the density difference between the liquid and the ice as well as the droplet deformation induced by the balance of the surface tension and gravity. The numerical simulations are validated by a comparison between the theoretical solutions and experimental observations, and the CSF-VOF spurious currents are shown to induce no effect on the icing process due to the small value of both the corresponding Weber and Capillary numbers for the considered cases.

We investigate the effect of the Stefan number and the ratio of solid density to liquid density on the height evolution of the icing front for both liquid films and droplets. We also study the whole freezing processes of droplets with different contact angles. Furthermore, the effect of gravity and the surface tension on freezing processes of drops are investigated. The temperature distribution, solidification shape, and evolution within the droplet are systematically analysed. We find that the final drop shape is in very good agreement with the experiments of Marin *et al.* [4] (see Fig. 1), and in particular the value of the tip angle of the iced droplet and the front-to-interface angle are very well reproduced.
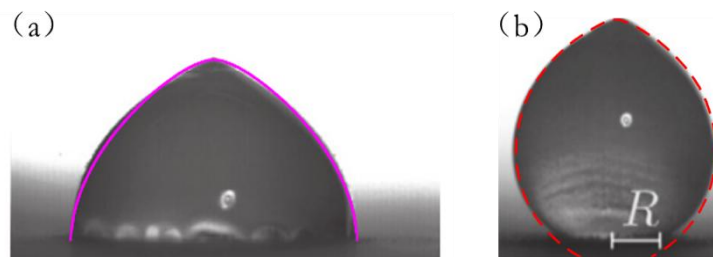
Figure 1. Final numerical droplet shapes (coloured lines) compared to the experiments of Marin *et al.* [4] for different contact angles: (a) θ=90°, (b) θ=150°.

In addition, we investigate the effect of the environmental medium (generally ignored) on a freezing droplet. We show that depending on the ambient conditions a liquid cavity can be entrapped below an ice shell encapsulating the droplet. The internal liquid cavity continues to solidify and consequently can drastically change the final fate of the freezing droplet, explaining non-smooth asymmetric frozen droplets observed in experiments.

References

[1] S. Lyu, K. Wang, Z. Zhang, A. Pedrono, C. Sun and D. Legendre, J. Comput. Phys. 432, 110160 (2021).

[2] J. B. Dupont and D. Legendre, J. Comput. Phys. 229, 2453 (2010).

[3] D. Legendre and M. Maglio, Comput Fluids 113, 2 (2015).

[4] A. G. Marın, O. R. Enrıquez, P. Brunet, P. Colinet and J. H. Snoeijer, Phys. Rev. Lett. 113, 054301 (2014).

Direct Numerical Simulation of Atomization of Vaporizing Liquids

Y. Ling[1], B. Boyd[2] and T. Mahmood[1]

[1]Department of Mechanical Engineering, Baylor University, Waco, Texas, USA
[2]Department of Mechanical Engineering, University of Canterbury, Christchurch, New Zealand
Contact E-mail : stanley_ling@baylor.edu

A novel simulation framework has been developed in this study for the direct numerical simulation of the breakup of vaporizing bulk liquids. The interfacial multiphase flow with phase change is resolved using a consistent geometric volume-of-fluid method. A novel method is proposed to distribute the volumetric source induced by vaporization at the interfacial cells, to the neighboring pure gas cells. With this simple but elegant treatment, the velocity at the interfacial cells is not influenced by the Stefan vapor flow and can be used to advect the interface directly. The newly developed numerical methods are implemented in the solver, *Basilisk*, in which the adaptive octree/quadtree mesh is used for spatial discretization. The simulation framework is extensively validated by a series of benchmark cases, including the 1D Stefan and the 2D film boiling problems. Furthermore, 2D axisymmetric simulations were performed to resolve the vaporization of a moving drop with a low Weber number in a high-temperature free stream. The computed rate of volume loss agrees well with empirical correlations for Reynolds numbers varying from 20 to 200. The validated solver is then used to simulate the breakup of an acetone drop in a high-temperature and high-speed gas stream. The free-stream gas velocity, pressure, and temperature are chosen to be similar to the post-shock conditions for Mach number 1.6, though the present simulation has neglected the effects of shock-drop interaction and compressibility. A fully 3D simulation is performed, and the morphological evolution of the drop is accurately resolved. The rate of vaporization is found to be significantly enhanced due to the drop deformation and breakup. The drop volume decreases nonlinearly in time and at a much higher rate than the empirical correlation for a spherical drop.
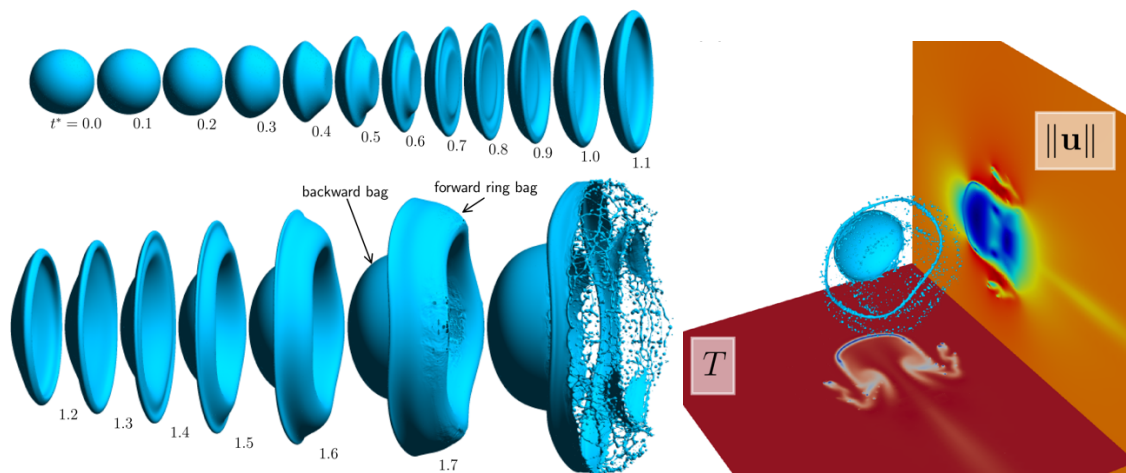
Figure 1. Breakup of a vaporizing liquid drop in a high-temperature and high-sped flow.

Liquid Velocity and Turbulence Measurements in Air-water Bubbly Flows using PIV-PLIF

**Qingqing Liu[1], Hanxing Sun[2], Yang Liu[2], Ted Worosz[3],
John Buchanan Jr.[3], and Xiaodong Sun[1*]**

[1]: Department of Nuclear Engineering and Radiological Sciences, University of Michigan
Ann Arbor, MI 48109-2104, USA
[2]: Nuclear Engineering Program, Mechanical Engineering Department, Virginia Tech
635 Prices Fork Road, Blacksburg, VA 24061, USA
[3]: Naval Nuclear Laboratory, PO Box 79, West Mifflin, PA 15122-0079, USA
Contact E-mail: xdsun@umich.edu

This paper presents an experimental study to measure the liquid-phase velocity and turbulence in an upward air-water two-phase flow loop using a particle image velocimetry-planar laser-induced fluorescence (PIV-PLIF) system. The test section is a confined vertical channel with a cross-section of 30×10 mm^2 and a height of 3.0 m [1]. Experimental data are collected at three instrumentation ports along the test section with normalized axial distances of $z/D_h = 8.8$, 72.4, and 136.0 from the exit of a two-phase injector (i.e., the inlet of the test section). Six bubbly flow conditions are studied with the liquid superficial velocity ranging from 0.4 to 4.0 m/s and the gas superficial velocity ranging from 0.03 to 0.1 m/s.

In the experiments, the void fraction is measured by double-sensor conductivity probes [2]. For the liquid-phase measurements, while the reflection and diffraction of the incident laser are filtered out, the induced fluorescence can also be diffracted and reflected by the gas-liquid interfaces (i.e., bubble surfaces) before being captured by the CCD camera of the PIV-PLIF system. Therefore, the acquired raw PIV images are first pre-processed to remove gas-liquid interface residuals, lower the noise level, and remove overexposed particles [3]. After the image pre-processing, Davis 10.0 (LaVision Inc.) is used to further process the images to obtain the liquid-phase velocity field. The transverse profiles of the time-averaged local liquid velocity, Reynolds stress, turbulence kinetic energy (TKE), and turbulence intensity are obtained from the PIV-PLIF measurements. To derive the bubble-induced turbulence, the liquid velocity and turbulence in single-phase flow are also measured with the liquid velocity ranging from 0.4 to 4.0 m/s. The bubble-induced turbulence is calculated based on the measured two-phase bubbly flow turbulence and the corresponding single-phase turbulence. This study adds a dataset of two-dimensional liquid-phase velocity and turbulence in bubbly flows in a confined flow channel to the literature, which could assist with two-phase turbulence model development and two-phase high-fidelity computational model assessment and validation.

Figure 1 shows the time-averaged streamwise liquid velocity and Reynolds normal stress measured at $z/D_h = 136.0$ (Port 3) for flow condition Run 5: $j_f = 4.0$ m/s and $j_g = 0.03$ m/s. In general, the streamwise liquid velocity (w) and Reynolds normal stress (R_{ww}) profiles show good symmetry along the x and y directions (i.e., the width and gap directions of the test section cross

section). The Reynolds normal stress is fairly uniform in the core region, which is due to the relatively uniform void fraction distribution in the bulk flow, but generally increases toward the wall due to wall-induced turbulence and large fluctuations in the boundary layer. Figure 2 shows the measured bubble velocity and void fraction distributions for the same flow condition. For bubbly flows of high bubble Reynolds numbers where the inertia effects are dominant, the bubble interaction with the wall results in an attractive lift force. Therefore, small bubbles tend to move towards the wall region, which causes a wall-peak bubble distribution. Additional results will be presented at the meeting.
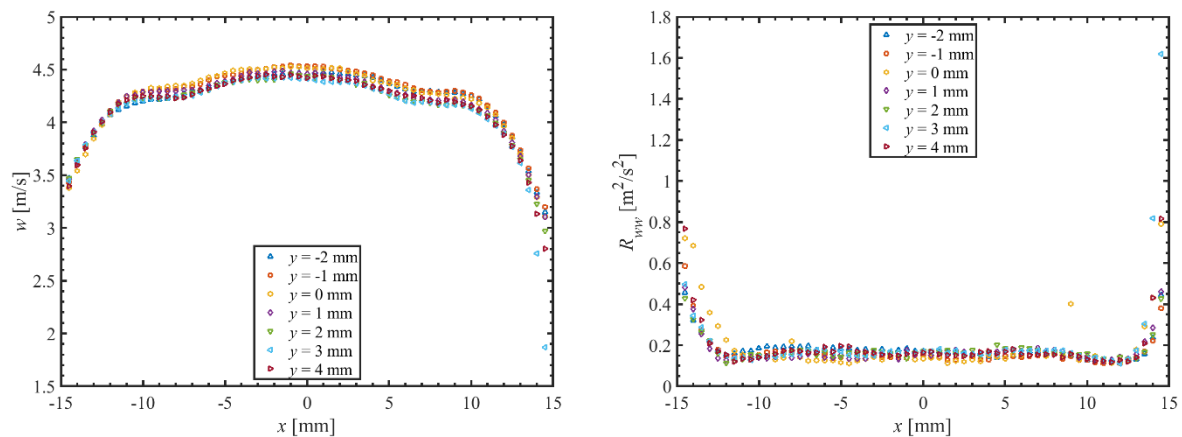

Figure 1. Liquid-phase velocity (left) and Reynolds normal stress (right) at Port 3 for Run 5.
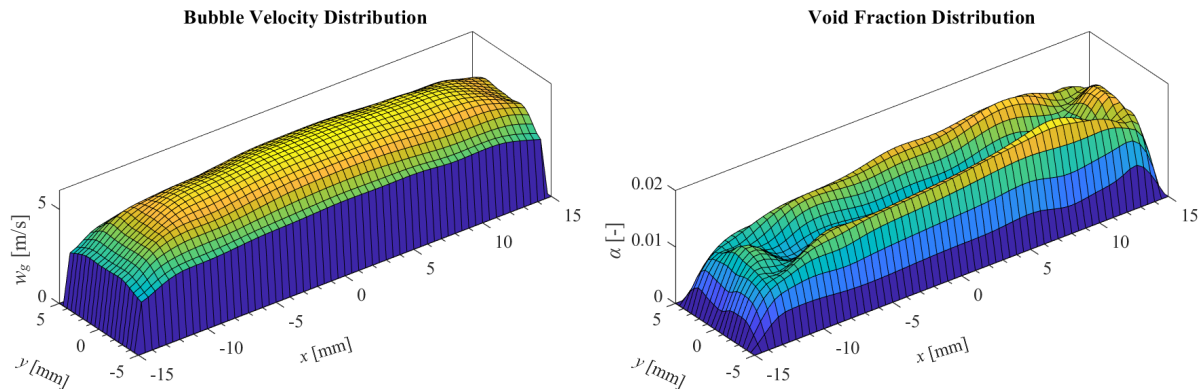

Figure 2. Bubble velocity (left) and void fraction (right) at Port 3 for Run 5

References

1. Fu, Y. and Y. Liu, Experimental study of bubbly flow using image processing techniques, *Nuclear Engineering and Design*, **310**, 570-579, 2016.
2. Wang, D., Fu, Y., Liu, Y., Talley, J.D., Worosz, T., Hogan, K., and Buchanan, J.R., Jr., A comprehensive uncertainty evaluation of double-sensor conductivity probe, *Progress in Nuclear Energy*, **136**, 103741, 2021.
3. Zhou, X., Doup, B., and Sun, X., Measurements of liquid-phase turbulence in gas-liquid two-phase flows using particle image velocimetry, *Measurement Science and Technology*, **24**(12), 125303, 2013.

Influence of contaminations on the flow structure in an aqueous bubble column

H. Hessenkemper and D. Lucas

Helmholtz-Zentrum Dresden – Rossendorf, Bautzner Landstr. 400, 01328 Dresden, Germany
Contact E-mail : d.lucas@hzdr.de

The lateral lift force obviously plays an important role for the transition from the homogeneous to the heterogeneous flow regime in a bubble column. Generally, a positive lift force coefficient, as observed for small bubbles, stabilizes the flow; contrary a negative coefficient, as observed for large deformable bubbles, acts in a destabilizing way. Lucas et al. (2005) derived a stability criterion by means of a stability analysis. For a discrete or continuous bubble size distribution, the respective stability parameters were introduced as follows:

$$\sum_i^N \frac{\alpha_i C_{L,i} d_{b,i}}{C_{D,i}} > 0 \quad , \quad \int_0^\infty \frac{C_L(d_b) \frac{d\alpha}{dd_b} d_B}{C_D(d_b)} dd_b > 0 \quad .$$

Lucas and Ziegenhein (2019) presented experiments in a rectangular bubble column to check the validity of this criterion. For that, the gas flow rate was kept constant, but the bubble size distribution was varied by the use of different sparger configurations and sparger needles. To calculate the stability parameter the lift force coefficient obtained for single bubbles in deionized water was used. The criterion above was well confirmed in these experiments.

Recently the setup to determine the lift force coefficient was used to determine a new correlation valid for deionized and tap water (Hessenkemper et al., 2021a) and to investigate the influence of contaminations (Hessenkemper et al., 2021b). While the correlation for water is rather close to the correlation of Tomiyama et al. (2002), it was shown that contaminations may change the lift force for small bubbles drastically. While very small concentrations of 1-Pentanol (up to about 350 ppm) caused an increase of the coefficient, larger contaminations lead to a decrease and at a concentration of 1000 pm only very small values very obtained for all bubble sizes.

This work presents results of experiments investigating bubbly flows in a rectangular bubble column with a width of 112.5 mm, a depth of 50 mm and a height of 2000 mm with and without contaminations. The gas flow rate was kept constant at 1 l/min for all experiments. Different sparger needles and sparger combinations were used to vary the bubble size distribution. However, because of the influence of the contamination on the initial bubble sizes it is not possible to compare cases with different contaminations and the same bubble size distribution directly. That makes the interpretation of the results more complex.

There is a clear effect of the contamination of the flow structure in the bubble column, which is characterized by the spanwise profiles of the gas volume fraction and the liquid velocity as shown in Fig. 1. The stability parameter is estimated for each single experiment based on the results obtained by Hessenkemper et al., 2021b. The role of the lift force on the modification of the flow structure is discussed on this basis.
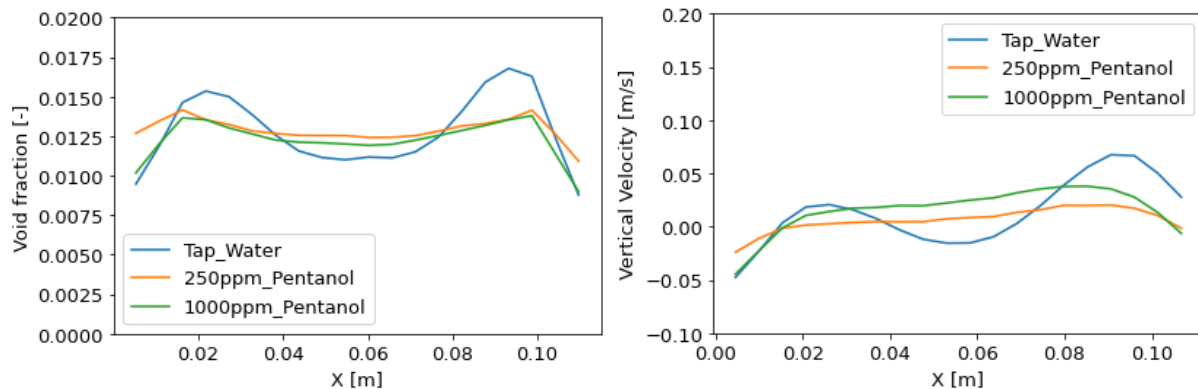

Figure 1. Void fraction profiles (left) and liquid velocity profiles (right) 1600 mm above the inlet.

References

Hessenkemper, H., Ziegenhein, T., Rzehak, R., Lucas, D., Tomiyama, A., 2021a. Lift force coefficient of ellipsoidal single bubbles in water. Int. J. Multiph. Flow 138, 103587.

Hessenkemper, H., Ziegenhein, T., Rzehak, R., Lucas, D., Tomiyama, A., 2021b. Influence of surfactant contaminations on the lift force of ellipsoidal bubbles in water. Int. J. Multiph. Flow 145, 103833.

Lucas, D. , Prasser, H.-M. , Manera, A. , 2005. Influence of the lift force on the stability of a bubble column. Chem. Eng. Sci. 60 (13), 3609–3619.

Lucas, D., Ziegenhein, T., 2019. Influence of the bubble size distribution on the bubble column flow regime. Int. J. Multiph. Flow 120, 103092.

Tomiyama, A., Tamai, H., Zun, I., Hosokawa, S., 2002b. Transverse migration of single bubbles in simple shear flows. Chem. Eng. Sci. 57, 1849–1858.

Two-phase frictional pressure gradient: to what extent are the ANN-based methods able to replace the deterministic models?

A.W. Mauro[1], R. Revellin[2], L. Viscito[1]

[1]Dept. of Industrial Engineering, Università degli Studi di Napoli Federico II. P.le Tecchio 80, 80125, Napoli (Italy)
[2]Univ de Lyon, INSA Lyon, CNRS, CETHIL, UMR5008, 69621 Villeurbanne, France
Contact E-mail : wmauro@unina.it

Two-phase flow frequently occurs in a wide range of applications of any kind, from gas/liquid streams in pipes employed in chemical and petroleum industries or natural gas transfer lines, to vapor/liquid flows of refrigerants inside tubes during convective evaporation or condensation in refrigeration and air-conditioning systems.

The correct prediction of the frictional pressure gradient during two-phase flow is therefore of utmost importance for a correct design of condensers and evaporators, as well as for the estimation of the pumping power required to transport two-phase fluids in all pipelines. On this regard, while pressure losses in a single-phase flow are correctly modeled with well-known expressions, accurate predictions of the frictional pressure gradient in two-phase flow have been proved to be more challenging because of added complexities related to the coexistence of the liquid and the vapor phase and their relative motion and distribution.

Over the last decades, different prediction methods have been proposed by several researchers. They can be mainly classified in two categories, namely homogeneous models and separate flow models, including mechanistic approaches and flow pattern-based correlations. Despite this great effort in developing an efficient predictive method, the correlation results are still not completely accurate if tested outside their original database, since significant assumptions of physical phenomena are involved. For this reason, the Artificial Intelligence (AI) can emerge as a very powerful tool of estimating or predicting data without an explicit understanding of the physical mechanism and are recommended to high non-linear applications and complex engineering problems [1]. Among the available AI techniques, Artificial Neural Networks (ANNs) imitate the neural aspect of the human brain, in which learning is based on experience and repetition rather than the application of principles and equations, and consist of a layered network of neurons, each of them connected to a large number of others [2].

In this context, the main objective of this work is to evaluate to what extent these innovative tools can be employed in successfully predicting the two-phase frictional pressure gradient, with respect to the accuracy of deterministic models. Different neural networks are then developed and a critical analysis is carried-out, testing their accuracy and sensibility by changing the ANN structure and the number of the input parameters. The assessment of some benchmark correlations and of the developed ANNs is finally proposed by using a large database made up of more than 8000 frictional pressure loss points in a wide range of operating conditions in terms of mass flux, reduced pressure, tube diameter and vapor quality.

References

[1] Cong, T., Su, G., Qiu, S., Tian,W., 2013. Applications of ANNs in flow and heat transfer problems in nuclear engineering: A review work. Prog. Nucl. Energy 62, 54–71. http://dx.doi.org/10.1016/j.pnucene.2012.09.003.

[2] Alizadehdakhel A., Rahimi M., Sanjari J., Alsairafi A.A., 2009. CFD and artificial neural network modeling of two-phase flow pressure drop, Int. Communication in Heat and Mass Transfer 36, 850-856. doi:10.1016/j.icheatmasstransfer.2009.05.005

Selected Aspects of Flow Boiling of R1233zd(E) at Medium and High Reduced Pressures

D. Mikielewicz

[1]Gdańsk University of Technology, Faculty of Mechanical Engineering and Ship Technology
Contact E-mail : dariusz.mikielewicz@pg.edu.pl

Recently there is observed an increased interest in development of new heat transfer installations where either flow boiling or flow condensation is employed under conditions close to the thermodynamic critical point. For example mentioned here can be the organic Rankine cycle (ORC) installations as well as high temperature heat pumps (HTHP) which are very attractive options for example in recovery of heat from industrial processes or waste heat. In these applications either new fluids are implemented or the known ones are used under conditions reaching the thermodynamic critical point. Prediction of pressure drop and heat transfer under such conditions can usually be made using empirical methods using models developed for specific fluids. Such methods suffer from not being general and cannot be applicable to a variety of fluids. Most of the experimental evidence of pressure drop and heat transfer characteristics come from the refrigeration applications. Literature review shows a gap in knowledge on flow boiling of low boiling point liquids at high saturation temperatures (above 120°C) for medium/high values of reduced pressure (0.5-0.9). Experimental data can be found in literature for similar values of reduced pressure but for the lower values of the saturation temperature. Most of the data presented in the literature relate to saturation temperatures in the range -20°C to 40°C due to the application of such fluids in refrigeration technology. With the increase in saturation temperature to and above critical values, reduced pressure increases, the density and viscosity of the vapor phase rises, while the opposite trend is noticed for the liquid phase. These influences directly contribute to velocity increase of liquid phase and reduction of the vapor phase, what results in similar values of the phase velocities. The increase in the reduced temperature also leads to reduction in surface tension, what renders gravitational forces to become dominant. Prediction of pressure drop and heat transfer under such conditions is very challenging. Existing two-phase pressure and heat transfer models rarely include the reduced pressure effect on their performance. Thermal-hydraulic mechanisms associated with strong changes in physical properties of working fluids near the critical point are responsible.

In the presentation attention will be focused on the accomplished experimental study of flow boiling of R1233zd(E) with particular focus on the influence of reduced pressure on the predictions of heat transfer during flow boiling at the high range of pressures. The experimental

results will also be compared with an in-house flow boiling model with respect to the selection of the appropriate two-phase flow multiplier, which is one of the distinctive elements of that model. For this purpose a few two-phase frictional pressure drop correlations were tested. In the paper are presented the results of calculations using the authors' own model to predict heat transfer coefficient during flow boiling. The model has been tested against a large selection of experimental data collected from various researchers to investigate the sensitivity of the in-house developed model on selected experimental flow boiling data of the following refrigerants: R134a, R1233zd(E), R1234yf, R600a and CO2.

Effect of Bilayer Porous Metal body on Critical Heat Flux Enhancement in a Saturated Pool Boiling

Shoji Mori [1] , Tadashi Sekiguchi [1], and Yuya Hayashida [1]

[1]Department of Mechanical Engineering, Kyushu University
744 Motooka, Nishi-ku, Fukuoka, 819-0395, Japan
Contact E-mail : morisho@mech.kyushu-u.ac.jp

In the present paper, we propose a critical heat flux (CHF) enhancement technique using a two-layer structured honeycomb porous plate (HPP). In a previous study, the CHF during saturated pool boiling of water was investigated experimentally using an HPP attached to a heated surface and was shown to be enhanced to more than twice (2.0 MW/m^2) that for a plain surface. According to the proposed capillary limit model as shown in Fig.1, the CHF can be increased by decreasing the thickness of the HPP because of the decrease in the frictional pressure drops caused by the liquid flow in the porous medium. However, the CHF could not be greatly enhanced when the thickness of the HPP was comparable to the thickness (approximately 100 μm) of the thin liquid film (the macro-layer thickness) formed beneath coalescent vapor bubbles. Based on the observation of the boiling configuration near the CHF, a large coalesced bubble forms on the heated surface and departs periodically as shown in Fig.2. Therefore, the CHF may occur when water contained in a porous material disappears due to evaporation during the bubble hovering period. In order to prevent the dry-out phenomenon during the hovering period of a large coalesced bubble and enhance the CHF, we herein propose that the structure of HPPs should be improved by the superposition of two kinds of HPPs shown in Fig.3 and that each of the HPPs must satisfy two conditions. First, an HPP simply attached to a heated surface should have very fine pores to supply water to the heated surface due to strong capillary action, and the HPPs should be as thin as possible in order to decrease the pressure drop caused by internal water flow. Second, the other HPP, which is stacked on top of the thin HPP, must be structured to hold a sufficient amount of water in order to prevent the inside of the HPP from drying out during the bubble hovering period over the plate. A metallic two-layer HPP was prepared by electrodeposition(Fig.4), and the CHF was enhanced more than four times(465 W/cm^2) higher than that of the bare surface.
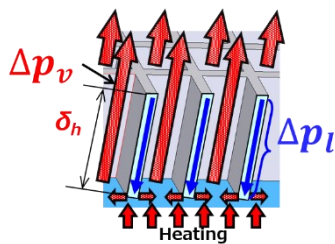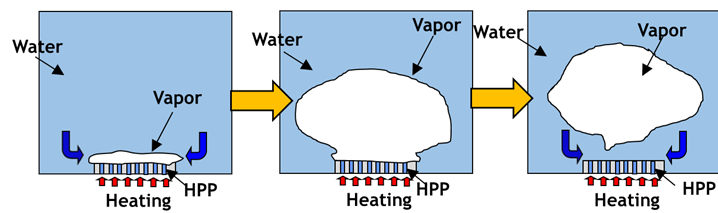
Fig.1 Capillary limit model

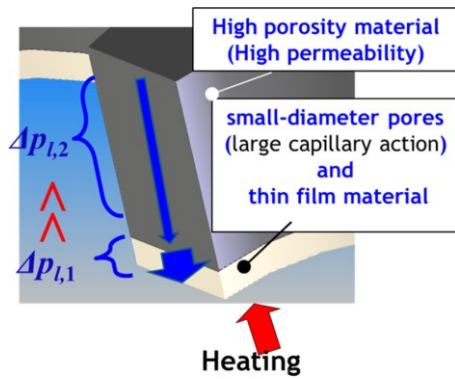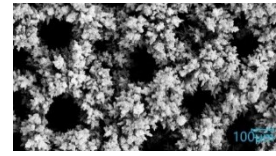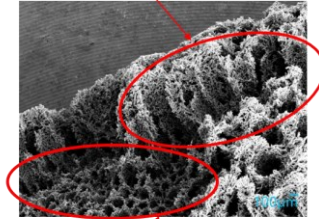Fig.2 Growth processes of the coalesced bubbles on an HPP.

Fig.3 Schematic diagram of a bilayer structured HPP capable of further enhancing the CHF.

Observed from above

Fig.4 SEM of porous metal prepared by electrodeposition method.

Numerical simulation of conjugate heat transfer effects on flow boiling in a multi-microchannel evaporator

F. Municchi[1], I. El Mellas[2], O. K. Matar[3], M. Magnini[2]

[1]Colorado School of Mines, 1500 Illinois St., Golden, CO 80401
[2]Department of Mechanical Engineering, University of Nottingham, NG7 2RD Nottingham, UK
[3]Department of Chemical Engineering, Imperial College London, London SW7 2AZ, UK
Contact E-mail : mirco.magnini@nottingham.ac.uk

While the recent advances in manufacturing technology enabled mass production of devices operating at high power densities (e.g., microelectronics, batteries, miniature fuel cells, etc.), they also led to a dramatic surge in the pressure for developing efficient cooling systems. Since such high-power devices tend to produce heat fluxes on the order of several MW/m^2, they require a heat-removal capability beyond that of traditional single-phase cooling systems, which is generally bounded to less than 1 MW/m^2. Multiphase flows with phase-change represent a viable technological solution since additional energy can be dissipated in the form of latent heat. Despite the large number of experimental studies conducted on boiling heat transfer in microchannels, there is still general disagreement on the underlying dynamics, because the existing experimental techniques cannot yet access the small spatial and temporal scales of the flow with sufficient resolution. This resulted into a lack of clarity about the best channel design to optimise heat transfer. On the other hand, numerical simulations have become a popular research tool to investigate the fundamental aspects of these flows, however, they are often limited to models reproducing only the fluidic part of the channel, while disregarding the solid material. Since two-phase flow in microchannels is typically arranged in multi-microchannel evaporators, where the heat sink is heated from one side only, and heat is transferred to the fluid through the evaporator base wall and the fins separating adjacent channels, the conjugate heat transfer between solid and fluid should be accounted for, in order to reproduce practical flow configurations. To mitigate the aforementioned shortcomings in the available literature, we have performed a systematic analysis of the impact of channel aspect-ratio and channel fins thickness on the bubble dynamics and boiling heat transfer performances of a microchannel. We emulate the unit channel of a multi-microchannel evaporator, which is composed of evaporator base and lateral channel fins; see Fig. 1(a). The heat load is applied to the evaporator base. The top of the channel is adiabatic. The lateral boundaries are symmetric. A fully-developed flow of liquid enters the channel at saturated conditions. Numerical simulations are performed using OpenFOAM v2106 and a self-developed Volume-Of-Fluid (VOF) solver which accounts for phase-change and conjugate heat transfer across the microchannel walls. The geometry and operating conditions are taken from the experimental work of Mukherjee et al. [1], that was considered as a validation benchmark. The microchannel has a hydraulic diameter of $D_h = 229$ μm and length of $20D_h$. The working fluid is water at the saturation pressure of $p_{sat} =$

1 atm. Width-to-height channel aspect-ratios of $\epsilon = W/H = 0.25 - 4$ are investigated, with W and H being the channel width and height, respectively. Thicknesses of the lateral fins in the range $W_f = D_h/8 - D_h$ are tested. The evaporator base thickness is fixed to an arbitrary value of 56 μm. The base heat load is $q_b = 100 \ kW/m^2$. The mass flux of water at the inlet is $G = 140 \ kg/(m^2 s)$. As initial condition, the velocity and temperature field in both liquid and solid regions are set according to preliminary steady-state liquid-only results, and a small vapour bubble of initial diameter of 50 μm is patched at the centre of the bottom wall. A contact angle of 30 degrees (hydrophilic wall) is set to all fluidic boundaries. Simulations are run till the bubble reaches the channel end. Figure 1(b) and (c) illustrate a snapshot of the numerical results extracted while the bubble is halfway through the channel, for aspect-ratio $\epsilon = 0.5$ and fin width $W_f = D_h/4$. The high heat transfer induced by the triple liquid-vapour-solid contact line is very effective in cooling down the internal surface of the walls, while the thermal inertia of the walls tends to dampen this effect when observed from the outside surface.

This study shows that, when conjugate heat transfer is considered, the temperature distribution on the walls at the fluid-solid boundary is much more uniform than what observed in simulations run without solid regions, where much higher temperatures are achieved at the corners of the channels. In single-phase flow, low aspect-ratio channels yield higher Nusselt numbers and lower evaporator base temperatures. In two-phase flow, the Nusselt number exhibits non-monotonic trends versus the aspect-ratio and these depend on the channel fins width, though low aspect-ratio channels seem to systematically lead to lower evaporator temperatures. The full results of this study are presented in a recent article from the authors [2].

References

[1] A. Mukherjee, S. G. Kandlikar, Z. J. Edel, "Numerical study of bubble growth and wall heat transfer during flow boiling in a microchannel", Int J. Heat & Mass Transfer, vol. 54, pp. 3702-3718, 2011.
[2] F. Municchi, I. El Mellas, O. K. Matar, M. Magnini, "Conjugate heat transfer effects on flow boiling in microchannels", Int J. Heat & Mass Transfer, vol. 195, 123166, 2022.
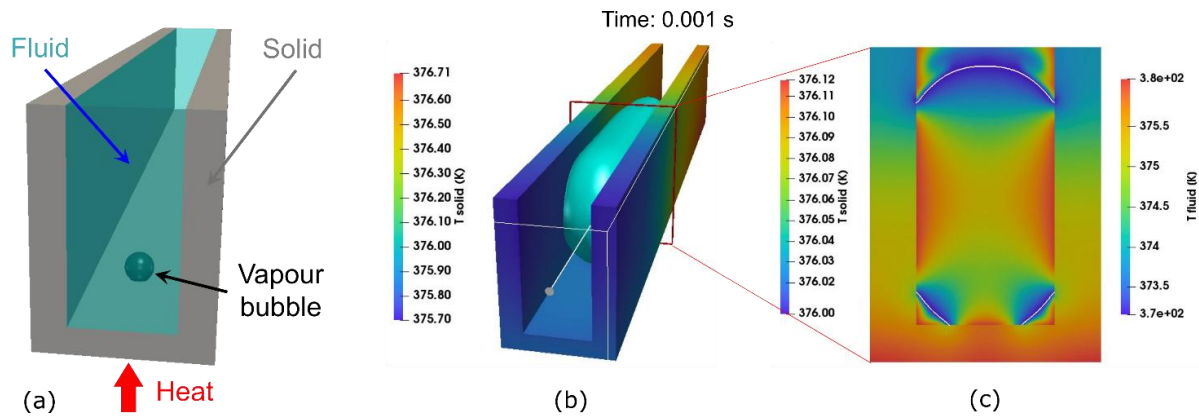
Figure 1. (a) Simulation setup for conjugate heat transfer analyses. (b) Snapshot of the bubble (in light blue) and temperature distribution in the walls and (c) temperature fields within fluid and walls on a cross-section extracted from (b); the white line in (c) identifies the liquid-vapour interface. The images refer to aspect-ratio $\epsilon = 0.5$ and fin width $W_f = D_h/4$.

EAJTPFGM22
CHAMONIX
— FRANCE —

Bubble splitters for a bubbly turbulent boundary layer

Y. Murai, R. Aoki, H. J. Park and Y. Tasaka

Laboratory for Flow Control, Hokkaido University, Sapporo, Japan
Contact E-mail : murai@eng.hokudai.ac.jp

Bubbly drag reduction on marine vessels is now in the stage of practical applications [1]. Recent technical concern is how to provide the bubbles in the best size into the turbulent boundary layer[2]. On this purpose, some devices that can promote bubble fragmentation in a bubbly two-phase turbulent boundary layer were examined experimentally. Using a 10 m-long horizontal water channel at the flow velocity of 1.1 m/s (Re=44,000), three kinds of array shown in Fig. 1 were attached on the upper surface where bubbles slide within a turbulent boundary layer. Ordinarily, bubbles will show their size at dynamically equilibrium condition between the surface tension and the shear stress in liquid[3][4][5]. This was realized inside the channel, having 5 mm in average as shown in Fig. 1. An array of finite cylinders (FC) promoted bubble fragmentation the most. An array of vortex generator (VG) slightly reduced the average size. Use of small hydrofoils (SH) breaded small bubbles.
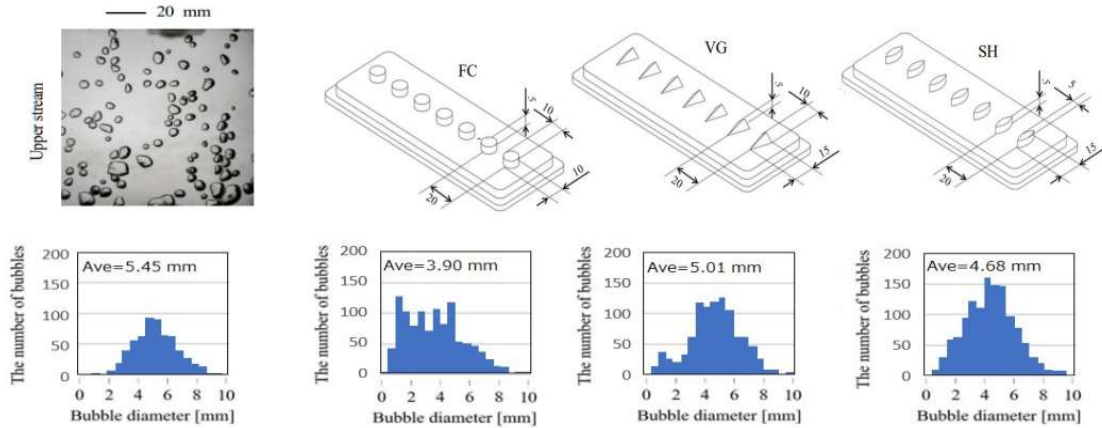

Figure 1. Performance of three different bubble splitter devices for horizontally sliding bubbles

According to these experimental results, we evaluated energy efficiency of the bubble fragmentation with following theories. When a single bubble of the initial radius r_1 is split into n, increase of surface energy is described as

$$e = \frac{8}{3}\pi\sigma r_1^2 \left(n^{1/3} - 1\right), \tag{1}$$

where σ is surface tension. Hence, the power required for the bubbles migrating at the velocity U with an interval λ is estimated by

$$L_B = \frac{U}{\lambda} e = \frac{2}{3} \pi \frac{U \sigma d^2}{\lambda} \left(n^{1/3} - 1\right), \quad d = 2r_1. \tag{2}$$

On the other hand, the power consumed for a single protrusive object with a height H and a width D in the array of the bubble splitter can be estimated by

$$L_D = F_D U = C_D \frac{1}{2} \rho U^3 HD, \quad F_D = C_D \frac{1}{2} \rho U^2 HD. \tag{3}$$

From Eqs. (2) and (3), the energy efficiency of bubble fragmentation is defined as

$$\eta = \frac{L_B}{L_D} = \frac{4}{3} \pi \frac{\sigma d^2}{C_D \rho U^2 HD\lambda} \left(n^{1/3} - 1\right) \tag{4}$$

Denoting Eq. (4) with a void fraction inside the boundary layer α, the efficiency is evaluated by

$$\eta = \frac{8}{C_D \cdot We} \cdot \frac{W}{D} \cdot \alpha \left(n^{1/3} - 1\right), \quad \alpha = \frac{\pi d^3/6}{HW\lambda}, \tag{5}$$

Where W is the spanwise spacing of the objects.

Using Eq. (5), the experimental data were processed to discuss on the difference in the energy efficiency as shown in Fig. 2. While the average number of fragmentations is the highest for SH, the energy efficiency is the highest for VG. This is explained by the smallest drag acting on the vortex generators among the three types of the array.
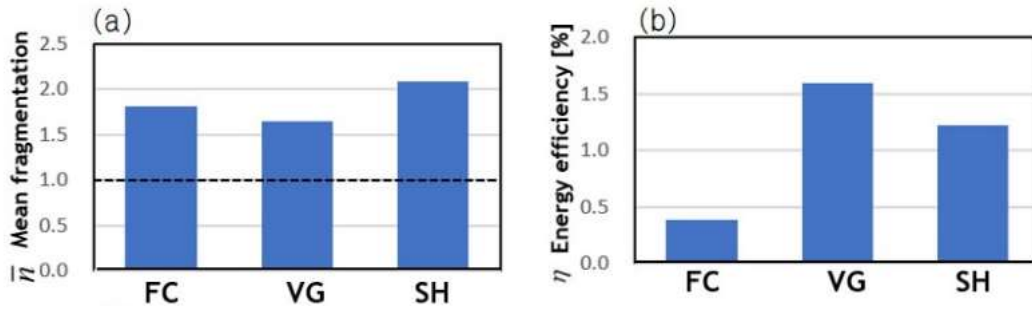

Figure 2. Comparison of statistic performance of three different bubble splitter devices

References
[1] American Bureau of Shipping, 2019. Air lubrication technology. https://ww2.eagle.org/.
[2] Murai, Y., Exp. Fluids, Vol. 55, 1773 (2014)
[3] Hinze, J. O., AIChE J., Vol. 1, 289–295 (1955)
[4] Sanders, W.C. et al., J Fluid Mech, Vol. 552, 353–380 (2006)
[5] Makiharju, S.A. et al., Int. J. Naval Arch. Ocean Eng., Vol. 4, 412-422 (2012)

Behaviour of Bubble Chain in Gallium Eutectic Alloy under Influence of Transverse Magnetic Field

H. Murakawa[1], X. Fu[1] and K. Adachi[1]

[1] Graduate School of Engineering, Kobe University
Contact E-mail : murakawa@mech.kobe-u.ac.jp

In the continuous casting process, argon gas is injected into the tundish to homogenize the melting steel and remove the undesired inclusion [1]. Furthermore, the molten steel flow is controlled by applying a magnetic field to the mold. The inclusion of argon gas as the molten steel flows into the mold can lead to product defects. Therefore, it is essential to predict the motion of the bubble in liquid metals under influence of the magnetic field. To clarify the effect of the magnetic field on the bubble-bubble interaction, the motion of a single-chain bubble in gallium eutectic alloy under influence of a horizontal magnetic field is investigated in this study. A high-speed ultrasonic tomography (UT) system [2] was employed for evaluating the bubble position and bubble shape of continuously released bubbles in a circular pipe with an inner diameter of 50 mm. The measurements were carried out at 500 frames/s both at the bottom and upper position in the container. Furthermore, the bubble rising velocities were evaluated using the pulsed Doppler method with changing of the magnetic field strength.

Figure 1 shows a schematic of the experimental setup. The test container was made of an acrylic resin pipe with an inner diameter of 50 mm. The working fluids were nitrogen gas and gallium eutectic alloy which is a liquid at room temperature. Ultrasonic tomography measurements were carried out at 40 mm or 160 mm from the bottom. Bubble rising velocities were measured from the bottom using the pulsed Doppler method. A horizontal magnetic field with a maximum magnetic field strength of 412 mT was applied by changing the current applied
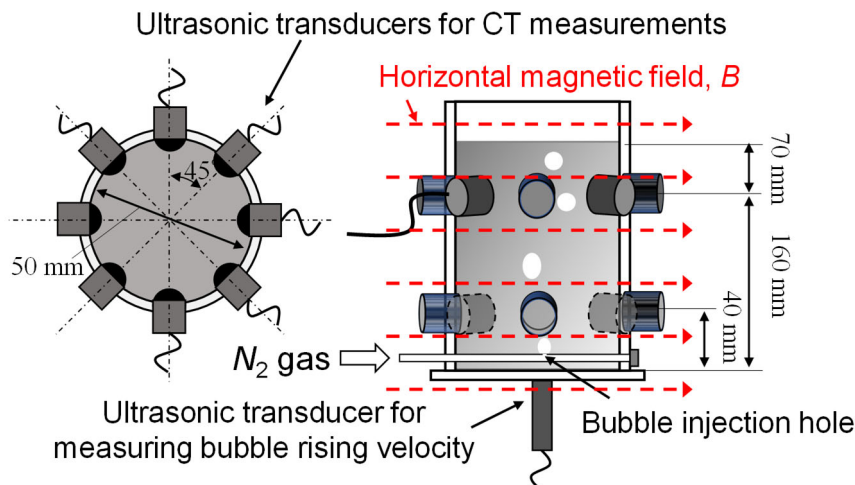

Figure 1. Schematic representation of the test section

to the electromagnet.

Figure 2 shows the change in bubble rising velocity, V_b, with bubble detachment frequency, f, and the Stuart number, $N = \sigma_l B^2 d_e / \rho_l V_T$, where B is the magnetic field strength, σ_l is the electrical conductivity of the gallium eutectic alloy, d_e is the equivalent bubble diameter, ρ_l is the liquid density and the V_T is the terminal velocity of bubbles. In this study, N was calculated by assuming that the $V_T = V_b$. It can be seen that the change in V_b with the N differs depending on f. At $f = 1$ and 2 Hz, V_b increases under influence of the magnetic field and reaches the maximum velocity around $N = 0.5$. When the magnetic field strength was further increased, V_b decreased. At $f = 4$ and 5 Hz, the V_b takes maximum values without magnetic field, $N = 0$. With increases of the N, V_b tends to decrease. Figure 3 shows overlay images of four two-dimensional intensity distributions of rising bubbles at the upper measurement position ($f = 1$ Hz). It can be seen that as the magnetic field strength increases, the bubbles crossing the measurement position become closer to the centre of the container. Although the CT measurement evaluates the bubble passage position in a particular cross-section, it is considered that the electromagnetic force caused by the bubbles' movement increased due to the increase in the magnetic field strength. As a result, it is assumed that the wobbling motion of the bubbles was suppressed resulting in rising bubbles almost straitly in the liquid metal.
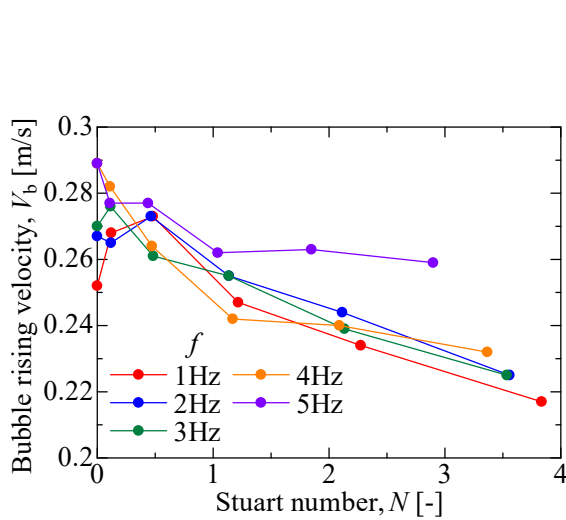

Figure 2. Change in bubble rising velocity with Stuart number and the bubble detachment frequency
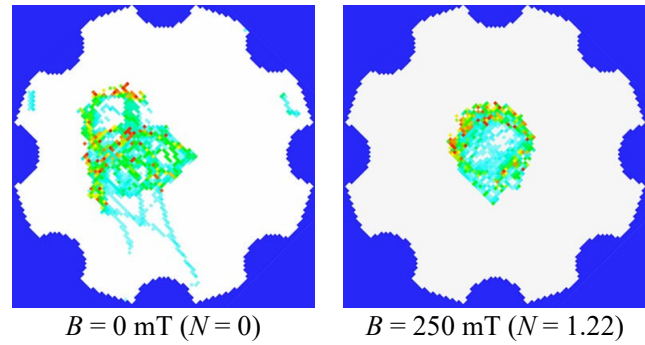
Figure 3. Overlay images of four two-dimensional intensity distributions of rising bubbles in a gallium eutectic alloy at the upper measurement position ($f = 1$ Hz)

References
[1] L. Zhang, *et al.*, Inclusion removal by bubble flotation in a continuous casting mold, Metallurgical and Materials Transactions B, 37, pp. 361–379, 2006.
[2] H. Murakawa, *et al.,* Development of a high-speed ultrasonic tomography system for measurements of rising bubbles in a horizontal cross-section, Measurement, 182, 109654, 2021.

Fragmentation of Liquid Drop Falling through Miscible Liquid due to Rayleigh-Taylor Instability

R. Nakajima[1] and K. Hayashi[2]

[1]Tennoji High School Attached to OKU, [2]Graduate School of Engineering, Kobe University
Contact E-mail : hayashi@mech.kobe-u.ac.jp

Fragmentation of a liquid drop falling through a miscible liquid was studied by Thomson and Newall (1886) more than hundred years ago. A drop shape becomes torus (vortex ring) and child drops are formed from some parts of the ring. After a century from Thomson and Newall, Arecchi et al. (1989) carried out a series of experiments on the fragmentation and discussed a scaling law of fragmentation. Shimokawa and Sakaguchi (2016; 2019) also carried out experiments on fragmentation of drops released from a nozzle placed 8 mm above the free surface. They pointed out that the number, m, of child drops formed from a ring increases with increasing the Archimedes number, Ar, for $Ar < 80$ and proposed a prediction model based on the growth of disturbances by the Rayleigh-Taylor instability. In this presentation, we will show the characteristics of m for a larger Ar range up to 1000 (Figure 1, 2), in which range m slightly decreases as Ar increases (Figure 2), and this trend different from that in the low Ar range can be understood from the change in the dominant force in the ring growth. Effects of the drop formation on m and the width of the fragmented drop will also be discussed.
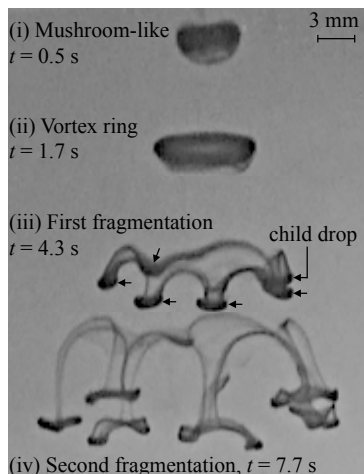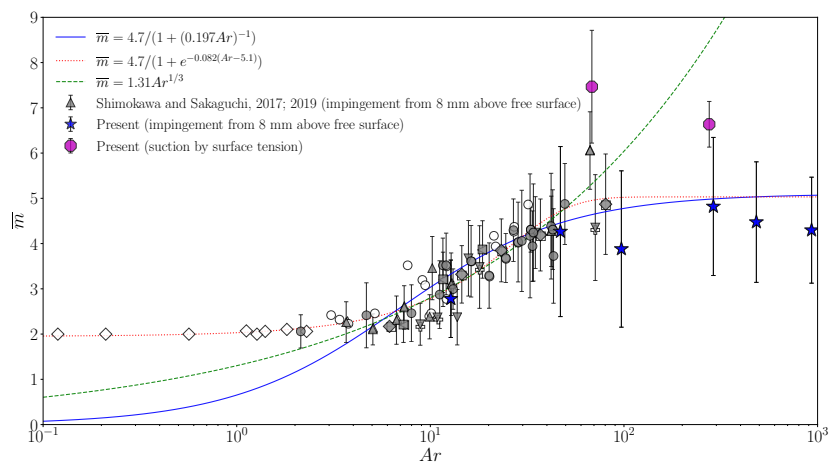
Figure 1. Fragmentation of drop   Figure 2. Number of child drops formed by fragmentation

Thomson and Newall, Proc. R. Soc. Lond. Ser. A Math. Phys. Eng. Sci., 39, 417-436, 1886
Arecchi et al., Europhys. Let., 15(4), 429-434, 1989
Shimokawa et al., Phys. Rev. E, 93, 062214, 2016
Shimokawa and Sakaguchi, Phys. Rev. Fluids, 4, 013603, 2019

Multiscale deformation and breakup in turbulence

Yinghe Qi, Shiyong Tan, Noah Corbitt, Carl Urbanik, Ashwanth K. R. Salibindla & Rui Ni
[1]Johns Hopkins University
Contact E-mail : rui.ni@jhu.edu

From air-sea gas exchange to flotation bioreactors, fragmentation of bubbles, particles, oil droplets in turbulence constitutes one of the most basic and practically important processes in turbulent multiphase flow. Most phenomenological models and simulations for this problem have been developed based on the classical Kolmogorov-Hinze framework, even though some of the key assumptions have never been tested and challenged. In this talk, I will first introduce a new experimental framework that measures the geometry of breaking bubbles and their surrounding turbulence simultaneously in 3D. From this new result, I will discuss two issues that we found in the classical framework: (i) the Kolmogorov's classical theory of turbulence is not sufficient for quantifying the turbulent stresses on the bubble interface, and (ii) the assumption that the most relevant and energetic scale of the flow is at the bubble diameter is incorrect. Here, by designing an experiment that can physically and cleanly disentangle eddies of various sizes, we report the experimental evidence to challenge this hypothesis and show that bubbles are preferentially broken by the sub-bubble-scale eddies. Our work also highlights that fragmentation cannot be quantified solely by the stress criterion or the Weber number; The competition between different time scales is equally important. Instead of being elongated slowly and persistently by flows at their own scales, bubbles are fragmented in turbulence by small eddies via a burst of intense local deformation within a short time. Our work underlines the importance of two missing mechanisms and paves the foundation for future studies on the fragmentation of bubbles, droplets, and particles in turbulence.
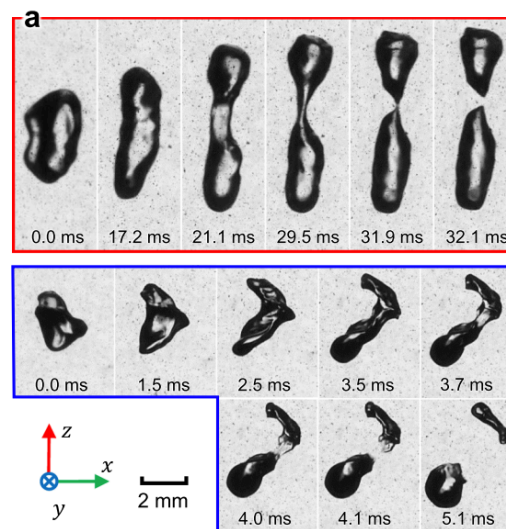
Figure 1. Examples of a primary breakup (red) driven by a smooth vortex ring and a secondary breakup (blue) driven by a turbulent cloud

Experiment on boiling entrainment from a falling liquid film

T. Okawa[1], J. Tabuchi[1], R. Firman[1], Y. Narushima[2], H. Furuichi[2], and K. Katono[2]

[1]The University of Electro-Communications, [2]Hitachi, Ltd.
Contact E-mail : okawa.tomio@uec.ac.jp

In flow boiling of relatively low mass flux, the critical heat flux condition is reached when a liquid film disappears in annular two-phase flow regime [1]. In annular flow, the liquid film flow rate G_f increases due to droplet deposition m_d and decreases due to droplet entrainment m_e and vaporization m_v. The axial variation of G_f is hence written by

$$\frac{dG_f}{dz} = \frac{4}{D}(m_d - m_e - m_v) \tag{1}$$

where z is the axial coordinate and D is the hydraulic-equivalent flow channel diameter. It is usually assumed that the deposition rate m_d is proportional to the droplet concentration in the vapor core flow and m_e is mainly caused by the shear force exerted by the vapor core flow on the liquid film surface to calculate the critical heat flux using Eq. (1) [2, 3]. Ueda et al. [4] however showed that nucleate boiling can also be an important mechanism to cause droplet entrainment at high wall heat flux. In fact, Barbosa et al. [5] observed that vapor bubbles are formed within a liquid film in annular two-phase flow.

To solve the radioactive waste problem, Hino et al. [6] proposed a new nuclear reactor design called the Resource-renewable Boiling Water Reactor (RBWR). Narushima and Katono [7] showed that the critical heat flux is underestimated if the boiling entrainment that is the droplet entrainment caused by nucleate boiling is neglected. Therefore, to ensure the safety of the RBWR, the boiling entrainment phenomenon should sufficiently be understood.

To explore the mechanisms of boiling entrainment, the process of droplet generation caused by nucleate boiling within a liquid film was observed using a high-speed camera. In the experiment, using water as the test liquid and a falling liquid film was formed in a rectangular flow channel of 15 mm in width, 10 mm in height, and 400 mm in length. Its one side wall of 15 mm in width was heated to cause nucleate boiling. Air was also flowed down along the liquid film to explore the effect of vapor core flow in diabatic annular flow.

In each experimental run, after setting the liquid flow rate J_l, the gas flow rate J_g, and the inlet liquid subcooling ΔT_{sub} at desired values, the wall heat flux q_w was increased step by step. At low heat fluxes, the boiling entrainment was not observed since nucleate boiling did not occur. The value of q_w was high enough, nucleate boiling commenced on the heated surface. As illustrated in Fig. 1(a), a thin liquid film was formed between the vapor bubble and air. The liquid film ruptured eventually to create a crater. Surface tension then acted to vanish the crater to minimize the surface energy. Since the bottom of crater was lifted at this stage, the liquid inertia formed a liquid column or jet that was similar to the central jet produced during droplet impact onto a quiescent liquid film [8]. Finally, droplets were pinched off at the tip of liquid jet to cause droplet entrainment. Since the droplets were produced from the jet tip, this mechanism is classified as the jet-type entrainment. The droplet size was generally small in the jet-type entrainment, and it was 0.15 mm in the case presented in Fig. 1(a). The jet-type entrainment was observed as soon as nucleate boiling was commenced. The wall heat flux was increased further,

the size of vapor bubble became larger. Then, as delineated in Fig. 1(b), during the process of rupture of a thin liquid film, a liquid filament appeared and it was disintegrated into produce a droplet. The size of produced droplets was much larger and it was 0.9 mm in the case presented in Fig. 1(b). It may be supposed that the boiling entrainment occurs when the inertia of the liquid flow induced by nucleation overcomes the surface tension. The present visualization results suggested that the critical condition for the onset of filament-type entrainment can conservatively be estimated by

$$We = \frac{\rho_l u_g^2 L_a}{\sigma} = 1.8 \tag{2}$$

where We is the Weber number, ρ_l is the liquid density, and σ is the surface tension. As for the characteristic scales of length and velocity to calculated We, the Laplace length $L_a = (\sigma/g\Delta\rho)^{1/2}$ and $u_g = q_{nb}/\rho_g\Delta h_v$ were used where g is the gravitational acceleration, $\Delta\rho$ is the density difference between the phases, q_{nb} is the heat flux spent for nucleate boiling, ρ_g is the vapor density, and Δh_v is the latent heat vaporization. To calculate the critical heat flux using Eq. (1), measurement of the rate of boiling entrainment is of primary importance in the future studies.
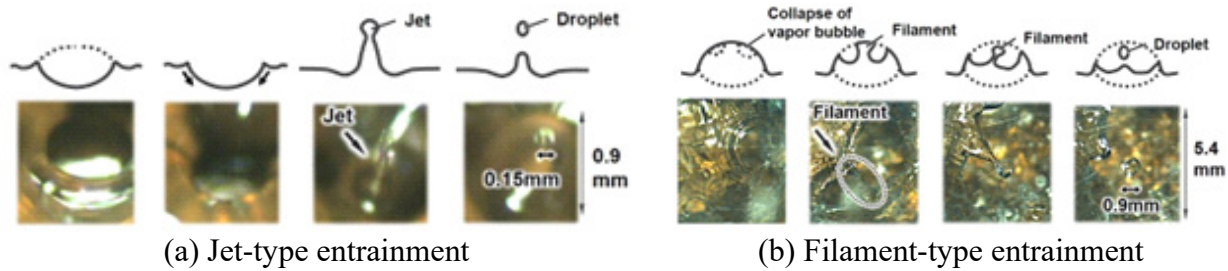
(a) Jet-type entrainment   (b) Filament-type entrainment
Figure 1. Droplet generation processes observed in the two types of boiling entrainment.

Reference

[1] P.B. Whalley, Boiling, Condensation, and Gas-Liquid Flow, Clarendon Press, Oxford, 1987.
[2] T. Okawa, T. Kitahara, K. Yoshida, T. Matsumoto, I. Kataoka, New entrainment rate correlation in annular two-phase flow applicable to wide range of flow condition, International Journal of Heat and Mass Transfer, 45 (1) (2001) 87-98.
[3] T. Okawa, A. Kotani, I. Kataoka, M. Naito, Prediction of critical heat flux in annular flow using a film flow model, Journal of Nuclear Science and Technology, 40 (6) (2003) 388-396.
[4] T. Ueda, M. Inoue, S. Nagatome, Critical heat flux and droplet entrainment rate in boiling of falling liquid films, Int. J. Heat Mass Transf. 24 (7) (1981), 1257-1266.
[5] J.R. Barbosa Jr., G.F. Hewitt, S.M. Richardson, High-speed visualisation of nucleate boiling in vertical annular flow, Int. J. Heat Mass Transf. 46 (26) (2003) 5153-5160.
[6] T. Hino, M. Otsuka, K. Moriya, M. Matsuura, Light water reactor system designed to minimize environmental burden of radioactive waste, Hitachi Rev. 63 (9) (2014) 602-609.
[7] Y. Narushima, K. Katono, Development of CHF prediction method based on the film flow model with nucleate boiling entrainment, in: Proceedings of 18th International Topical Meeting on Nuclear Reactor Thermal Hydraulics, Portland, 2019, pp. 473-383.
[8] T. Okawa, T. Shiraishi, T. Mori, Production of secondary drops during the single water drop impact onto a plane water surface, Experiments in Fluids, 41 (6) (2006) 965–974.

Dispersion of a passive scalar around a Taylor bubble

D. Picchi and P. Poesio

Dept. of Mechanical and Industrial Engineering, University of Brescia, via Branze 38, 25123
Brescia, Italy
Contact E-mail : davide.picchi@unibs.it

The motion of Taylor bubbles in capillaries is typical of many engineering and biological systems, ranging from subsurface flows to small-scale reactors. Although the hydrodynamics of elongated bubble has been object of several studies, the case where a solute is transported in the surrounding liquid and surface mass-transfer mechanisms act on the solid wall or the bubble-fluid interface is much less understood. To fill this gap, we investigate the transport problem around a confined Taylor bubble to access the competition between advection, diffusion, and surface mass-transfer in the different regions of the bubble. To this aim, we derive a one dimensional Advection-Diffusion-Mass-Transfer equation where the transport mechanisms are described through an effective velocity, an effective diffusion coefficient, and an effective Sherwood number. Our model generalises the Aris-Taylor dispersion to the case of a Taylor bubble and clarify the impact of surface mass-transfer in the advection and diffusion dominated regimes for both the front and rear menisci. Interestingly, the effective diffusion coefficient scales with the square of the Péclet number based on the film thickness and, when the Péclet number balances with the Sherwood number, there exist conditions that leads to the formation of hot spots of concentration. We also show that the typical shape oscillations of the bubble rear locally enhance superficial mass-transfer. Finally, we study the transport problem in the uniform film region.
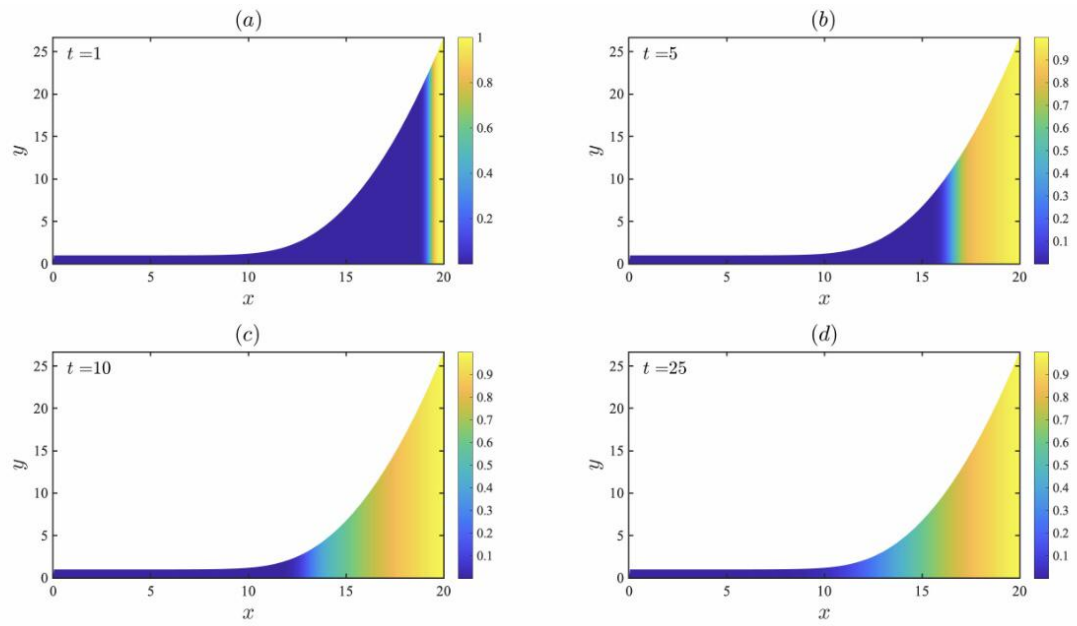
Figure 1. Time evolution of the concentration field in the bubble front.

Low to Moderate Frequency AC Electric Field Effects on Convective Boiling in the Bubbly Flow Regime

S. Ahmadia[2], M. Eraghubi[1], A.J. Robinson[1]

[1] Department of Mechanical, Manufacturing & Biomedical Engineering, Parsons Building, Trinity College Dublin, Ireland.

[2] School of Mechanical Engineering, College of Engineering, University of Tehran, P. O. Box: 11155-4563, Tehran, Iran.

Contact E-mail : arobins@tcd.ie

An experimental investigation has been performed for upward flow boiling of HFE 7000 considering the influence of AC electric fields. The study focusses on EHD augmentation of a baseline bubbly flow regime, here established for the conditions; mass flux of $G=100$ kg/m^{2}s, heat flux of q"=10 kW/m^2, and inlet subcooling of $\Delta T_{sup}=2$ K. The AC high-voltage (10 kV$_{p-p}$) establishes an electric field between a concentric electrode and the low potential tube wall, and tests were performed over a low to moderate frequency range of 1-100 Hz. A related study by Ahmadi et al. (2021) revealed strong evidence of electrophoretic influences for higher (100-10,000 Hz) applied high voltage frequencies. Interestingly, for the initially bubbly flow regime, a peak in heat transfer enhancement was observed at 1000 Hz, and this was hypothesized as being due to the ideal interplay between electrophoretic and polorization forces. For the working fluid tested, HFE 7000, the charge relaxation time based on manufacturer property specifications is about $t_R=65$ ms. It is hypothesized here that stronger interplay between electrophoretic and polarization forces will exist for voltage frequencies that are closer to $f_R=1/t_R=15$ Hz since it will switch between dominant electrophoretic and polarization forces. To this end, an experimental campain was carried out that spans f_R by a decade on either side.

Figure 1 (a) depicts the baseline bubbly flow regime for the 1.0 Hz test case. Subsequent to initialization of the +10 kV square pulse, the vapour bubles are repulsed towards the wall, redistributing the phases, and is indicative of polarization force interaction on the bubbles (t<70 ms in Figs 1 & 2(a)). This short initial phase reditibution is followed by a longer phase where the flow resembles a churn flow (70ms<t<220ms), afterwhich the flow begins to recover and resemble the baseline bubbly flow. When the electrode switches to -10 kV, the bubbles are in fact attracted to the electrode and the vapour held there, which is clear indication of charge injection causing electrophoretic forces that dominate over polarization forces. After a phase commensurate with the charge relaxation time, the vapour gradually entrains into the core liquid flow and bubbly flow is reestablished prior to the next cycle.

Figure 2(b) shows the convective boiling heat transfer coefficient enhancement over the baseline field-free case for the range of voltage frequencies tested. The figure confirms the initial hypothesis, that approximately matching the voltage frequency with $f_R=1/t_R$ maximizes the heat transfer, ostensibly eliminating the intermediate regions of bubbly flow, which is the least effective regime with regard to the boiling heat transfer.

The results are quite promising with regard to using frequency as a control parameter for engineering smart and small heat exchangers for both ground and space applications.
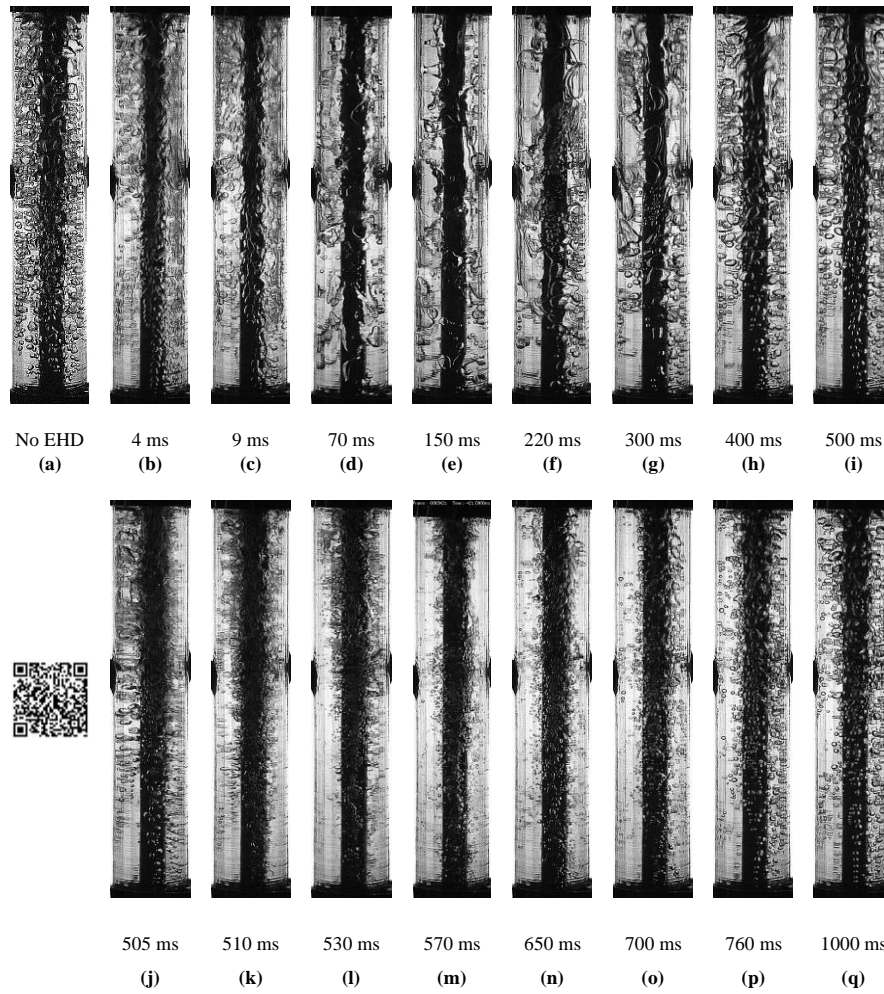
Figure 1. Flow regime observations for a f=1.0 Hz square wave, 50% duty cycle, at G=100 kg/m^{2}s, q"=10 kW/m^2 and V=10 kV$_{p-p}$ (see QR code for video).
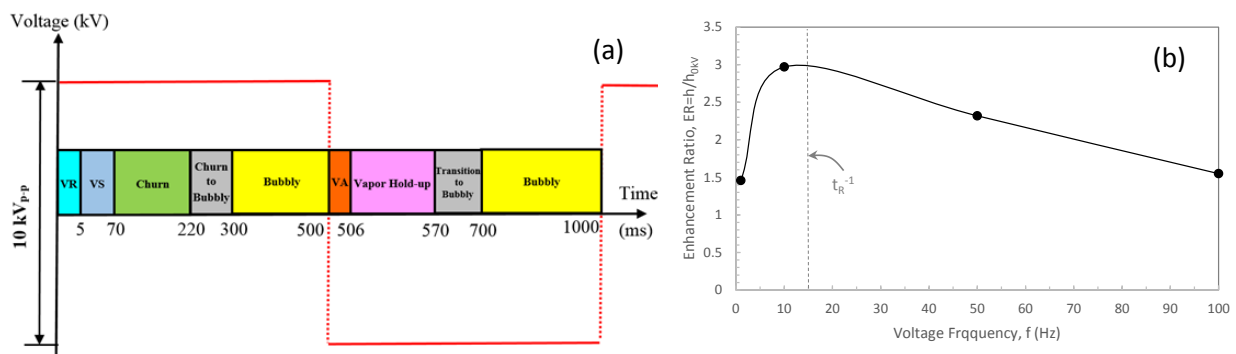

Figure 2. (a) Observed phase dynamics for one period at 1.0 Hz AC frequency, and (b) heat transfer coefficient enhancement ratio versus frequency: G=100 kg/m^{2}s, q"=10 kW/m^2 and V=10 kV$_{p-p}$.

References

S. Ahmadi, P. Hanafizadeh, M. Eraghubi and A. J. Robinson, "Upward flow boiling of HFE-7000 in high frequency AC electric fields," *International Journal of Thermofluids* 10 (2021) 100076.

Influence of density and viscosity on deformation, breakage, and coalescence of bubbles in turbulence

A. Roccon[1,2], F. Mangani[1], G. Soligo[3] and A. Soldati[1,2]

[1]Institute of Fluid Mechanics and Heat Transfer, TU-Wien, 1060 Vienna, Austria
[2]Polytechnic Department, University of Udine, 33100 Udine, Italy
[3]Complex Fluids and Flows Unit, OIST, 904-0495 Okinawa, Japan
Contact E-mail : alessio.roccon@uniud.it

We investigate the effect of density and viscosity differences on a swarm of large and deformable bubbles dispersed in a turbulent channel flow. For a given shear Reynolds number, Re_τ=300, and a constant bubble volume fraction, $\Phi \simeq 5.4\%$, we perform a campaign of direct numerical simulations of turbulence coupled with a phase-field method accounting for interfacial phenomena. For each simulation, we vary the Weber number (We, ratio of inertial to surface tension forces), the density ratio (ρ_r, ratio of bubble density to carrier flow density) and the viscosity ratio (η_r, ratio of bubble viscosity to carrier flow viscosity). Specifically, we consider two Weber numbers, We=1.50 and We=3.00, four density ratios, from ρ_r=1 down to ρ_r=0.001, and five viscosity ratios, from η_r=0.01 up to η_r=100. Our results show that density differences have a negligible effect on breakage and coalescence phenomena, while a much stronger effect is observed when changing the viscosity of the two phases. Increasing the bubble viscosity with respect to the carrier fluid viscosity damps turbulence fluctuations, makes the bubble more rigid, and strongly prevents large deformations, thus reducing the number of breakage events. Local deformations of the interface, on the contrary, depend on both density and viscosity ratios: as the bubble density is increased, a larger number of small-scale deformations, small dimples and bumps, appear on the interface of the bubble. The opposite effect is observed for increasing bubble viscosities: the interface of the bubbles become smoother. We report that these effects are mostly visible for larger Weber numbers, where surface forces are weaker. Finally, we characterize the turbulence structures inside the bubbles by analyzing the mixing of a passive scalar in the multiphase system.
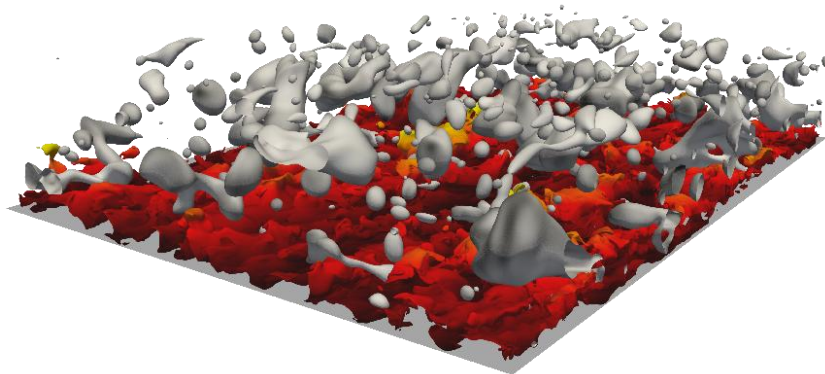
Figure 1. Instantaneous representation of a swarm droplets released in a turbulent channel flow. The flow field is visualized via the streamwise velocity isosurface (corresponding to $u = 15$) and is colored by the distance from the bottom wall (black, near wall; yellow, channel center).

Study of Plateau-Rayleigh instability in stratified liquid-liquid pipe flow: PIV/PLIF experiments and numerical solution

P. J. Miranda-Lugo[1], Jorge E. Arrollo-Caballero[1], Marlon M. Hernandez-Cely[2] and O. M. H. Rodriguez[1]

[1]University of São Paulo (USP), São Carlos School of Engineering (EESC), Mechanical Engineering Department, Industrial Multiphase Flow Laboratory (LEMI), Av. Trab. São Carlense, 400, São Carlos - SP, 13566-590, Brazil.

[2] Federal University of Pelotas, Engineering Center, Rua Benjamin Constant, n° 989, Porto, Pelotas - RS, 96010-020, Brazil.

pjosemiranda@usp.br, oscarmhr@sc.usp.br

Keywords: Oil-water flow, Stratified flow, Capillary instability, PIV, PLIF, Velocity contours.

1. INTRODUCTION

The accurate prediction of liquid-liquid flow patterns transition is important for many industries and have been studied by several researchers (Trallero et al., 1997; Angeli and Hewitt, 2000; Elseth, 2001; Amundsen, 2011). Rodriguez and Castro (2014) suggested that for high-viscosity-ratio stratified flow the interface's cross-section curvature is related to capillary instability, which can be relevant at high water volumetric fractions. Those authors derived a new interfacial-tension term that was included in a general transition criterion based on the linear hydrodynamic stability analysis. However, to the best of the authors knowledge, there is no experimental study that quantifies that specific capillary effect in stratified flow. We are focused on the study of a horizontal stratified oil-water pipe flow, experimentally, via 2-D PIV-PLIF, and numerically, via the matrix method to solve the linearized problem. The effect of the interfacial-tension term related to the interface's cross-section curvature on the flow instability will be evaluated.

2. NUMERICAL WORK

A two-layer flow configuration in a horizontal channel was adopted as a first step for the numerical study the stability of liquid-liquid stratified flow. Differently from the classical approach, we propose a linear stability analysis considering the linearized perturbed equations of continuity and momentum in their primitive variables, where the perturbed velocities and pressure fields are written as $u_j = \bar{U}_j + \tilde{u}_j$, $v_j = \tilde{v}_j$, $p_j = \bar{P}_j + \tilde{p}_j$, and $n = \tilde{n}$ gives the interface's disturbance. The governing equations of the stability analysis for a two-plate horizontal geometry are described as follows:

$$i\alpha\bar{u}_j(y) + \bar{v}_j(y) = 0 \tag{1}$$

$$i\alpha c\bar{u}_j(y) + i\alpha\,\bar{U}_j\bar{u}_j(y) + \bar{v}_j(y)\frac{\partial\bar{U}_j}{\partial y} = -i\alpha\frac{\rho_1}{r\rho_j}\bar{p}_j(y) + \frac{1}{\mathrm{Re}_2}\frac{\bar{v}_j(y)}{v_2}\frac{\partial^2\bar{U}_j}{\partial y^2} \tag{2}$$

$$i\alpha c\bar{v}_j(y) + i\alpha\,\bar{U}_j\bar{v}_j(y) = -\frac{\rho_1}{r\rho_j}\bar{p}_j(y) \tag{3}$$

The velocities satisfy the no-slip impermeable wall boundary conditions at the channel walls:

$$y = -\eta,\ \ \bar{u}_1 = \bar{v}_1 = 0,\ \text{and}\ \ y = 1,\ \ \bar{u}_2 = \bar{v}_2 = 0 \tag{4}$$

Boundary conditions at the interface $y = 0$ require continuity of velocity components and the tangential stresses. The jump of the normal stress due to the surface tension is also needed.

$$y = 0, \qquad \bar{u}_1 = \bar{u}_2,\ \text{and}\ \bar{v}_1 = \bar{v}_2 \tag{5}$$

$$y = 0, \qquad \vec{t}\cdot\sum\cdot\vec{n} = \left[\frac{m\mu}{\mu_1}\left\{\left(\frac{\partial\bar{u}}{\partial y}+\frac{\partial\bar{v}}{\partial x}\right)\left(1-\left(\frac{\partial\eta_0}{\partial x}\right)^2\right)-4\frac{\partial\bar{u}}{\partial x}\frac{\partial\eta_0}{\partial x}\right\}\right] = 0 \tag{6}$$

$$y = 0, \qquad \vec{n}\cdot\sum\cdot\vec{n} = \left[p+\frac{m\mu}{\mu_1}\frac{2\mathrm{Re}_2^{-1}}{1+\left(\frac{\partial\eta_0}{\partial x}\right)^2}\left\{\frac{\partial\bar{u}}{\partial x}\left(1-\left(\frac{\partial\eta_0}{\partial x}\right)^2\right)+\left(\frac{\partial\bar{u}}{\partial y}+\frac{\partial\bar{v}}{\partial x}\right)\frac{\partial\eta_0}{\partial x}\right\}\right] = \mathrm{We}_2^{-1}\frac{\frac{\partial^2\eta_0}{\partial x^2}}{\left(1+\left(\frac{\partial\eta_0}{\partial x}\right)^2\right)^{3/2}} \tag{7}$$

In addition, the interface displacement and the normal velocity components at the interface satisfy the kinematic boundary condition:

$$y = 0, \qquad \tilde{v}_j = \frac{D\tilde{\eta}}{Dt} = \frac{\partial\tilde{\eta}}{\partial t}+\tilde{u}_j\frac{\partial\tilde{\eta}}{\partial x}\ \ \text{or}\ \ \bar{v} = -i\alpha c\eta_0 + i\alpha\bar{U}\eta_0 \tag{8}$$

The matrix method can be used to solve Eq. (1) - (3) with the boundary condition (4) - (8). This numerical approach uses Chebyshev polynomials to approximate the solution in each sublayer. The differential problem is reduced to a generalized eigenvalue problem of the form $Lv = \omega Fv$, where $v = [\bar{u}_j, \bar{v}_j, \bar{p}_j, \eta_0]^T$ represents the eigenfunctions, ω are the eigenvalues, and L and F are block matrixes.

3. EXPERIMENTAL WORK

One can see in Fig. 1 a schematic view of the new test facility designed and built up to study the dynamics of stratified liquid-liquid flow. There are two independent supply lines, one for water and another for oil, and two test sections (F and K), made of borosilicate-glass pipes with lengths (L_p) of 4.5 and 7.5 m and internal diameters (D) of 9.7 and 20.5 mm, respectively. The fluid distribution system is driven by gravity from two reservoirs (A and B). The liquids are injected into the test section through a set of flow straighteners (C, D, H, and I) and a specially designed inlet section (E and J). Both flow lines have an array of liquid flowmeters (1, 2, 4, 5), thermocouples type K (3, 6, 7, 8), and differential/gauge pressure transducers (9, 10, 11).
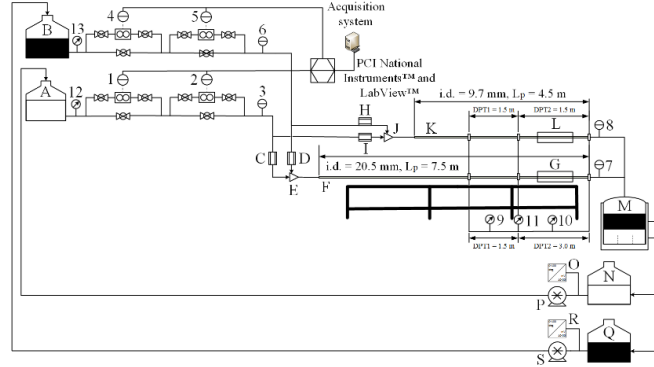
Figure 1. Schematic representation of the new liquid-liquid flow test facility of USP at São Carlos campus.

4. PRELIMINARY RESULTS

One can see in Fig. 2 the application of a mapping technique to correct the distorted original images collected at -45° from the horizontal in a pipe's cross-section plane. The technique uses a calibration pattern and a polynomial function to correct distorted images. Once the original images are corrected, a scanning algorithm identifies the oil-water interface and fits a circle to it through the least-squares method. The interface's cross-section curvature radius is determined by a probability density function of the circles' sizes.

| (a) | (b) | (c) | (d) |
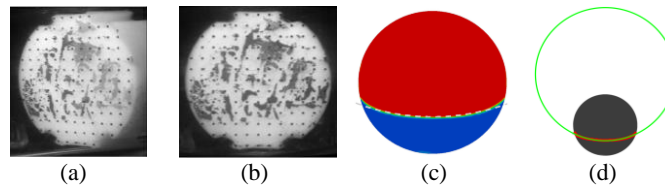
Figure 2. Mapping technique to correct the distorted images of stratified flow. (a) Distorted original image. (b) Corrected image. (c) Expected cross-section view, Bochio et al. (2021). (d) Circle fitting to determine the interface's cross-section curvature radius.

One of the challenges of modeling this problem is incorporating the destabilizing interfacial-tension term. The proposed matrix method was validated considering the core-annular flow studied by Boomkamp (1969). A comparison of our numerical solution and Boomkamp's results is presented in Fig. 3. One can observe a quite good agreement for the two considered transversal wave numbers (n=1 and n=5).
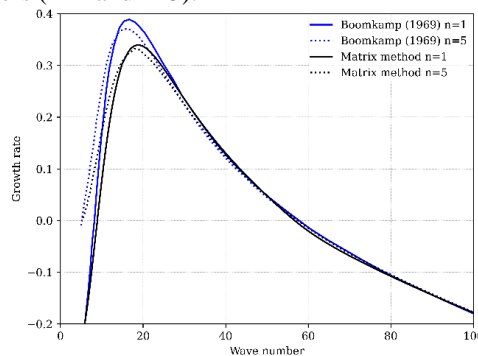

Figure 3. Comparison of Boomkamp's core-annular flow results and the numerical solution obtained using the matrix method considering two transversal waver numbers (n=1, n=5).

4. CONCLUSIONS

A new experimental setup and preliminary results of an on-going research on capillary instability in liquid-liquid stratified flow are presented. The adopted methodology is the use of 2D PIV-PLIF experiments and the matrix method to solve the linearized governing equations. The aim is to quantify the destabilizing effect of the interfacial-tension term. One can expect that the larger the interface's cross-section curvature, the stronger its effect is.

5. REFERENCES

Amundsen, L., 2011. *An experimental study of oil-water flow in horizontal and inclined pipes*. Ph.D. thesis, The Norwegian University of Science and Technology (NTNU), Trondheim.

Angeli, P., Hewitt, G., 2000. "Flow structure in horizontal oil-water flow". *International Journal of Multiphase Flow*, Vol. 26, pp. 1117–1140.

Bochio, G, Cely, MMH, Teixeira, AFA, Rodriguez, OMH., 2021. "Experimental and numerical study of stratified viscous oil-water flow". *AIChE Journal,* Vol. 67, pp. e17239.

Boomkamp, A. M., 1969. *Stability of parallel two-phase flow*. Ph.D. thesis, The Norwegian University of Science and Technology (NTNU), Dordrecht.

Elseth, G., 2001. *An experimental study of Oil/water flow in horizontal pipes*. Ph.D. thesis, University of Twente, Porsgrunn.

Rodriguez, O.M., Castro, M.S., 2014. "Interfacial-tension-force model for the wavy-stratified liquid–liquid flow pattern transition". *International Journal of Multiphase Flow*, Vol. 58, pp. 114–126.

Trallero, J.L., Sarica, C., Brill, J.P., 1997. "A Study of Oil-Water Flow Patterns in Horizontal Pipes". *SPE Production & Facilities*, Vol. 12, pp. 165–172.

Heat Transfer of Flow Boiling Carbon Dioxide in Vertical Upward Direction

R. Revellin[1], D. Schmid[2,3], B. Verlaat[2], P. Petagna[2], J. Schiffmann[3]
[1]Univ Lyon, INSA Lyon, CNRS, CETHIL, UMR5008, F-69621 Villeurbanne, France
[2]European Organization for Nuclear Research (CERN), CH-1211 Geneva 23, Switzerland,
[3]Ecole Polytechnique Fédérale de Lausanne, EPFL STI IGM LAMD, CH-2002 Neuchâtel, Switzerland
Contact E-mail : remi.revellin@insa-lyon.fr

Carbon Dioxide (CO_2) has been identified as an excellent and sustainable candidate for the thermal management of the new Inner Particle Tracking Detectors of the ATLAS and CMS experiments at the European Organization for Nuclear Research (CERN). For the proper development of evaporative cooling systems, it is imperative to understand the two-phase flow behaviour inside the channels and due to the lack of experimental data, the heat transfer mechanisms of flow boiling CO_2 have been investigated in vertical upward direction at heat fluxes of ~5 kW m^{-2} and ~11 kW m^{-2}, mass velocities between 100 kg m^{-2} s^{-1} and 450 kg m^{-2} s^{-1} and saturation temperatures from -25 °C to +5 °C. The inner tube diameter of the evaporator is 8 mm and its length is 8 m.

The dryout is influenced by the heat flux, the mass velocity and the saturation temperature and is observed to occur at lower vapour qualities compared to other refrigerants. As a result, a new dryout inception model is proposed for the experimental domain of the present study. The heat transfer coefficients of two-phase upflow of CO_2 are enhanced compared to other refrigerants and many established prediction methods underpredict the experimental measurements. To incorporate these phenomena, enhancement factors are suggested for two established prediction models to capture the trends of vertical two-phase upflow of CO_2.
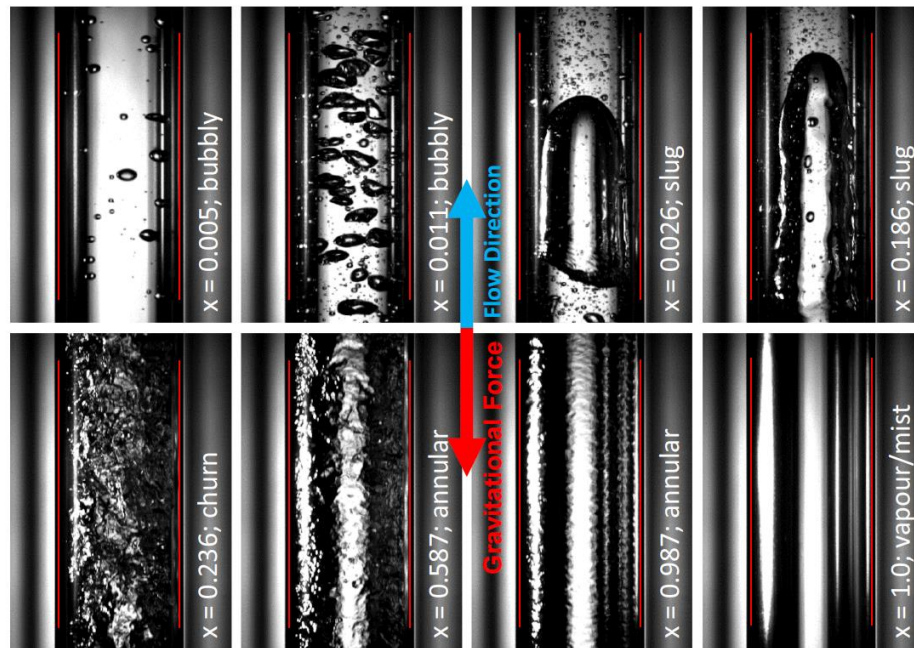
Figure 1. Flow pattern observations of CO_2 in vertical upward direction at T_{sat} = -25 °C; G = 200kg m^{-2} s^{-1}; vapour quality increasing from top left to bottom right: bubbly, bubbly, slug, slug, churn, annular, annular, vapour/mist. The red lines represent the inner tube walls.

HEAT TRANSFER AND PRESSURE DROP CHARACTERISTICS OF SINGLE AND TWO-PHASE FLOWS IN A FINNED RECTANGULAR CHANNEL

Y. Saito[1], H. Zhang[2], D. Ito, N. Odaira[1], and K. Ito[1]

[1]Institute for Integrated Radiation and Nuclear Science, Kyoto University
[2]Graduate School of Energy Science, Kyoto University
Contact E-mail : saito.yasushi.8r@kyoto-u.ac.jp

1. INTRODUCTION

In recent years, there has been a need for cooling technology that can deal with the increasing of heat generation by the miniaturization and high output of the electronic devices. Therefore, it is necessary to develop a higher performance cooling technology. In order to remove the high-density heat flow, various cooling technologies using a finned surface or phase change (such as boiling) have been proposed. The finned surface, which is used mainly for single-phase flow can expand its heat transfer area and improve the heat transfer ability by promoting turbulence[1]. On the other hand, boiling cooling has an extremely high heat transfer ability compared to single-phase flow [2]. However, the boiling cooling can only be used under boiling conditions. In this study, boiling cooling with finned surface has been considered.

Although finned surface can improve the heat transfer efficiency for single-phase flow, the pressure drop through the heat sink increases especially for boiling two-phase flow. As a result, higher pressure drop may deteriorate the cooling efficiency under boiling conditions. Therefore, it is important to predict the pressure drop of fin-type heat sink from non-boiling region to boiling region. In previous studies, although pressure drop of fin-type heat sink has been studied under various conditions, the optimization of the design is still difficult for various arrangement and shape of the fin for single-/two-phase flows. The purpose of this study is to treat the fin-type heat sink as a packed-bed bed and generalize the unique characteristics of the fin-type heat sink by using the packed-bed model. Pin-fin heat sink is used to measure the pressure drop of single-/two-phase flow and the packed-bed model such as Ergun/Lipinski model is employed to evaluate the experimental results.

2. EXPERIMENT APPARATUS AND METHOD
2.1 Experimental Apparatus

As shown in Fig.1, the test section is a rectangular flow path with length of 795 mm, width of 30 mm and height of 8mm. The bottom plate of the test section is made of stainless steel and the top plate is made of transparent polycarbonate for the visualization. A high-speed camera is set above the heat sink to visualize the flow between finned section. The liquid phase

is supplied from the inlet at the bottom plate, through the finned section and flows out to the outlet at top plate. Same as the liquid phase, air is injected from three nozzles at the bottom plate. A resin porous sponge is set at the inlet of the flow path to rectify the mixed two-phase flow.

Fig.1 Schematic of Test section

2.2 Heat Sink

The heat sink as shown in Fig.2 is used for this study. The heat sink is made of aluminum and the base part area of the heat sink is 65×30 mm^2. The shape of the fin is square prism with edge length of 2 mm, pitch of 4 mm and height of 8 mm. The arrangement of the fin is in-line arrangement.

Fig.2 Pin-fin heat sink.

3. RESULTS

Figure 3 shows the pressure drop of fin-type heat sink with single-phase flow. Circular symbols denote the experimental data and solid line denotes the prediction by the Ergun model. As can be seen, the Ergun model overpredicts the pressure drop for the pin-fin heat sink. Therefore, the Ergun model has been modified to predict the measured data, which is shown by the dotted line in this figure.

For two-phase flow, various existing models have been compared with experimental data for pin-fin heat sink. As a result, Schulenberg-Mueller model predicts experimental data with highest accuracy, as shown in Fig.4. It should be noted that the cofficients in the governing equations are optimized for the single-phase flow experiments.

Fig. 3 Variation of pressure drop for single-phase flow.
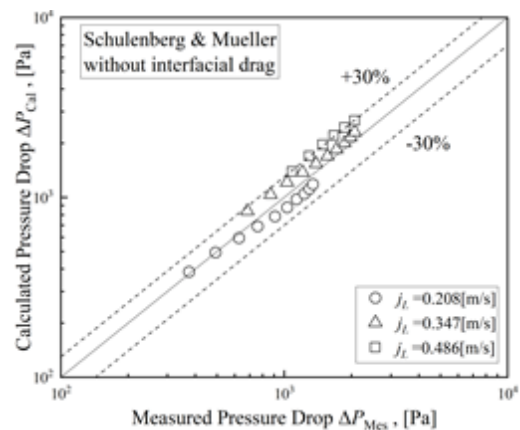
Fig. 3 Comparison of measured and predicted pressure drop for two-phase flow.

REFERENCES

[1] Tzer-Ming Jeng, Thermal performance of in-line diamond-shaped pin fins in a rectangular duct, International Communications in Heat and Mass Transfer 33, 1139-1146(2006).

[2] Han Ju Lee, Sang Yong Lee, Heat transfer correlation for boiling flows in small rectangular horizontal channels with low aspect ratios, International Journal of Multiphase Flow 27, 2043-2062 (2001).

Gas Removal from Closed-End Small Holes using Pressure Fluctuation

T. Sanada[1]

[1]Shizuoka University
Contact E-mail : sanada.toshiyuki@shizuoka.ac.jp

Wet cleaning methods using liquids are widely applied in many industrial fields. In such methods, it is first necessary to cover the object to be cleaned with the liquid. A small hole with one end closed is difficult to deform the gas-liquid interface due to its surface tension, making it difficult to fill with liquid. Therefore, it is necessary to have an efficient method to remove gas from closed-end holes. Here we demonstrate the gas removing method from small holes utilizing droplet train impingement in the air or irradiating acoustic waves in the liquid.

First, we observed this liquid infiltration process through droplet train impingement into a closed-end hole and compared it with the liquid column impact. The filling process was visualized with two high-speed video cameras. Our observations illustrate the importance of the oscillation and deformation of the gas-liquid interface inside the holes following droplet impingement. Intermittent droplet impingement causes small droplets or large interface deformations to form, and then the gas column inside the hole becomes separated. This separated gas column is then gradually ejected. Therefore, the liquid infiltration can be increased by using a droplet train formed of a small surface-tension liquid.

Second, we directly generated interface oscillation by irradiating acoustic waves in the liquid. We estimated the natural frequency of gas columns and irradiated sweep frequency of the acoustic wave, i.e., monotonically increasing the frequency including natural frequency. As a result, we succeeded in completely removing the gas inside the small holes. From a high-speed observation, we found two important frequencies for the gas removal, the natural frequency of the gas column and the bubble inside a hole. Finally, we found that combining two different frequencies enabled complete gas removal in water within 2 sec. We discuss the gas removing mechanism from a closed-end hole.
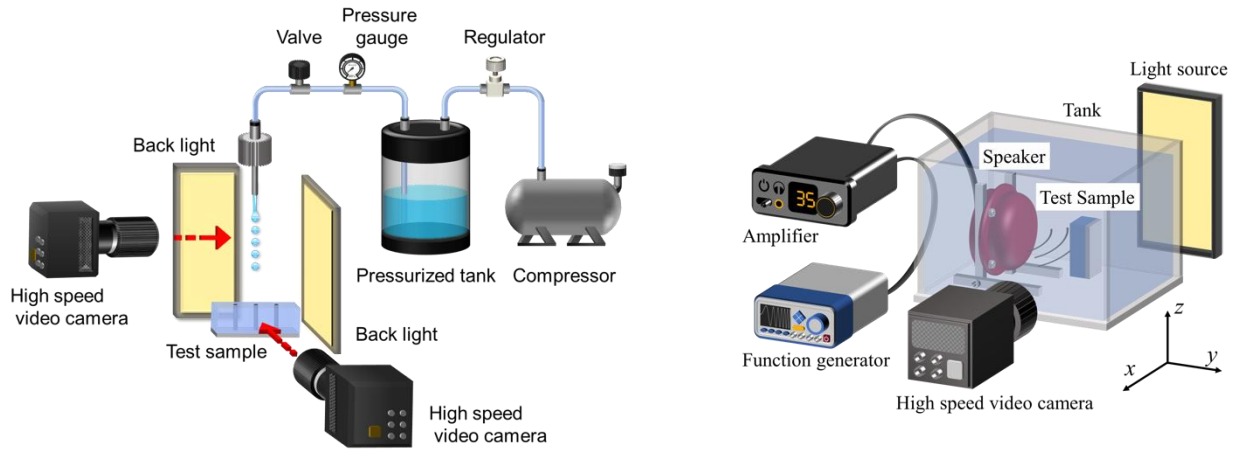
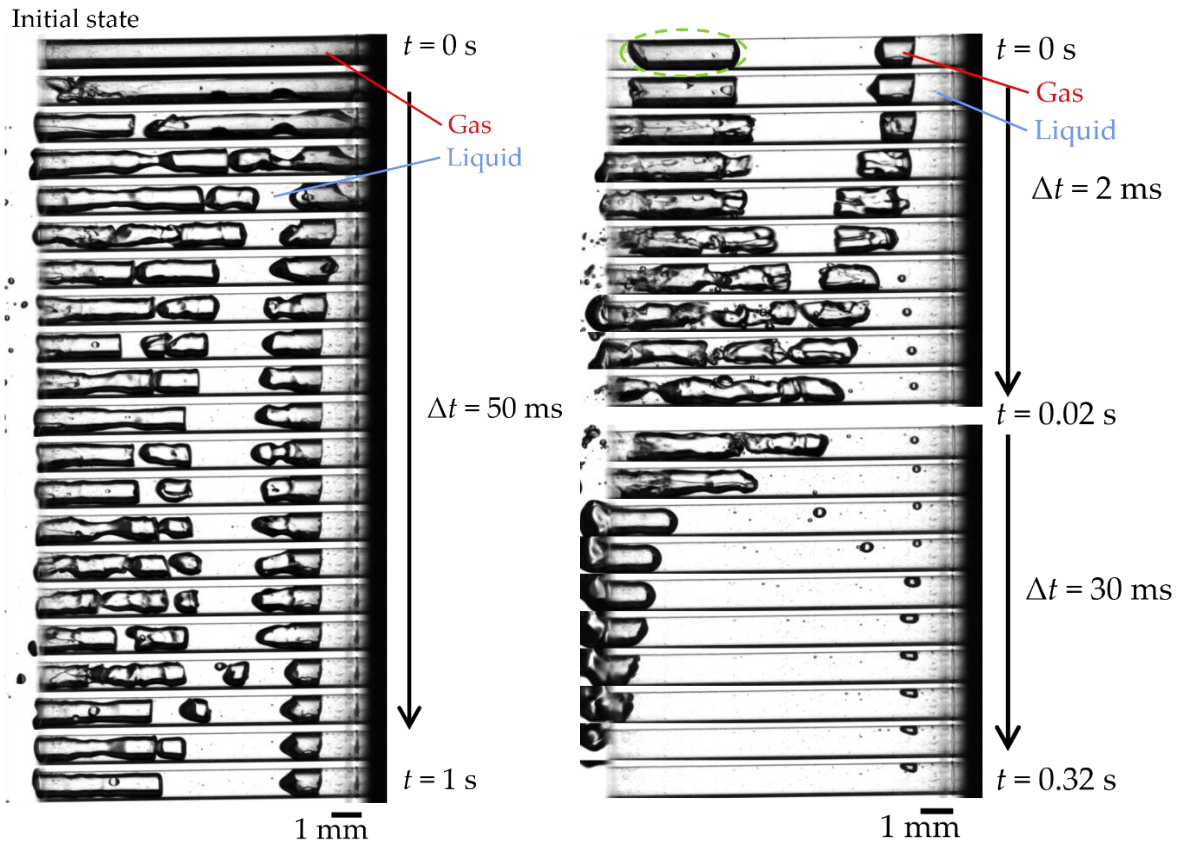Figure 1. Experimental setup left droplet impingement, right acoustic wave irradiation.

Figure 2. Gas removal process, the black stripes and the white areas are gas and liquid, respectively: (left) First stage irradiation (600 Hz, Δt = 50 ms), (right) Second stage irradiation (1100 Hz).

EXPERIMENTAL ANALYSIS OF THE FLOW-INDUCED NOISE, STRUCTURE ACCELERATION, AND TWO-PHASE FLOW JET VELOCITY AT THE OUTLET OF A THERMAL EXPANSION VALVE

Erivelto dos Santos Filho*, Leopoldo Pisanelli Rodrigues de Oliveira, Gherhardt Ribatski
Heat Transfer Research Group, EESC-USP, Avenida Trabalhador São-carlense, 400, São Carlos - SP, 13566-590, Brazil
*erivelto.filho@usp.br

Keywords: Flow-induced noise, Fluid-structure vibration, Jet velocity, Thermal expansion valve, Two-phase flow

1. INTRODUCTION

Designing expansion devices with low refrigerant induced noise still is a great challenge, since this kind of noise occurs irregularly during the thermodynamic cycle. The expansion devices can produce mechanical vibration as a combination of shear, turbulence and/or shock wave interaction during the expansion process (REETHOF, 1977). These mechanical vibrations may propagate through the components being able to produce resonance and propagates as sound waves through the air, reaching the human ear (SINGH et al., 1999). The flow-induced noise by refrigerant has not been extensively studied, but only as a subject of interest for trouble shooting of refrigerator and air-conditioning units (AOYAMA et al., 2006). The most effective and least expensive way to reduce unwanted noise is to reduce the noise at the source (ASHRAE, 2013). In this context, the present study aims to contribute knowledge concerning flow-induced noise and fluid-structure vibration characteristics of a thermal expansion valve (TXV). The experiments were performed for R134a flowing through the flow restriction region of a commercial expansion valve assembled between two borosilicate glass tubes. The noise and the structure vibration were evaluated through an external microphone, and a single axis accelerometer, respectively. Moreover, the transparent section allowed the investigation of the two-phase flow topology immediately upstream the flow restriction and along the expansion process. The tests were performed for a mass flow rate of 0.03 kg/s with inlet pressures of 3.1 (30 ºC), 4.8 (35 ºC), and 6.1 (40 ºC) bar, and an outlet saturation pressure of 4.1 bar (10 ºC) with inlet subcooling degree ranging from -15ºC up to vapor quality of 17%.

2. RESULTS AND DISCUSSION

The results displayed in Fig. 1 revealed, in general, similar behaviors for the TSPL and the structure acceleration, regardless of the pressure drop through the valve. Additionally, the TSPL and structure acceleration intensify as the pressure drop increases. Among the experimental conditions, superior noise was observed for the pressure drop of 6.1 bar at a vapor quality of 2%. It is important to highlight that as flow at the inlet of the valve shifts from subcooled liquid to two-phase flow, the intensity of these parameters sharply increase. It can be speculated that, under isolated bubble (I.B.) and coalescence bubble (C.B.) flow pattern, as the pressure drop increases the bubble contraction and expansion process as it crosses the valve orifice leads to a superior noise and structure vibration. The inlet flow patterns were characterized based on visual observations. As mentioned by Ishii and Watanabe (2019), the energy of a spherical bubble shock wave increases as its pressure increases. As vapor mass fraction increases the C.B. evolves into annular flow pattern at the valve inlet. Under annular flow pattern the TSPL and structure acceleration results in a constant signal and inferior to I.B. and C.B.. At this point, it is important to highlight that during the experimental campaign, although qualitatively, it was possible to distinguish the I.B. from the other flow patterns only by hearing its generated noisy. As each bubble passed through the valve orifice, it resulted in a characteristic popping noise. According to Fig. 1c, the jet velocity at the valve outlet for inlet vapor qualities lower than 4% exhibited similar values for pressure drops of 3.6 and 6.1 bar, and slighted superior velocity for a pressure drop of 4.8 bar and higher. For inlet vapor quality superior to 4%, the jet velocity increases sharply under pressure drop of 4.8 and 6.1 bar, while under a pressure drop of 3.6 bar, it remains around 22 m/s. Overall, the present results indicate an abrupt increase in the TSPL, structure acceleration, and jet velocity as the inlet flow shifts from saturated liquid to two-phase flow.

3. CONCLUSIONS

The following remarks summarize the conclusion of the present investigation: (i) The TSPL and the structure acceleration increase as the pressure drop across the valve orifice increases; (ii) Superior noise and structure vibration

occurred for I.B. flow pattern, while superior jet velocity was observed for vapor quality superior to 9% (annular) at the TXV inlet; (iii) Inferior TSPL, structure acceleration, and jet velocity were found for only liquid at the valve inlet for a given pressure drop.
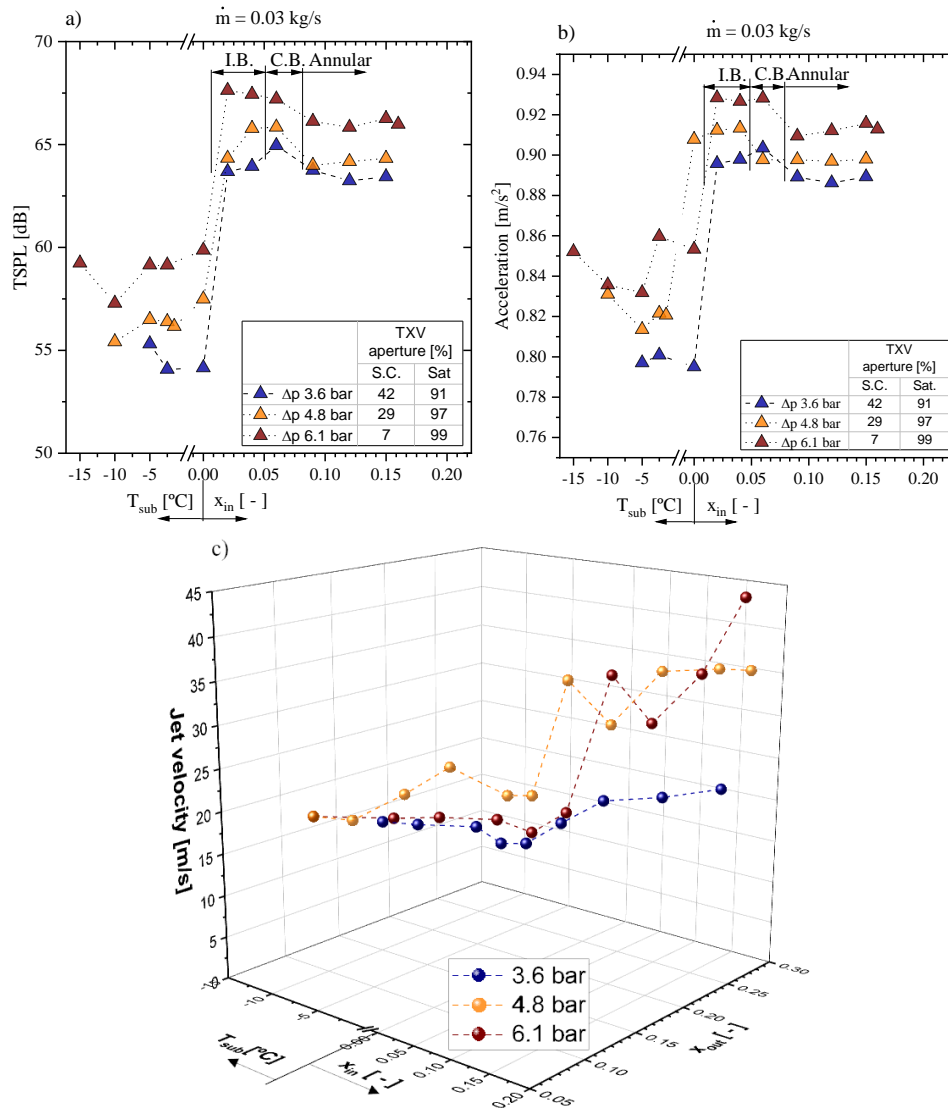

Figure 1 – a) External TSPL flow-induced noise, b) flow-induced structure acceleration, and c) jet velocity at the valve outlet for pressure drops of 3.6, 4.8, and 6.1 at mass flow rate of 0.03 kg/s.

4. REFERENCES

1. ASHRAE, F. Fundamentals handbook. IP Edition, v. 21, 2013.
2. AOYAMA, S. et al. Analyzing for refrigerant induced noise for split type air conditioner indoor unit. Transactions of the Korean Society for Noise and Vibration Engineering, The Korean Society for Noise and Vibration Engineering, v. 16, n. 3, p. 240–246, 2006.
3. ISHII, K.; WATANABE, N. Shock wave generation by collapse of an explosive bubble in water. Proceedings of the Combustion Institute, Elsevier, 2018.
4. REETHOF, G. Control valve and regulator noise generation, propagation, and reduction. Noise Control Engineering, Institute of Noise Control Engineering, v. 9, n. 2, p. 74–85, 1977.
5. SINGH, G. M. et al. Noise generation from expansion devices in refrigerant. [S.l.], 1999.

String Cavitation Flow in Multi-Hole Fuel Injector and Spray

Akira Sou[1]

[1]Graduate School of Maritime Sciences, Kobe University, Japan
Contact E-mail : sou@maritime.kobe-u.ac.jp

When super cavitation is developed in an orifice of a fuel injector for diesel engines, it induces a strong turbulence at the exit of the orifice and promotes fuel spray atomization [1-3]. The inception and development process of cavitation as well as cavitation bubble size distribution were visualized and measured by X-ray phase contrast imaging technique at a synchrotron radiation facility Spring-8 [4]. The effects of the cross-sectional area of the sac at the upstream of an orifice [5], liquid fluid properties [1], length-to-diameter ratio of the orifice [6], inlet edge roundness of the orifice [7], time scale of transient flow dynamics [8], ambient pressure [9] on cavitation in the orifices and spray have been clarified and were found to be predictable quantitatively by using modified cavitation number based on local pressure at the vena contracta of the orifice.

In recent diesel engines, a multi-hole fuel injector has been employed to distribute fuel spray in a combustion chamber. It was reported that when the needle lift is very low at the beginning of needle valve opening and just before the needle valve closing, spray angle often becomes very large and fuel droplets is atomized largely even with a very low fuel velocity. In order to clarify the reasons of the atomization enhancement and the increase in spray angle, we manufacture various transparent multi-hole mini-sac diesel fuel injector replicas with various fixed needle lifts, needle tip shapes, sac diameters, orifice positions, orifice diameters and orifice numbers to carry out high-speed visualization, 3D3C-PIV with four cameras and a high speed camera as well as high-speed PIV of turbulent cavitating flows in the injectors and sprays for various flow velocities by refractive index matching of diesel fuel [10-16]. Figure 1 shows some of the transparent injectors whose sac diameters are 10 mm and orifice diameters are 2 mm.
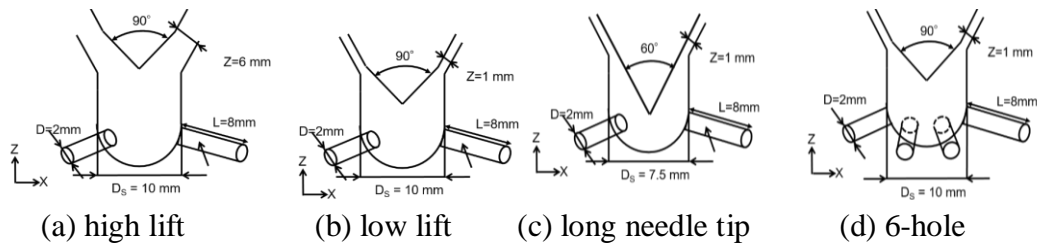
(a) high lift   (b) low lift   (c) long needle tip   (d) 6-hole
Figure 1. Transparent multi-hole mini-sac diesel fuel injector replicas

Figure 2(a) shows typical images of twin string cavitation connecting two neighbouring orifices, and Figure 2(b) shows those of single string cavitation connecting an orifice and the

needle surface as well as hollow-cone sprays whose spray angles are increased largely. Figures 3(a) and (b) show a toroidal vortex flow with twin string cavitation by 3D-PIV and a steady vortex flow around single string cavitation for an orifice. The results clarify that the large local inertia of the inflow into the sac induces the vortex flows, and the strong circulation of the vortex flow largely increases spray angle by the centrifugal force even with very low fuel flow velocity.

Following the results of the high-speed images and measured velocity distributions under wide variety of experimental conditions, we derive three dimensionless parameters for orifice wall cavitation, twin string cavitation flow and single string cavitation flow, and confirm that we can predict the string cavitation regime and spray angle by using the dimensionless parameters.
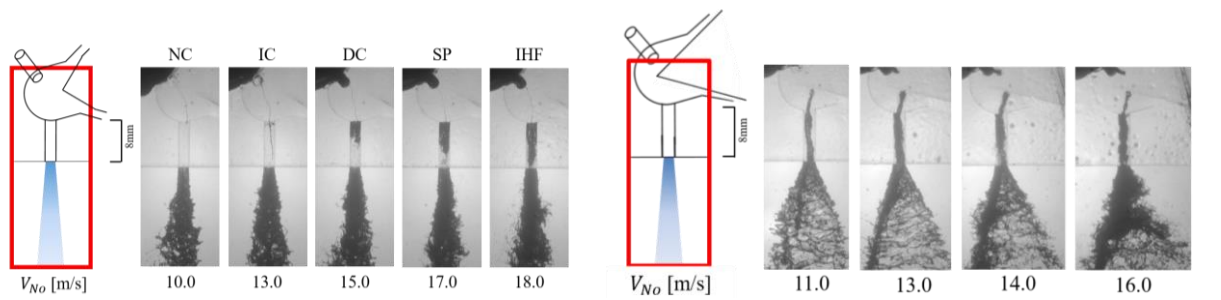
(a) twin string cavitation and spray   (b) single string cavitation and a hollow-cone spray
Figure 2. Images of string cavitation and orifice wall cavitation in injectors and sprays
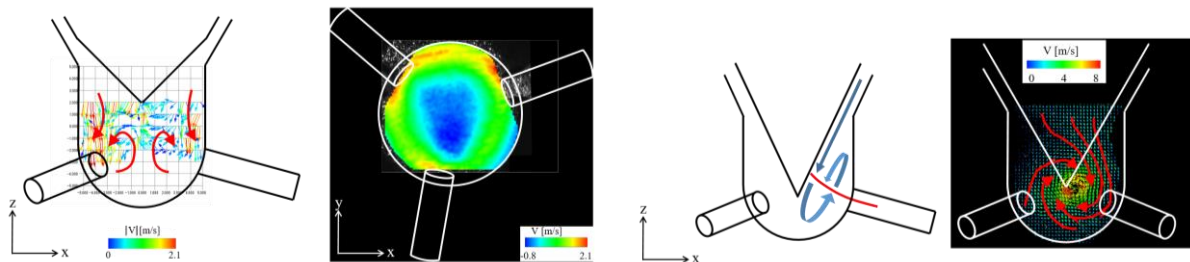
(a) toroidal vortex flow with twin string by 3D-PIV   (b) steady vortex flow with single string
Figure 3. Measured velocity distributions in the injectors by 3D3C-PIV and high-speed PIV

References
[1] Akira Sou, et al., Int. J Heat and Mass Transfer, Vol. 50, Iss. 17-18, (2007), pp. 3575-3582.
[2] Akira Sou, et al. J. Fluid Science and Technology, Vol. 3, No. 5, (2008) pp. 633-644.
[3] Christophe Dumouchel, Akira Sou, et al., Experiments in Fluids, (2019).
[4] Rubby Prasetya, Akira Sou, et al., Atomization and Sprays, Vol. 29, No. 1, (2019) pp. 59–78.
[5] Akira Sou, et al., J. Fluid Science and Technology, Vol. 3, No. 5, (2008) pp. 622-632.
[6] Akira Sou, et al., Atomization and Sprays, Vol. 20, Iss. 6, (2010) pp. 513-524.
[7] Makoto Mashida and Akira Sou, Int. J Automotive Engng, Vol. 9, No. 1, (2018), pp. 9-15.
[8] Rubby Prasetya, Akira Sou, et al., Atomization & Sprays, Vol. 29, No. 2, (2019) pp. 123–141.
[9] Rubby Prasetya, Akira Sou, et al., J. Fluid Sci and Technol, Vol. 14, No. 1, JFST0005, (2019).
[10] Raditya Hendra Pratama, Akira Sou, et al., Atomization & Sprays, Vol. 27, Iss. 3, (2017).
[11] Rubby Prasetya, Akira Sou, et al. Int. J of Engine Research, (2019).
[12] Samsu Dlukha Nurcholik, Akira Sou, et al., Proc. ICLASS 2021, (2021).

Drag reduction of a spherical bubble with oscillation in shear-thinning power-law fluid

Kazuyasu Sugiyama[1, 2], Xianping Zhang[1, 2], and Tomoaki Watamura[3, 2]

[1] Graduate School of Engineering Science, Osaka University
[2] RIKEN Center for Advanced Photonics
[3] Department of Mechanical Engineering, Kyoto Institute of Technology
Contact E-mail : kazuyasu.sugiyama@me.es.osaka-u.ac.jp

The speed of a rising drop or falling particle in a resting pseudo-plastic fluid is enhanced by ultrasound irradiation. The speed-up mechanism is qualitatively explained from that owing to the enhanced strain rate resulting in viscous stress reduction. However, it is non-trivial to examine how the drag force is quantitatively determined because of the spatiotemporally multiscale nature of the system. Especially when the frequency of the irradiated ultrasound is high and/or the oscillation amplitude is large, the time-average drag force would be much smaller than the level of the instantaneous external force. In the present study, oscillation-enhanced shear-thinning effects on a spherical bubble moving in a power-law fluid are numerically and theoretically studied. As the simplest model system, we neglect the fluid compressibility associated with the ultrasound propagation but consider incompressible fluid flows around the bubble with prescribed translational and oscillating velocities. We obtain drag forces D on the bubble as numerical solutions to the unsteady Stokes equation with the power-law viscosity for various power-law indices n and oscillation velocity amplitudes A. The drag reduction ratio $1-D/D_0$ (here, D_0 is D at $A = 0$) is proportional to A^2 for small A. It is explained by weak nonlinearity in the power-law viscosity. While for large A, the scaled drag force D/D_0 is proportional to A^{n-1} as shown in figure 1. Examining the instantaneous force and energy loss, we discuss the drag reduction mechanism using the nearly irrotational velocity.
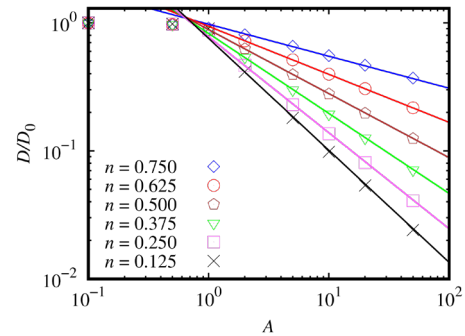
Figure 1. Time-averaged scaled drag force D/D_0 versus oscillation velocity amplitude A for various power-law indices n. The solid curve for each n indicates the curve proportional to A^{n-1}.

Acknowledgments

Generation of Microbubble Encapsulated Vesicles and the Manipulations using Ultrasound Field

S. Takagi[1], R. Kakukawa[1], R. Kiyozumi[1], B. Chen[1] and M. Ichiyanagi[2]
[1]The University of Tokyo
[2]Sophia University,
Contact E-mail : takagi@mech.t.u-tokyo.ac.jp

Microbubble-Encapsulated Vesicle (MEV) is expected to be a drug carriers which is used for Drug Delivery System (DDS) using ultrasound. MEVs are required to be smaller than 5 μm with mono-dispersed size in order to pass through capillaries and to be controlled with ultrasound. In this study, we used a flow focusing type microchannel and an inverted emulsion method to generate MEVs which satisfy the above requirements. First, we generated microbubble-encapsulated droplets by putting water containing microbubbles and mineral oil into a flow focusing device. Then, these droplets were converted to MEVs by an inverted emulsion method. The snapshot taken by high-speed video camera is shown in Fig.1. For this experimental condition, relatively larger droplets are formed, and a tiny microbubble of a few micro-meter radius is observed in the droplet. Optimizing the experimental conditions, the droplets size can be drastically reduced, and we succeeded in generating 5μm MEVs with this method (Fig.2). We currently have the problem of low production rate of small vesicles containing microbubbles. To overcome this problem, we have been developing the ultrasound device to manipulate the microbubble encapsulated bubble. Some results for this study will be discussed in the talk.
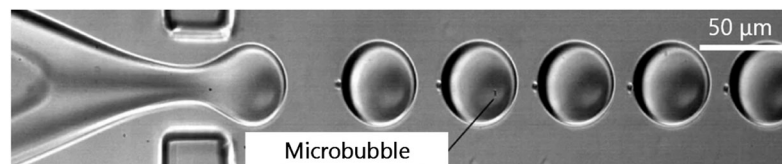
Figure 1 Flow Focusing Device for generating
Microbubble-Encapsulated Droplet
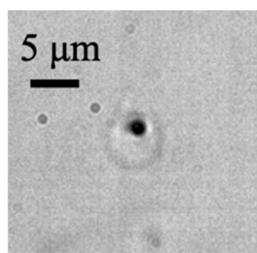
Figure 2 Generated Microbubble
-Encapsulated Vesicle

Bubble Cloud Formation by the Backscattering of High Intensity Focused Ultra Sound from a Bubble Interface

H. Takahira[1], M Nakao[2], T. Ogasawara[1]

[1] Osaka Metropolitan University
[2] Osaka Prefecture University
Contact E-mail : takahira@omu.ac.jp

INTRODUCTION

High-intensity focused ultrasound (HIFU) has been investigated for a minimally invasive cancer treatment. The collapse of cavitation bubble clouds appeared near the focus of HIFU can be a candidate to improve the efficiency of the treatment although it may destroy the healthy cell near the cancerous tissue. Thus, controlling the bubble clouds is a key to develop such effective utilization. Maxwell et al.[1] proposed the mechanism of the cavitation bubble clouds in HIFU. They showed that the negative pressure due to the backscattering of HIFU from the interface of the first cavitation bubble generated at the focus makes another cavitation bubbles leading to a bubble cloud. However, identifying the initial cavitation inception position is needed to understand details of bubble cloud formation. Ogasawara et al.[2] and Horiba et al.[3], therefore, used a laser-induced bubble as an initial cavitation and controlled the inception position. They observed the forming process of a cone-shaped bubble cloud in HIFU and measured the cavitation inception pressure at the tip of the bubble cloud. In the present study, we first review the experimental results by Horiba et al. for the mechanism of cavitation bubble formation in HIFU. Then we propose a multiscale numerical method and simulate the experiments.

RESULTS

Figure 1 shows a typical experimental result for bubble cloud formation. A large bubble in each frame is a laser-induced bubble used as a reflector of HIFU. The HIFU propagates from right to left and reflects at the interface of the laser-induced bubble, which generate a negative pressure with high intensity, leading to the first cavitation inception close to the laser-induced bubble at t=152 μs. Then, cavitation occurs continuously in a line in the perpendicular direction to the HIFU propagation during t=160 μs and 166 μs, and a bubble layer, which can be a new reflector of HIFU, is formed. Repeating this inception procedure results in the formation of a cone-shaped bubble cloud.

Numerical calculations are conduted to simulate the bubble cloud formation as shown in Fig. 1. Figure 2 shows an arrangement of bubble 1 as a reflector and bubble nuclei. In the simulation, 136 bubble nuclei with an initial radius of 1.8 nm are placed near bubble 1. The governing

equations are the two-dimensional axisymmetric Euler equations. The pressure field around bubbles is calculated by the ghost fluid method (GFM). Until a bubble nucleus grows enough for its interface to be captured with the level-set function, the equation of motion of a single spherical bubble, the Keller equation, is utilized to calculate the growth of nuclei. When an arranged bubble nucleus grows enough, the level set function is used to express the bubble surface. When switching the method, the velocities by the nuclei growth are superposed to those in the microscopic field calculated with the GFM. Figure 3 shows the pressure distributions around bubbles and the formation of a bubble cloud. When each nucleus' radius grows larger than threshold radius in which their interfaces can be captured with the level-set function, the numerical method changes from Keller equation to the level-set method; the bubble interfaces appear and the bubbles start to interact with the HIFU's pressure field ($t/T = 11.640$). These bubbles stand in a line in the perpendicular direction with respect to the propagation axis and forms a bubble layer ($t/T = 11.919$). Backscattering of HIFU from the bubble layer makes negative pressure with high intensity; the new nuclei start to grow and make another layer of bubbles ($t/T = 12.637$). Continuing these processes make a cone-shaped bubble cloud like the experiment ($t/T = 13.481$). This mechanism in the simulation agrees with the experiment.

REFERENCES

(1) Maxwell, A. D. et al, J. Acoust. Soc. Am., Vol. 130(4), 1888-1898 (2011).
(2) Ogasawara, T. et al, Fluid Dyn. Res., Vol. 50(6), 1-16 (2018).
(3) Horiba, T. et al, J. Acoust. Soc. Am., Vol. 147(2), 1207-1217 (2020).
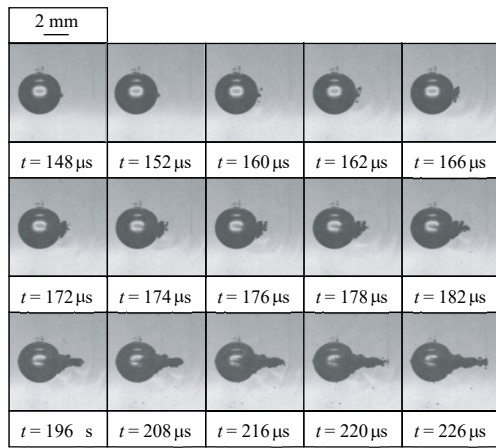
Fig. 1   Snapshots of bubble cloud formation.
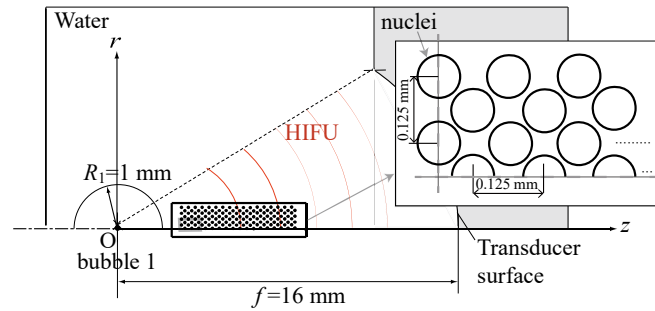
Fig. 2   Schematic of numerical model for the pressure field with bubble nuclei.
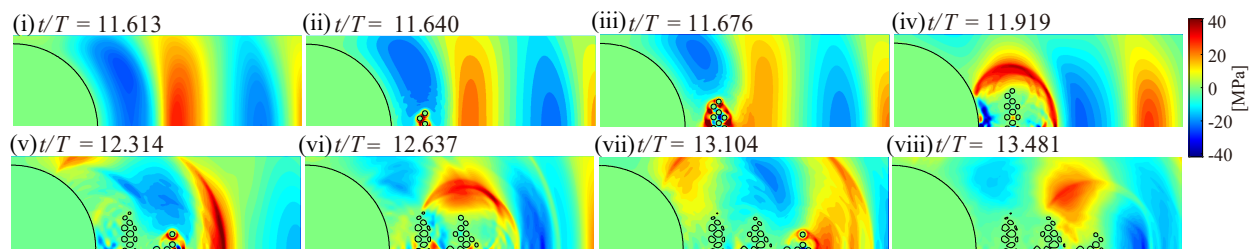
Fig. 3   Bubble cloud formation and pressure distributions around bubbles

Industrialization of Micro-Two-Phase Flow and Heat Transfer Research: Where Are We?

John R. Thome[1]
[1]JJ Cooling Innovation Sàrl
Technical Director
EPFL Innovation Park, Bldg. A
Lausanne, Switzerland

Contact E-mail : john.thome@jjcooling.com

Many of us present have been heavily involved in fundamental research on microchannel two-phase flow, flow boiling and convective condensation (experimentally, visually, modelling and numerically) for over two decades now. Extensive advances have been made in all these areas, and many new results will be presented here this week. So the question for our community arises: *Is This Fundamental Research Being Translated into Engineering Practice?* The answer seems to be a big *YES*! Notably, applications are always a great stimulus for more focused research once a technology roadmap has begun and numerous issues need to be confronted. This lecture will try to highlight some of these applications and new devices, both personal and from tech talks of others at conferences. In general, they fall into the following categories and nearly all are for electronics cooling: (1) pumped two-phase cooling loops, (2) gravity-driven two-phase cooling loops, (3) micro-evaporator designs and (4) pulsating heat pipes. In most instances, the goal is higher performance cooling using less energy (electricity) to drive the cooling system, so a timely topic. The goal in this talk is not to be exhaustive in details, but to stimulate discussion on how the current fundamental work can contribute more to this technology/energy challenge and thus to our "green" environment goals.

Interface Retaining Coarsening of Multiphase Flows

X. Chen, J. Lu, and G. Tryggvason

Johns Hopkins University, Baltimore, MD, USA
Contact E-mail : gtryggv1@jhu.edu

Multiphase flows are characterized by the presence of a sharp interface. In many situations such flows also consists of a large range of scales, making fully resolved numerical simulations expensive or unfeasible. For predictions of the behavior of systems of practical interest it is therefore necessary to use coarse models where large scales are evolved deterministically and small scales are represented statistically. The interface is usually a prominent feature of multiphase flows and in coarse models it may therefore be important to retain a sharp interface for the resolved scales, in a similar way that modeling of disperse flows often retain bubbles or drops as point particles. Equations for the evolution of coarse grained flows are usually derived from equations for the fully resolved flow by adding closure terms to account for the effect of unresolved scales, the coarse field is generated by explicit filtering, and the closure terms constructed using the filtered fully resolved solution. An alternate approach is to find the closure terms directly from the evolution of the coarse field by asking how the traditional fluid equations need to be modified to ensure that the coarse field evolves correctly. The second approach allows the coarsening to be done in a variety of different ways, including using strategies that preserve a sharp interface. We describe a systematic process to coarsen fully resolved numerical solutions for multiphase flows while retaining a sharp interface [1]. The different phases are identified by an index function that takes different values in the different phases and is coarsened by solving a constant coefficient diffusion equation, while tracking the interface contour. Small flow scales of one phase, left behind when the interface is moved, are embedded in the other phase by solving a nonlinear diffusion equation with a modified diffusion coefficient that is zero at the interface location to prevent diffusion across the interface, along with a pseudo pressure equation to preserves the incompressibility of the coarsened volumetric velocity field. Several examples of different levels of coarsening are shown. The dynamics of the small scales in the mixed regions can be modeled in many different ways, including using homogeneous mixture, drift flux, and two fluid Euler-Euler models, as well as Euler-Lagrange models. While classical models for the flow away from the interface can be used, those are usually developed in highly empirical ways and we have started explore the use of data-driven techniques for more systematic development of models for the whole flow field, including the interface. The interface dynamics is modeled using simple physics bases models, with coefficients determined using filtered data, and the flow in the bulk is modeled

using a very simple mixture model. Comparison of the model results for different level of filtering with filtered fully resolved results show that for a short time the coarse model predicts the detailed evolution of the filtered data but for long times we need to compare the evolution of the statistical properties of the flow. Opportunities and challenges for more complex coarse models, as well as other coarsening strategies, are also discussed.

[1] Xianyang Chen, Jiacai Lu and Gretar Tryggvason. "Interface Retaining Coarsening of Multiphase Flows." Physics of Fluids 33, 073316 (2021).
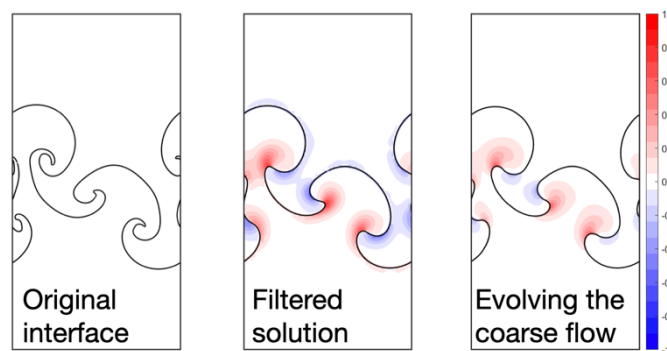
Figure 1. The Rayleigh–Taylor instability at late time. The left frame shows the unfiltered interface, and the middle frame shows the interface and the perturbation volume fraction obtained by smoothing the flow by diffusion. The perturbation volume fraction in the right frame is obtained by evolving a simple mixture model in time.

Gas-liquid flow hydrodynamics in jumpers of subsea gas production systems

A. Yurishchev[1], B. Ravid[1], A. Ullmann[1], N. Brauner[1]

[1] School of Mechanical Engineering. Tel-Aviv University, Tel-Aviv 69978, Israel
Contact E-mail : ullmann@tauex.tau.ac.il

Subsea jumpers are widely used in deep-water offshore gas production systems. They are used to connecting two subsea production structures, such as the wellhead to the Infield Gathering Manifold (IMF), and the IMF to the export flow lines, via their respective PLET (i.e. Pipe Line End Termination). Rigid jumpers are standard-shaped pipes that are designed to accommodate high static and dynamic loads due to thermal expansion, high internal pressure, hydrodynamic loads from the internal two phase flow and external currents. Two-phase flow is encountered due to the presence of liquid phase (e.g., water from the reservoir, condensates, mono-ethylene glycol (MEG) solutions added to prevent hydrates formation). The two-phase flow patterns in the jumper are dependent on the various system parameters, which include the gas pressure and flow rate, the amount of liquid present in the system and the particular jumper shape and size. Each of the flow patterns is associated with a range of pressure fluctuation frequencies, which interact with the jumper structure and may induce harmful Flow-Induced Vibration (FIV).

The study is focused on transient operational conditions during the production start-up, which follows a shut down. It addresses the issue of removing the liquids accumulated in jumpers, the associated gas-liquid flow patterns, pressure variations and the FIV. Experiments and numerical simulations are combined to enable the identification of the minimal gas velocity for removing the accumulated liquids, the maximal pressure built-up and the forces acting on the jumper elbows. A description of the experimental setup of a downscaled jumper (pipe diameter ID=50mm) is shown in Figure1. OpenFOAM is used for the simulations. Several issues, such as turbulence model selection (e.g., κ-ε or κ-ω SST) and gas compressibility effects were studied and discussed. A simple mechanistic model is established for predicting the transient behavior of the gas pressure for various gas superficial velocities and amounts of accumulated liquids.

A demonstration of the experimental results for the pressure variations in the inlet to the jumper (atmospheric outlet pressure) is shown in Figure 2 (LHS).The accumulated liquid in the horizontal section is initially at rest, and the gas flow rate is increased to the final indicated value (U_{GS} is the superficial at atmospheric pressure). The time is scaled with the residence time of the gas in the jumper. The pressure variations predicted by the simulations and the mechanic model are demonstrated in the RHS of Figure 2. Here, a step change in the gas flow rate to the final value

(worst case scenario) was considered. As shown, mechanistic model predictions of the maximal pressure are in good agreement with the simulation results. The pressure rise during the transient process of water removal is mainly due to the acceleration of the liquid and can be attenuated by moderating the gas flow rate rump-up.
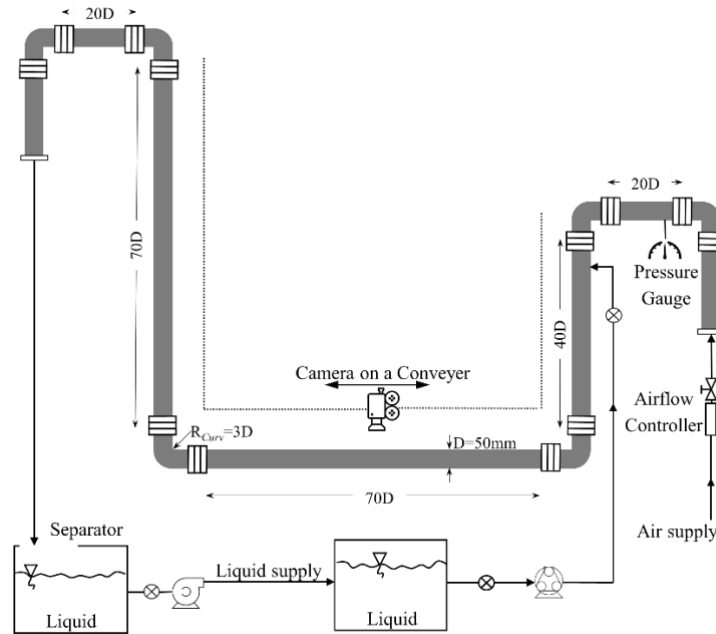

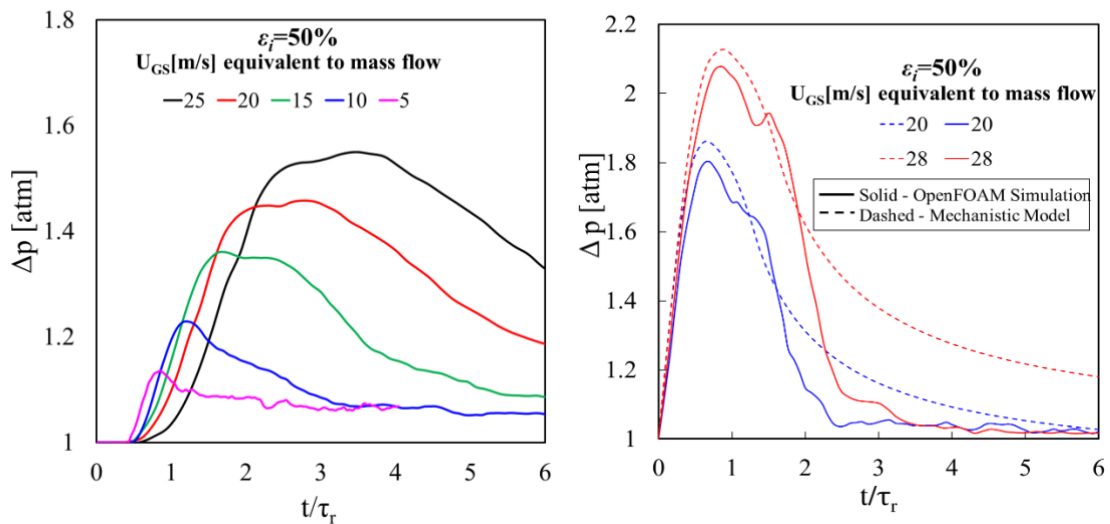Figure 1. Schematic description of the jumper experimental set-up.

Figure 2. Time variation of the pressure drop over the jumper during removal of accumulated liquid in the horizontal section (the initial water holdup in the horizontal section is 50%). LHS figure: experimental results during 2sec ramp-up of the gas flow rate to the final U_{GS} value. RHS figure: Pressure drop for a step change in the gas flow rate predicted by CFD simulations and the mechanistic model.

The percolation law of the boiling crisis

Limiao Zhang[1], Chi Wang[1], Guanyu Su[1], Artyom Kossolapov[1], Gustavo Matana Aguiar[1], Jee Hyun Seong[1], Florian Chavagnat[1], Bren Phillips[1], Md Mahamudur Rahman[1,2], Matteo Bucci[1]

[1]Massachusetts Institute of Technology, Cambridge, MA, USA.
[2]University of Texas at El Paso, El Paso, TX, USA

Contact E-mail : mbucci@mit.edu

Nucleate boiling is an exceptionally effective heat transfer process. However, a boiling crisis suddenly occurs when the heat flux to remove from a heated surface is too high. The maximum heat flux that can be sustained by nucleate boiling depends on surface properties and operating conditions, and it is an important operational limit in many scientific and industrial applications. Many scientists and engineers have attempted to describe this phenomenon and predict this limit mechanistically. However, a universal theory has eluded the thermal science community for almost a century.

Here, we reveal theoretically and experimentally the presence of a unifying law of the boiling crisis. This law emerges from an instability in the near-wall bubble interaction phenomenon, described as a percolation process driven by three fundamental boiling parameters: nucleation site density, average bubble radius and product of bubble growth time and detachment frequency. Our analysis demonstrates that the boiling crisis occurs on a well-defined critical boundary in the multidimensional space of these parameters for a wide variety of boiling surfaces and operating conditions (see Figure 1). We anticipate that this fundamental property of the boiling process can inspire the design of engineered surfaces that enhance the nucleate boiling limit, as well as mechanistic modelling criteria for the design of advanced two-phase heat transfer systems.
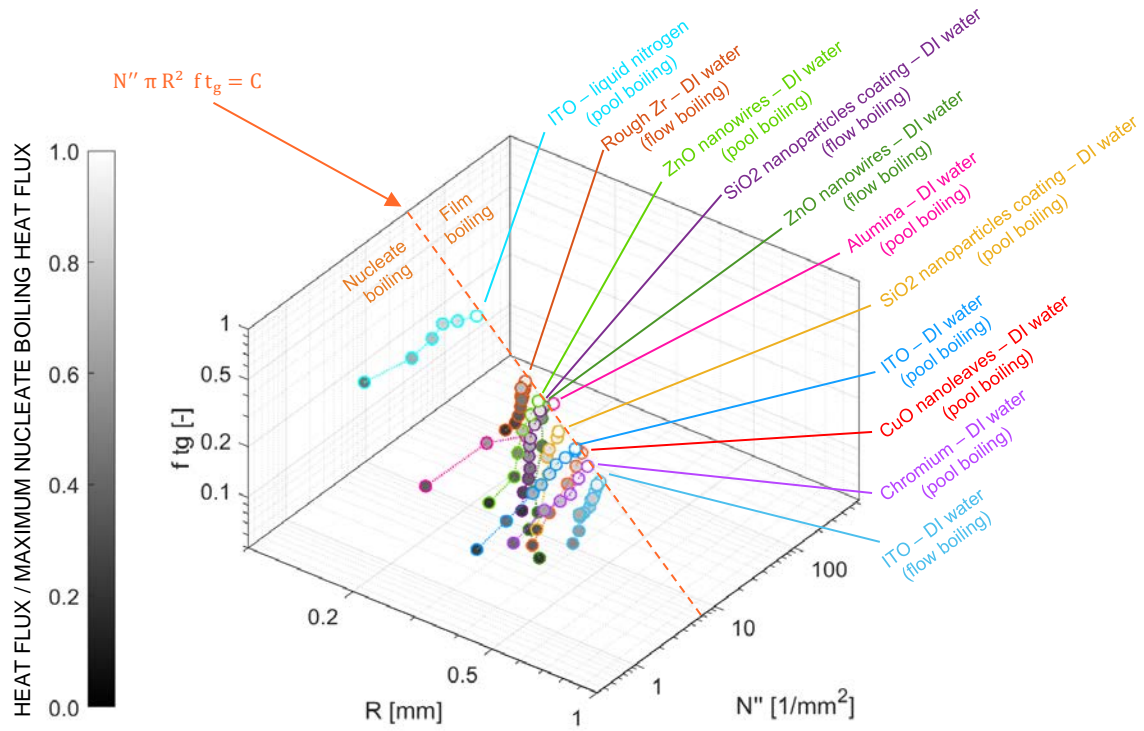
Figure 1. Representation of the experimental boiling triplets $(N'', R, f t_g)$ for several boiling surfaces and operating conditions. The dot grayscale is proportional to the ratio between the heat flux and the maximum heat flux that each surface (represented by different line colors) can remove in nucleate boiling. White dots indicate the experimental boiling crisis and lie on the theoretical critical surface $N'' \pi R^2 f t_g = C$.

Author Index